SCIENTIFIC RESEARCHES

EDITOR
Sevi ÖZ

AUTHORS
Ayça AKTAŞ KARAÇELİK
Aysel ÇIMEN
Bülent DEDE
Cristian Ştefan DUMITRIU
Elif AŞIKUZUN
Güvenç GÖRGÜLÜ
Murat KIRANŞAN

İKSAD
Publishing House

SCIENTIFIC RESEARCHES

EDITOR

Sevi ÖZ

AUTHORS

Ayça AKTAŞ KARAÇELİK

Aysel ÇIMEN

Bülent DEDE

Cristian Ștefan DUMITRIU

Elif AŞIKUZUN

Güvenç GÖRGÜLÜ

Murat KIRANŞAN

İKSAD
Publishing House

(The Licence Number of Publicator: 2014/31220)
TURKEY TR: +90 342 606 06 75
USA: +1 631 685 0 853
E mail: iksadyayinevi@gmail.com
www.iksadyayinevi.com

ISBN: 978-625-8061-25-3
Cover Design: İbrahim KAYA
December / 2021
Ankara / Turkey
Size = 16x24 cm

CONTENTS

FOREWORD

I am delighted to write the foreword for this scientific book. This book contains seven chapters. I want to say thanks to all IKSAD publication team and the authors who have contributed to this book. It is my hope and expectation that this book will provide an effective learning experience and referenced resource for all science professionals.

Prof. Dr. Sevi ÖZ
Ankara Hacı Bayram Veli University

CHAPTER 1

PREPARATION AND APPLICATION OF SP-CPTS-2-AMINO-3-PYRIDINOL MICROCAPSULE

Assoc. Prof. Dr. AYSEL ÇIMEN[1]

[1] University of Karamanoğlu Mehmetbey, Faculty of Kamil Özdağ Science, Department of Chemistry Karaman, Turkey. E-mail: acimen@kmu.edu.tr and ayselcimen42@hotmail.com, Orcid ID:0000-0001-7492-8950. This book chapter is adapted from the thesis work.

INTRODUCTION

With the development of industry, water pollution has begun to destroy the living spaces of living things all over the world (Bhatnagar.2010, Bhatnagar.2011, Santhosh. 2016). There are many pollutants in the world that pollute the waters. However, the most deadly of these pollutants are heavy metals. Because they poison living things even in small amounts (Santhosh. 2017, Sarojini.2021, Ukhurebor.2021). As a result, new generation adsorbents are necessary to remove harmful metals from wastewater with high efficiency and low cost. Sporopollenin and silica materials containing can be recommended for this process.

To remove many impurities and purify wastewater; membrane, photocatalyst, electrodialysis and adsorption etc. methods are used (Lu.2017, Sarin. 2006, Li.2017). Among these methods, the adsorption method has been suggested as the most suitable method due to its low cost, easy application and high separation capacity. It has been determined that *Cr (VI)* is a very toxic and mutagenic ion for the ecological and biological environment (Tang. 2014). It is used in many areas of the industrial sector such as chrome casting industry, metallurgy, automotive industry, chemistry, kitchen and bathroom materials (Cheng. 2014, Liu. 2020, Aigbe.2020).These industrial establishments send waste containing *Cr(VI)* to water sources after productionAccumulation of *Cr (VI)* in doses that exceed the exposure limit in the human body causes many diseases such as sadness, spiking confusion, mind loss and allergic rashes.

(Bhusari. 2016, Sarojini. 2021 Jang. 2020). The average limit value of *Cr(VI)* ions that should be present in drinking water has been determined as 0.05 mg/L by the World Health Organization (WHO) (Peng. 2020, Pietrelli. 2020). Therefore, much attention should be paid that *Cr(VI)* amount in wastewater does not exceed this limit value. Sporopollenin is a biological polymer that is stable in molecular structure, resistant to chemical agents, has a very high adsorption ability, can be modified with a multifunctional group, can be obtained in a short time and quite easily, and has a low cost.

In this study, firstly, the surface of Sporopollenin was activated and modified with *3-chloropropyl trimethoxysilane (CPTS)* compound. It was then modified with the compound 2-amino-pyridin-3-ol. The kinetic parameters about the adsorption of *Cr(VI)* on the *Sp-CPTS-2-amino-pyridin-3-ol* has been investigated. At the same time, the effects of variables such as pH, touch time, amount of adsorbent, temperature and concentration were studied to eliminate *Cr(VI)* ions from wastewater.Since the results are very efficient and compatible with the literature, *Sp-CPTS-2-aminopropyl-3-ol* adsorbent can easily be recommended to eliminate *Cr (VI)* from wastewater.

1. MATERIALS AND METHODS

1.1. Reagents and Chemicals

The chemicals used in the study are of analytical purity. They were purchased from Sigma and Aldrich companies. It is*Sporopollenin (Sp), 3-chloropropyl trimethoxysilane (CPTS),*Toluene (C_7H_8), Potassium dichromate ($K_2Cr_2O_7$), 2-amino-3-pyridinol ($C_5H_6N_2O$).

1.2. Instrument

In experimental studies, devices such as pH meter (Orion ion meter), FT-IR, UV-Vis Spectroscopy (Perkin Elmer), thermostatic shaker (A HeidolphUnimax 2010) and SEM (Scanning Electron Microscope) were used.

1.3. Synthesis of Sp-CPTS-2-amino-3-pyridinol Microcapsules

5.0 g of Sporopollenin (Lycopodium Clavatum) and 12 ml of 3-chloropropyl-triethoxysilane were added to 100 mL of anhydrous toluene and the resulting mix was stirred under reflux for 72 hours. After filtering, it was washed with methyl alcohol and ethyl alcohol, respectively. The compound *3-chloropropyl-trimethoxysilane-sporopollene (Sp-CPTS)* was dried under vacuum at 60 °C for 24 hours (Bilgiç. 2019, Qu. 2021).

100 mL of anhydrous toluene was added on 5.0 g of *3-chloropropyl-trimethoxysilane-sporopollenin (Sp-CPTS)* and 1.0 g of 2-amino-3-pyridinol and themixwas stirred under reflux for 12 hours at 65 °C (Bilgiç. 2019). The mixture which was at room temperature was filtered and the solid adsorbent (Sp-CPTS-2-amino-3-pyridinol) was washed with methanol, ethanol and diethyl ether respectively.Then, the synthesized adsorbent (*Sp-CPTS-2-amino-3-pyridinol*) was dried in a vacuum at 60 ^{o}C for 24 hours (Goswami et al., 2002). The expected formation reaction of *Sp-CPTS-2-amino-3-pyridinol* adsorbent is shown in Figure 1 (Bilgiç. 2019, Qu. 20219).

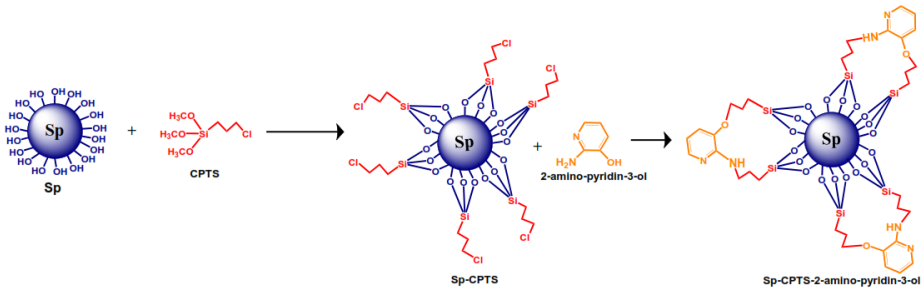

Figure 1. The Expected Structures of Sp, Sp-CPTS and Sp-CPTS-2 amino-3-pyridinol.

1.4. Adsorption Procedure

To be used in adsorption experiments, 0.0294 g $K_2Cr_20_7$ was put into 1L bottle and completed with pure water. Thus, $1x10^{-4}$ M. Cr (VI) stock solution was prepared. The pH values used in the experimental studies were adjusted with 10^{-1} M HCl and NaOH solutions. Experiments were also carried out for the waste chromium solution under the same conditions. Adsorption studies were performed using batch method. There are important parameters that affect the adsorption efficiency, such as pH (2-7), concentration (8-40 mg/L), amount of adsorbent (0.1-0.75 g), contact time (30-180 minutes) and temperature (20-50 ^{o}C). Various experiments were carried out with stock solution and waste solution to determine these parameters (Nur-E-Alam. 2020). The concentrations of *Cr(VI)* remaining in the filtrate were measured by UV-Vis. Spectroscopy. Experimental results were evaluated and optimum conditions were determined. The percent adsorption was found from the following Equation 1.

$$Adsorption\% = \frac{(C_0 - C_e)}{C_0} x100 \quad (1)$$

The adsorption coefficient (q_e in mg.g-1) was seen Equation 2 (Cimen. 2015).

$$qe = \frac{(C_0 - C_e)V}{W} \quad (2)$$

2. CONSEQUENCE AND NEGOTIATION

2.1. Characterization ofSp-CPTS-2-amino-3-pyridinol

FTIR spectra of *Sp-CPTS-2-amino-3-pyridinol* adsorbent were recorded using a Perkin Elmer spectrophotometer in the wavenumber range of 400–4000 cm^{-1}. In addition, the morphology of the adsorbent was examined by SEM. Cr(VI) ions in solution were analyzed with a UV–Vis spectroscopy.

Adsorption is an event that occurs on the surface and its size is proportional to the specific surface area. Adsorption is a surface phenomenon, and its width is proportional to its surface. Therefore, the adsorption efficiency increases in adsorbents with a large surface area and pore volume, a certain pore distribution and particle structure (Othmani.2021). Surface morphologies of the *Sp-CPTS-2-amino-3-pyridinol* adsorbent were observed under SEM. SEM images *of Sp*, *Sp-CPTS* and *Sp-CPTS-2-amino-3-pyridinol* are shown in Figure 2. According to these images, pure Sp (Figure. 2a) shows a much smoother morphology than *Sp-CPTS* (Figure. 2b). Geometric structures of *Sp-CPTS-2-amino-3-pyridinol* adsorbent are shown in Figure 2c. Here, it is seen that the structure is deteriorated and an irregular morphology covered with foreign matter such as 2-amino-3-

pyridinol is formed. As seen in Figure 2c, the presence of particles, i.e., (2-amino-3-pyridinol) attached to the surface of the sporopollenin confirms the immobilization.

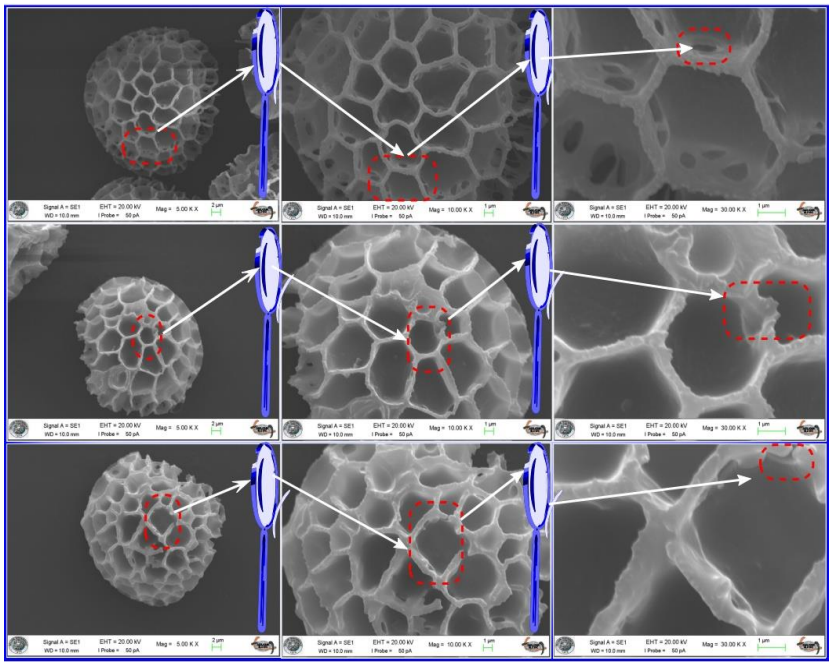

(a) (b) (c)

Figure.2. SEM images of Sp (a), Sp-CPTS (b) and Sp-CPTS-2-amino-3-pyridinol

2.2. FTIR Investigations

The FTIR spectra of *Sporopollenin (Sp), sporopollenin-3-chloropropyl-trimethoxysilane (Sp-CPTS)* and *sporopollenin-3-chloropropyl-trimethoxysilane-2-amino-3-pyridinol(Sp-CPTS-2-amino-3-pyridinol)* are given in Figure 3.

The peak at 3321 cm^{-1} result from the OH stretching bond. The peaks between 2850-2921 cm^{-1} result from the aliphatic (-CH, -CH2, -CH3)

group. The peaks at 1706 cm^{-1} result from the carbonyl (C=O) group (Lu.2017).

The vibrational of the –OH group in Sp shifted from 3321 cm^{-1} to 3361 cm^{-1} in Sp-CPTS.In addition, deep large peaks seen at 1100 cm^{-1} indicate C-O-C (similarly Si-O-C) or C-O (similarly Si-O) symmetrical or asymmetric stress (Das. 2021Singh. 2021, Shang. 2021).

The peaks at 2921–2850 cm^{-1} for Si-CPTS result from the CH stretching bond. The absorption band at 692 cm^{-1} for *Si-CPTS* belongs to the C–Cl stretching vibration from the silylating agent *(CPTS)* (Liu. 2021). The peak at 3361 cm^{-1} for–OH group in Sp-CPTS shifted to 3354 cm^{-1} in the *Sp-CPTS-2-amino-3-pyridinol*.

The peak at 1271cm^{-1} in the structure of *Sp-CPTS-2-amino-3-pyridinol* result from the –C–N.–C = N peak in Sp structure shifted from 1706 cm^{-1} to 1603 cm^{-1} in Sp-CPTS. Peaks seen in 2-amino-3-pyridinol and Sp-CPTS structures in the range of 2921-2840 cm^{-1} see as three different peaks in the *Sp-CPTS-2-amino-3-pyridinol*structure. The observation of different CH, CH_2 or CH_3 groups in the *Sp-CPTS-2-amino-3-pyridinol* compound confirms that the 2-amino-3-pyridinol composite is immobilized on the *Sp-CPTS* surface.

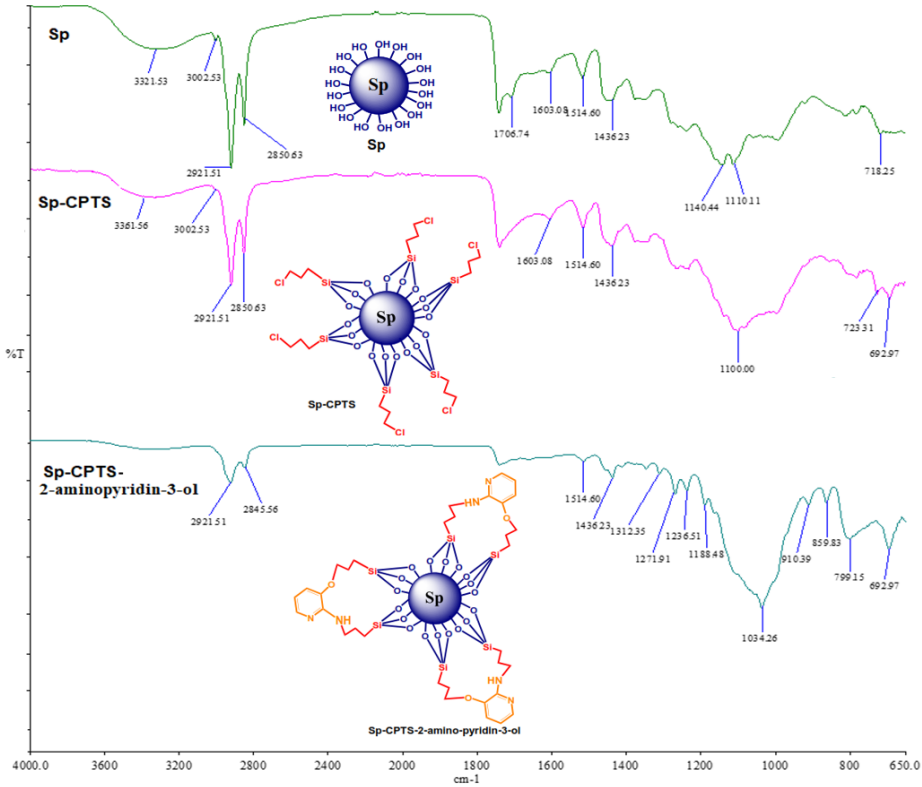

Figure 3. FTIR spectrums of activated Sp, Sp-CPTS and Sp-CPTS-2-amino-3-pyridinol.

2.3. Effective Parameters on The Adsorption Process

2.3.1. Effect of pH

One of the significant parameters affecting the adsorption efficiency is pH. It also determines the formation and stability of different *Cr(VI)* ions in solution. The adsorption efficiency can be influenced by the charge density on the newly prepared adsorbent surface and the *Cr(VI)* solution. In order to find the efficiency of adsorbing *Cr (VI)* ions in

solution with adsorbent having different amine groups, a series of experiments were carried out at different pH (1-7) using the *Bach Method*.

The effect of pH on adsorption according to experimental data is shown in Figure 4a.

There are various ionic forms of *Cr(VI)* ions ($HCrO_4^-$, $Cr_2O_7^-$, and CrO_4^{2-}) in nature. The stability of these ions is determined by the total CrO_4^{2-}concentration and pH of the solution (Lu.2017). Therefore, high adsorption efficiency was achieved at low pH (Ukhurebor. 2021).

As seen in Figure 4b, *Cr(VI)* removal was 97% at pH 2 and decreased to 20% at pH 7. In this case, as the pH increased, the positive charges on the adsorbent surface decreased. Thus, the adsorption efficiency increases as electrostatic attraction occurs between the negative charges of the adsorbent (NH_2- and OH-) and the positive charges of *Cr(VI)* (Maleki.2016).

2.3.2. Effect of Touch Time

Figure 4b shows that the amount of heavy metal adsorption increases with increasing contact time for *Cr(VI)* ions. The efficiency of removing *Cr(VI)* ions from the aqueous solution with the newly prepared adsorbent reached the highest level in 150 minutes and remained stable after this minute. The percentages of removal in solution and wastewater are 44% and 32%, respectively.

2.3.3. The effect of the dosage of adsorbent

The adsorbent dosage is an important parameter, which influences the extent of metal elimination from the solution. It is clear that the removal rate of metal ions increases as the adsorbent dosage increases, since there are more surface areas on the adsorbent with more adsorbent amount. Removal percentages of *Cr(VI)* ions from solution and wastewater were calculated by Equation 2. Figure 4c shows the effect of adsorbent amount on metal removal percentage in aqueous solution and wastewater. As can be seen from Figure 4c, the removal of metal ions increased as the amount of adsorbent increases. The highest amount of adsorbent was calculated as 0.05 g for the adsorption of Cr(VI) ions in both solution and wastewater.

2.3.4. Effect of concentration

The effect of concentration on the adsorption of *Cr(VI)* ions is shown in Figure 4d. As can be seen from the graph, the amount of substance retained on the surface increased in parallel by the increase in the dosage of metal ions in the solution. This process ends when the system is in equilibrium and the surface area is full.

2.3.5. Effect of temperature

Experimental studies were carried out in the range of 20-50^{o}C. The reason for metal removal at these temperatures is to increase the dynamism of the metal ion and create a swelling effect in the structure of the adsorbent, thereby allowing larger metal molecules to penetrate the adsorbent more. The amount of adsorption is affected because the

temperature changes the molecular movements, solubility and reactions. The reason for the increase in removal is the chemical reactions that occur between the functional groups of the metal ions and the adsorbent molecule (Figure 4e).

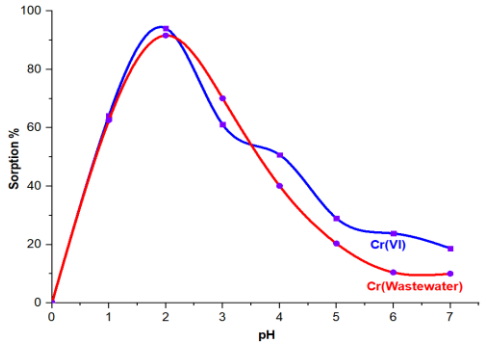

(a)

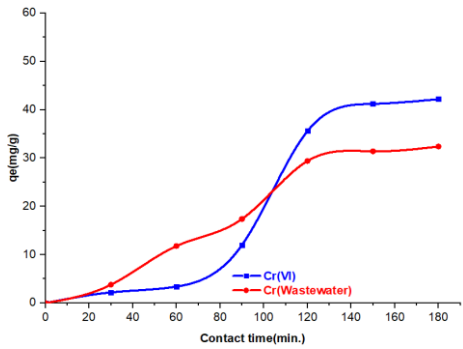

(b)

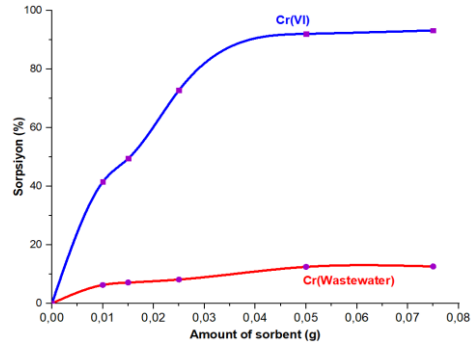

(c)

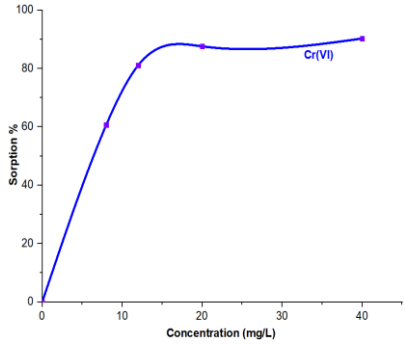

(d)

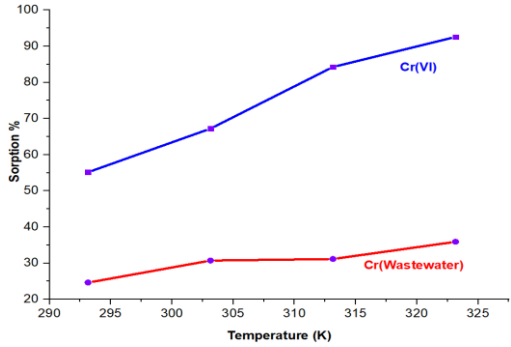

(e)

Figure. 4. The effect of pH (a). The effect of the contact time (b). The effect of the amount (c).
The effect of concentration (d). The effect of temperature (e).

2.4. Isotherm studies

Langmuir, Freundlich and Dubinin-Radushkevich isotherm models were applied to explain the data of adsorption isotherms. Langmuir isotherm data were calculated according to Equation 3 (Çimen. 2019).

$$\frac{C_e}{q_e} = \frac{C_e}{q_o} + \frac{1}{q_o} b$$

(3)

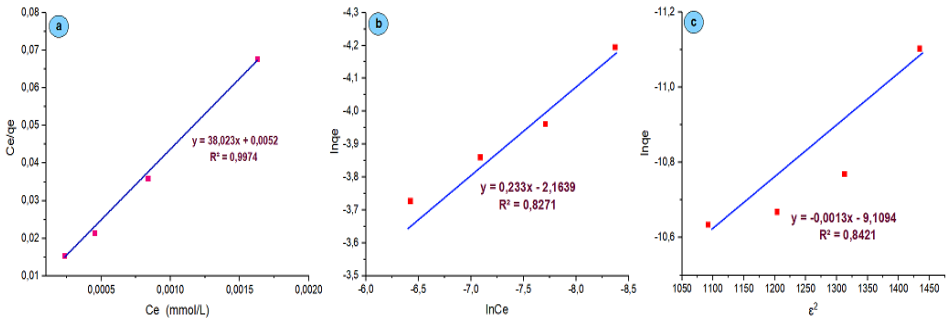

Figure. 5. Langmuir isotherm (a), Freundlich isotherm (b), D-R isotherm (c).

The Langmuir isotherm graph is shown in Figure 5a. In this graph, $1/q_o b$ is equal to the slope of the line, and $1/q_o$ is the point where the line intersects the y-axis. Adsorption of heterogeneous surfaces is explained by the Freundlich isotherm model, which is one of the isotherm models (Liu.2021). It is expressed by the following Equation4 (Maria. 1994).

$$\mathrm{Ln}q_e = \ln K_F + \frac{1}{n}\ln C_e \quad (4)$$

As seen in Figure 5b, when $\ln q_e$values versus $\ln C_e$ values are plotted, the graph gives a straight line and the y-intercept of this line gives the

K_F value and the *n* value is equal to the slope (Equation 4) (Ghanizadeh.2012 Liu. 2021). The valuations of 1/n for*Sp-CPTS-2-amino-3-pyridinol* are <1, confirming a high adsorption capacity. Calculation of the K_F value as 0.107 from the experimental measurements indicates that a high level of adsorption of Cr(VI) ions in the solution and waste water occurs with the *Sp-CPTS-2-amino-3-pyridinol* adsorbent (Almeida. 2019).Appropriate adsorption conditions are expressed by values of n > 1 (Bajpai. 2004). The K_F and *n* values were calculated by finding the intersection point and slope of the graph in Figure 5b. The results are given in Table 1. The adsorption energy was calculated with the DR isotherm. The calculations were made with Equation5 (Çimen. 2016).

$$lnq_e = lnq_m - k\varepsilon^2 \quad (5)$$

The ε^2 values against the lnqe values were plotted and the resulting graph gave a straight line. The point where this line intersects with the y-axis gives the q_m value and its slope gives the *k* value (Figure 5c).

Average free energy value *(E)* calculated using Equation 6 and some parameters calculated using the values obtained from the isotherms are given in Table1.

$$E = (2k)^{-1/2} \quad (6)$$

In this study, the average energy for *Cr(VI)* ions in solution was calculated to be 19.61 $kJmol^{-1}$ (Table 1). It is known that adsorption occurs chemically when the average energy is above 8 $kJmol^{-1}$

(Çimen.2020). Accordingly, the adsorption of *Cr(VI)* in aqueous medium was carried out by chemical adsorption (Çimen. 2020).

Table1. Isotherms parameters for Cr(VI) ions by Sp-CPTS-2-amino-3- pyridinol.

	1/n	K_F	q_o L/mol	b(mol^2 $(KJ^2)^{-1}$)	k ($mol^2K^{-1}J^{-1}$)	q_m(mol/g)	E ($kJmol^{-1}$)
	0.233	0.107	0.026	5570.91	0.0013	0.097	19.61

2.5. Thermodynamic studies

In physicochemical studies, thermodynamic factors such as enthalpy change *(ΔH°)*, entropy change *(ΔS°)* and free energy change *(ΔG°)* should be known in order to predict the mechanism of the reaction and the possible structure of the obtained substance (Karthik.2014).

Also, these factors are very important to explain the adsorption phenomenon and should be carefully studied to determine as they determine whether a reaction is voluntary or involuntary.

The effect of temperature (20 °C – 50 °C) on the adsorption of *Cr(VI)* ions to immobilized *Sp-CPTS-2-amino-3-pyridinol* adsorbent was investigated. Thermodynamic factors were calculated according to the Equations 7, 8 and 9 (Çimen. 2019).

$$K_D = \left(\frac{C_0 - C_e}{C_e}\right) \times \frac{V}{W} (7)$$

$$\log K_D = \frac{\Delta S^\circ}{2.303R} - \frac{\Delta H^\circ}{2.303RT} \quad (8)$$

$$\Delta G^\circ = \Delta H^\circ - T\Delta S^\circ \quad (9)$$

Table 2. Thermodynamic Parameters for Sorption of Cr(VI) and Cr(wastewater) ions of *Sp-CPTS*-2-amino-3- pyridinol.

Metal	**ΔH^o (kJmol^{-1})**	**ΔS^o (JK^{-1}mol^{-1})**	**$-\Delta G^o$(kJmol^{-1})**			
			298K	303K	313K	323K
Cr(VI)	44.81	181.74	11.46	12.28	13.55	14.41
Cr(wastewater)	40.44	50.17	10.27	10.69	11.08	11.52

Enthalpy and entropy change values for the adsorption of *Cr(VI)* ions were evaluated with Van't Hoff graphs (Figure 6) and Free energy change values also were calculated using Equation 8. They are given in Table 1 and 2 (Maria.1994 ,Çimen201). The plot of *1/T* versus $logK_D$is shown in Figure 6.

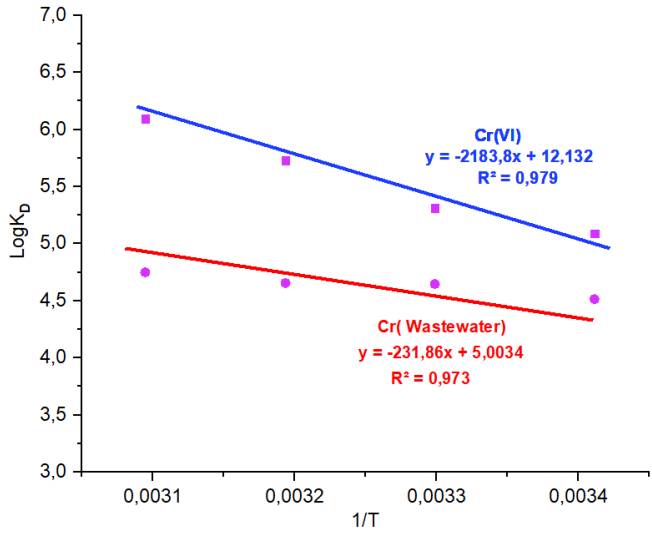

Figure. 6. Plot of log K_D versus 1/T

$\Delta H°$ and $\Delta G°$ values were calculated using experimental data. As seen in Table 2, $\Delta H°$ values are positive and $\Delta G°$ values are negative. According to this results, adsorption is endothermic and adsorption increases with temperature. Negative $\Delta G°$ values indicate that adsorption formation varies inversely with temperature. In addition, the presence of $\Delta H°$ as positive (+) also supports this statement. In the light of this information, it can be said that the adsorption took place inversely proportional to the temperature. The positive value of $\Delta S°$ shows the increase in incidental adsorption at the solid-solution interface and the existence of ion exchange reactions. *Cr(VI)* ions and water molecules in solution are bound to the adsorbent by covalent bonds. As a result of the liberation of water molecules, the degree of randomness, the type of mechanism, and the strength of the binding adsorption energy increase the value of ΔH^o. Since small energies are required for physical adsorption to occur, the reaction time is fast and

generally reversible. The energy required for H bond formation and for Van der Waals interactions is 4-8 kJ mol^{-1} and 8-40 kJ mol^{-1}, respectively. The chemical adsorption enthalpy starts at about 40 kJ mol^{-1}. The values below refer to physical adsorption (X. 2020).

The $\Delta H°$ values in solution and wastewater were found to be 44.81 and 40.44 kJ mol^{-1}, for the - ions in the 25°C–50°Crespectively.

CONCLUSION

Sp-CPTS-2-amino-3-pyridinol adsorbent was synthesized for the first time. This synthesis was confirmed by FT-IR spectroscopy and SEM. *Sp-CPTS-2-amino-3-pyridinol* adsorbent has a high separation capacity, is insoluble in water and many acids, is inexpensive, suitable for removing heavy metals from wastewater, and has a very large active surface area. The appearance of the *Sp-CPTS-2-amino-3-pyridinol-Cr*can be estimated in Figure. 7.

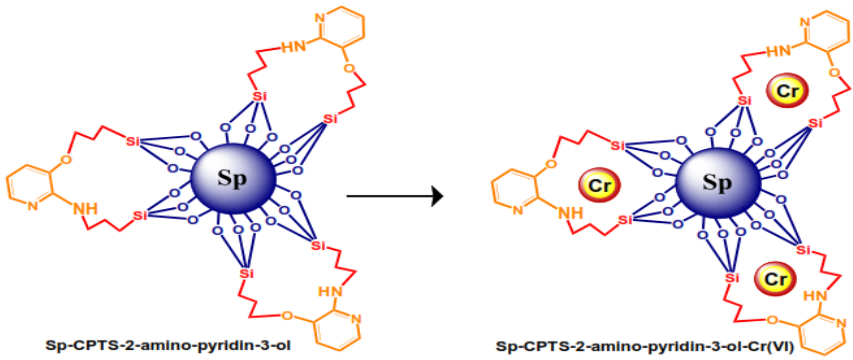

Figure.7. Estimated structure of Sp-CPTS-2-amino-3- pyridinol-Cr.

According to the parameters interpreted in this study, the best Cr removal was achieved at pH = 2.0, 0.05 g adsorbent and 325.15 K' temperature, 20 mg L^{-1} concentration and 150 minutes contact time. The adsorption phenomenon is suitable for the Langmuir isotherm model, which is one of the adsorption isotherm models. It mainly depends on pH. The best percentage of adsorption occurred at pH 2. The mean adsorption energies for the *Sp-CPTS-2-amino-3-pyridinol* adsorbent were found to be 19.61 for Cr*(VI)* in aqueous solution. Experimental results show that adsorption occurs chemically. According to the experimental results, a positive *ΔH°* value indicates that the adsorption reaction is endothermic, and a positive ΔG^o value indicates that the reaction is spontaneous. The adsorption of *Cr(VI)* ions on*Sp-CPTS-2-amino-3- pyridinol* increases at high temperatures. *Sp-CPTS-2-amino-3- pyridinol* adsorbent has fairly high capability for adsorption *Cr(VI)* ions from the wastewater (Çimen.2021).For this reason, this study presents new opportunities to explore feasible and economical methods for the treatment of wastewater containing *Cr(VI)* and other heavy metals (Kılıçel. 2018).

REFRENCES

Shang, Y., Zhu, G., Yan, D., Liu, Q., Gao, T., & Zhou, G. (2021). Tannin cross-linked polyethyleneimine for highly efficient removal of hexavalent chromium. *Journal of the Taiwan Institute of Chemical Engineers*, *119*, 52-59.

Ahmad, W., Qaiser, S., Ullah, R., Mohamed Jan, B., Karakassides, M. A., Salmas, C. E., ... & Ikram, R. (2021). Utilization of Tires Waste-Derived Magnetic-Activated Carbon for the Removal of Hexavalent Chromium from Wastewater. *Materials*, *14*(1), 34.

Aigbe, U. O., & Osibote, O. A. (2020). A review of hexavalent chromium removal from aqueous solutions by sorption technique using nanomaterials. *Journal of Environmental Chemical Engineering*, 104503.

Bhatnagar, A., & Sillanpää, M. (2010). Utilization of agro-industrial and municipal waste materials as potential adsorbents for water treatment—a review. *Chemical engineering journal*, *157*(2-3), 277-296.

Bhatnagar, A., Kumar, E., & Sillanpää, M. (2011). Fluoride removal from water by adsorption—a review. *Chemical engineering journal*, *171*(3), 811-840.

Bhusari, V. N., Dahake, R., Rayalu, S., & Bansiwal, A. (2016). Comparative study of removal of hexavalent chromium from water using metal oxide nanoparticles. *Advances in Nanoparticles*, *5*(1), 67-74.

Bilgiç, A., & Çimen, A. (2019). Removal of chromium (VI) from polluted wastewater by chemical modification of silica gel with 4-acetyl-3-hydroxyaniline. *RSC Advances*, *9*(64), 37403-37414.

Cheng, Q., Wang, C., Doudrick, K., & Chan, C. K. (2015). Hexavalent chromium removal using metal oxide photocatalysts. *Applied Catalysis B: Environmental*, *176*, 740-748.

Çimen, A., Bilgiç, A., & Yılmaz, İ. (2015). Chemical modification of silica gel with hydrazine carbothioamide derivative for sorption studies of Cu (II), Ni (II) and Co (II) ions. *Desalination and Water Treatment*, *55*(2), 420-430.

Çimen, A., Torun, M., & Bilgiç, A. (2015). Immobilization of 4-amino-2-hydroxyacetophenone onto silica gel surface and sorption studies of Cu (II), Ni (II), and Co (II) ions. *Desalination and Water Treatment*, *53*(8), 2106-2116.

Das, M., Bramhanand, P. S., & Laxminarayana, K. (2021). Performance and efficiency services for the removal of hexavalent chromium from water by common macrophytes. *International Journal of Phytoremediation*, 1-9.

Jang, E. H., Pack, S. P., Kim, I., & Chung, S. (2020). A systematic study of hexavalent chromium adsorption and removal from aqueous environments using chemically functionalized amorphous and mesoporous silica nanoparticles. *Scientific reports*, *10*(1), 1-20.

Li, Y., Xu, Z., Liu, S., Zhang, J., & Yang, X. (2017). Molecular simulation of reverse osmosis for heavy metal ions using functionalized nanoporous graphenes. *Computational Materials Science*, *139*, 65-74.

Liu, D. M., Dong, C., & Xu, B. (2021). Preparation of magnetic kaolin embedded chitosan beads for efficient removal of hexavalent chromium from aqueous solution. *Journal of Environmental Chemical Engineering*, *9*(4), 105438.

Liu, Y., Ke, X., Wu, X., Ke, C., Chen, R., Chen, X., ... & Van der Bruggen, B. (2020). Simultaneous removal of trivalent chromium and hexavalent chromium from soil using a modified bipolar membrane electrodialysis system. *Environmental Science & Technology*, *54*(20), 13304-13313.

Lu, W., Li, J., Sheng, Y., Zhang, X., You, J., & Chen, L. (2017). One-pot synthesis of magnetic iron oxide nanoparticle-multiwalled carbon nanotube composites for enhanced removal of Cr (VI) from aqueous solution. *Journal of colloid and interface science*, *505*, 1134-1146.

Nur-E-Alam, M., Mia, M. A. S., Ahmad, F., & Rahman, M. M. (2020). An overview of chromium removal techniques from tannery effluent. *Applied Water Science*, *10*(9), 1-22.

Othmani, A., Magdouli, S., Kumar, P. S., Kapoor, A., Chellam, P. V., & Gökkuş, Ö. (2021). Agricultural waste materials for adsorptive removal of phenols, chromium (VI) and cadmium (II) from wastewater: A review. *Environmental Research*, 111916.

Peng, H., & Guo, J. (2020). Removal of chromium from wastewater by membrane filtration, chemical precipitation, ion exchange, adsorption electrocoagulation, electrochemical reduction, electrodialysis, electrodeionization, photocatalysis and nanotechnology: a review. *Environmental Chemistry Letters*, 1-14.

Pietrelli, L., Francolini, I., Piozzi, A., Sighicelli, M., Silvestro, I., & Vocciante, M. (2020). Chromium (III) removal from wastewater by chitosan flakes. *Applied Sciences*, *10*(6), 1925.

Qu, J., Wang, Y., Tian, X., Jiang, Z., Deng, F., Tao, Y., ... & Zhang, Y. (2021). KOH-activated porous biochar with high specific surface area for adsorptive removal of chromium (VI) and naphthalene from water: Affecting factors, mechanisms and reusability exploration. *Journal of Hazardous Materials*, *401*, 123292.

Santhosh, C., Nivetha, R., Kollu, P., Srivastava, V., Sillanpää, M., Grace, A. N., & Bhatnagar, A. (2017). Removal of cationic and anionic heavy metals from water by 1D and 2D-carbon structures decorated with magnetic nanoparticles. *Scientific reports*, *7*(1), 1-11.

Santhosh, C., Velmurugan, V., Jacob, G., Jeong, S. K., Grace, A. N., & Bhatnagar, A. (2016). Role of nanomaterials in water treatment applications: a review. *Chemical Engineering Journal*, *306*, 1116-1137.

Sarin, V., & Pant, K. (2006). Removal of chromium from industrial waste by using eucalyptus bark. *Bioresource technology*, *97*(1), 15-20.

Sarojini, G., Babu, S. V., Rajamohan, N., Kumar, P. S., & Rajasimman, M. (2021). Surface modified polymer-magnetic-algae nanocomposite for the removal of chromium-equilibrium and mechanism studies. *Environmental Research*, *201*, 111626.

Sarojini, G., Babu, S. V., Rajamohan, N., Kumar, P. S., & Rajasimman, M. (2021). Surface modified polymer-magnetic-algae nanocomposite for the removal of chromium-equilibrium and mechanism studies. *Environmental Research*, *201*, 111626.

Singh, V., Singh, N., Yadav, P., & Mishra, V. (2021). Removal of Hexavalent Chromium from Aqueous Media Using Eco-Friendly and Cost-Effective Biological Methods. *Biosorption for Wastewater Contaminants*, 246-268.

Tang, L., Yang, G. D., Zeng, G. M., Cai, Y., Li, S. S., Zhou, Y. Y., ... & Luna, B. (2014). Synergistic effect of iron doped ordered mesoporous carbon on adsorption-coupled reduction of hexavalent chromium and the relative mechanism study. *Chemical Engineering Journal*, *239*, 114-122.

Ukhurebor, K. E., Aigbe, U. O., Onyancha, R. B., Nwankwo, W., Osibote, O. A., Paumo, H. K., ... & Siloko, I. U. (2021). Effect of hexavalent chromium on the environment and removal techniques: a review. *Journal of Environmental Management*, *280*, 111809.

Maleki, A., Hayati, B., Najafi, F., Gharibi, F., & Joo, S. W. (2016). Heavy metal adsorption from industrial wastewater by PAMAM/TiO2 nanohybrid: preparation, characterization and adsorption studies. *Journal of Molecular Liquids*, *224*, 95-104.

Maria, R. M. C. (1994). Synthesis, characterization, chemisorption and thermodynamic data of urea immobilized on silica. *Journal of Materials Chemistry*, *4*(9), 1479-1485.

Çimen, A., & Bilgiç, A. (2019). Immobilization of 2-(2-hydroxybenzylidinoamino) pyridin-3-ol on silica gel and application to ındustrial wastewater. *Desalination and Water Treatment*, *147*, 116-124.

Ghanizadeh, G., Asgari, G., Mohammadi, A. S., & Ghaneian, M. T. (2012). Kinetics and isotherm studies of hexavalent chromium adsorption from water using bone charcoal. *Fresenius Environmental Bulletin*, *21*(5A), 1296-1302.

Almeida, J. C., Cardoso, C. E., Tavares, D. S., Freitas, R., Trindade, T., Vale, C., & Pereira, E. (2019). Chromium removal from contaminated waters using

nanomaterials–a review. *TrAC Trends in Analytical Chemistry*, *118*, 277-291.

Bajpai, P., Shaman, V., Ealer, K. G., & Gupta, A. K. (2004). Adsorption of Cr (III) and Cr (VI) from aqueous solution by Bacillus cereus biomass. *Electron. J. Biotechnol*, *7*(3), 399-403.

Çimen, A., Karakuş, E., & Bilgiç, A. (2016). Chemical modification of silica gel with 4, 4′-((1Z, 8Z)-2, 5, 8-triazanona-1, 8-diene-1, 9-diyl) diphenol and applications to chromium Cr (VI) ions in industrial wastewaters. *Desalination and Water Treatment*, *57*(16), 7219-7231.

Wang, Y., Yu, L., Wang, R., Wang, Y., & Zhang, X. (2020). A novel cellulose hydrogel coating with nanoscale Fe0 for Cr (VI) adsorption and reduction. *Science of the Total Environment*, *726*, 138625.

Karthik, R., & Meenakshi, S. (2014). Removal of hexavalent chromium ions using polyaniline/silica gel composite. *Journal of Water Process Engineering*, *1*, 37-45.

Çimen, A. (2015). Removal of hexavalent chromium by chemical modification of 4, 4′-((1Z, 11Z)-2, 5, 8, 11-tetraazadodeca-1, 8-diene-1, 11-diyl) diphenol: kinetic and equilibrium modeling. *Journal of Water Reuse and Desalination*, *5*(3), 312-325.

X. Wang, X. Liu, C. Xiao, H. Zhao, M. Zhang, N. Zheng, W. Kong, L. Zhang, H. Yuan, L. Zhang. (2020) Triethylenetetramine-modified hollow Fe3O4/SiO2/chitosan magnetic nanocomposites for removal of Cr (VI) ions with high adsorption capacity and rapid rate, Micropor. Mesopor. Mat., 297, 110041.

Çimen, A., Bilgiç, A., & Karademir, B. (2021). Synthesis of eco-friendly Sp-EN-CPA adsorbent and its application for removal of Cr (VI) from aqueous solutions.

Kılıçel, F., & Karapınar, H. S. (2018). Determination of trace element contents of some spice samples by using FAAS.

CHAPTER 2

OXIMES

Prof. Dr. Bülent DEDE[1]

Assoc. Prof. Dr. Güvenç GÖRGÜLÜ[2]

[1] Süleyman Demirel University, Faculty of Arts and Science, **Department of Chemistry,** Isparta, Türkiye.bulentdede@sdu.edu.tr
[2] Mehmet Akif Ersoy University, Faculty of Education, **Department of Science Education,** Burdur, Türkiye guvencgorgulu@mehmetakif.edu.tr

INTRODUCTION

Coordination chemistry is undoubtedly the most developed and interested branch of inorganic chemistry in the last century. One of the most important factors in the development of coordination chemistry is oximes and their activities. The complexes that oxime compounds form with metals through the atoms in their structure are quite stable. The activities of oximes and their stable complexes with metals attract the attention of many fields of chemistry and science. In this section, it is aimed to give information about the important chemical and physical properties of oximes.

1. NOMENCLATURE AND PROPERTIES OF OXIMES

Oximes are compounds that are formed as a result of the reaction of aldehydes and ketones with hydroxylamine and contain carbon-nitrogen double bonds (C=N) in their structure as shown in Figure 1. In fact, the name oxime is an abbreviation of the words oxy-imine (Chakravorty, 1974).

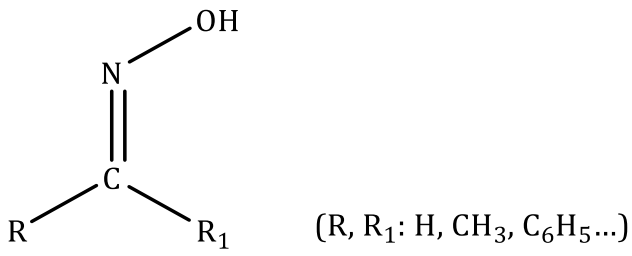

Figure 1. General Structure of Oximes

Oxime compounds are named according to the main structures from which they are obtained. If it is obtained from aldehydes, it is called aldoxime, if it is obtained from ketones, it is called ketoxime (Singh et al., 1978). For example, the oxime of acetone is known as acetoxime $(CH_3)_2CHNOH$. Oximes are separated according to the number of oxime groups they carry in their structures, by being named as monoxime and dioxime. In dioximes, if each of the two oxime groups is attached to one of the adjacent carbon atoms; These oximes are called vicinal, which means adjacent, or *vic*-dioximes for short (Chakravorty, 1974). The simple structure of monoxime and *vic*-dioximes is shown in Figure 2.

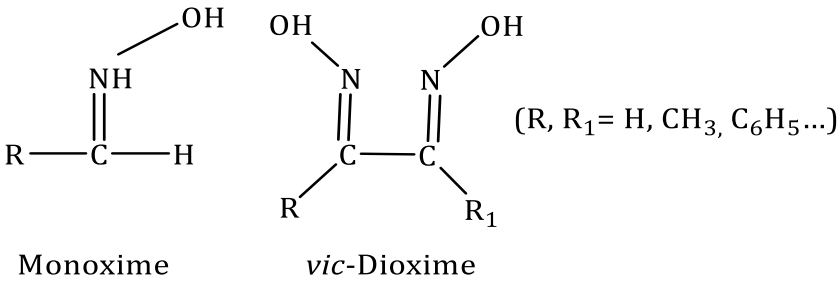

Figure 2. General Structure of Monooximes and *vic*-Dioximes

The position of the -OH group around C=N in oximes causes geometric isomerism. For this reason, oxime compounds are named by specifying the isomeric structure. Simple oximes and their derivatives have syn- and anti-geometric isomers. The syn- prefix is used when the H and OH groups around the C=N double bond are on

the same side of the double bond plane and the anti- prefix is on the opposite side (Fig. 3) (Kurtoğlu, 1999).

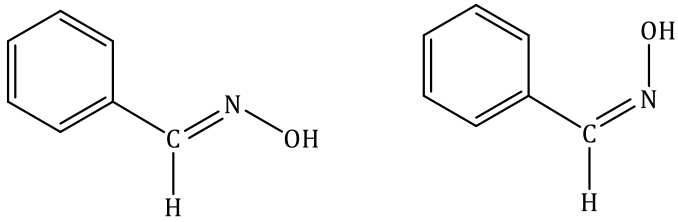

syn-benzaldoxime anti-benzaldoxime

Figure 3. Nomenclature of Aldoximes

In *vic*-dioximes, three isomeric structures emerge according to the orientation of the –OH groups to each other and these orientations are taken into account when naming. The anti-, syn- and amphi-isomers of these structures are given in Figure 4.

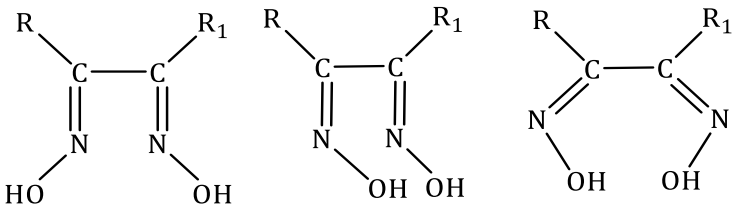

anti- amphi- syn-

(R, R_1= H, CH_3, C_6H_5...)

Figure 4. Isomer Structures of *vic*-Dioximes

2. PROPERTIES OF OXIMES

An oxime group is an amphiprotic group having a slightly basic nitrogen atom and a slightly acidic hydroxyl group. Oximes play an important role in the development of coordination chemistry (Chakravorty, 1974).

Oximes are generally colorless organic substances that melt at moderate temperatures. Their solubility in water is very low. Those with low molecular weight are volatile. While oximes with amphoteric character show acidic properties due to the proton of the OH group in their structure, they show weak basic properties due to their unpaired electrons on the N atom. They behave like both weak acids and weak bases, but more like acidic than bases. They form salts with very strong acids and bases. Due to the proton of the OH group of oximes, the dissociation constants vary between 10^{-10}-10^{-12} (Kurtoğlu and Serin, 2006).

The most important feature of oxime ligands is that they show oximato group ability with additional metal ions thanks to their N and O bridging functions. This property is frequently used in the field of molecular magnetics for the design and synthesis of polynuclear assemblies (Chaudhuri, 1999). While the acidity of aliphatic oximes generally decreases with increasing molecular weight, the presence of the carbonyl group adjacent to the oxime group increases the acidity. The degree of acidity in aromatic oximes varies depending on the substituents of the aromatic ring (Migrdichian, 1957).

Oximes are difficult to dissolve in concentrated mineral acids due to the basic character of the C=N groups in their structures. They precipitate in case of dilution with water and hydrochloride crystals are formed (Karipcin, 2001).

3. SYNTHESIS OF OXIMES

3.1. Reaction of aldehydes and ketones with hydroxylamine

This method is one of the most used methods to synthesize new oxime ligands. Oximes are obtained from the reaction of aldehydes and ketones with hydroxylamine hydrochloride in an alcoholic medium at appropriate pH and temperature conditions (Macit, 1996). The reactions of aldehydes and ketones with hydroxylamine are shown below. Aldehydes generally react more readily than ketones, and aliphatic ketones are more reactive than aromatic ketones. The basicity of the reaction medium is of great importance during oxime formation. When the variation of the reaction rate depending on the solution pH is examined, it is observed that the rate is maximum near the neutral point. The addition of a suitable base to the hydroxylamine hydrochloride creates a buffering effect.

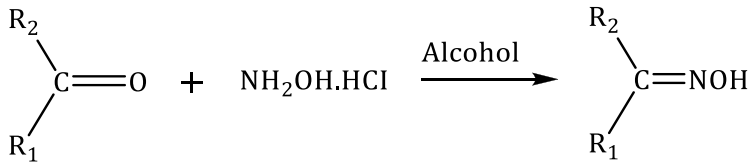

Figure 5. Reactions of Aldehydes and Ketones with Hydroxylamine Hydrochloride

3.2. Reaction of Ketimines with Hydroxylamine

Oximes are easier to obtain from ketimines than ketones. Ketimines are compounds containing -C=NH in their structure (Özcan, 1985).

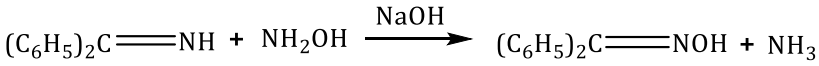

Figure 6. Synthesis of Oxime from Ketimines

3.3. Nitrosylation Method

By nitrosylation method as shown in Figure 7, it is possible to prepare α-ketoximes from ketones. Active methylene groups are needed in the reaction.

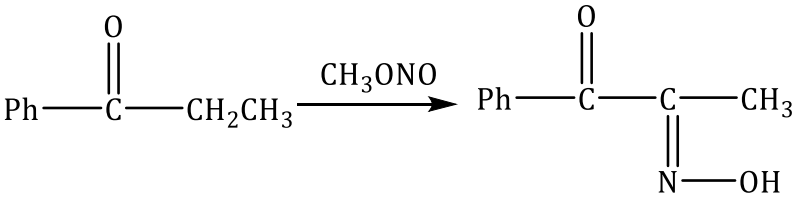

Figure 7. Synthesis of Oxime by Nitrosylation Method

3.4. Reduction of aliphatic nitro compounds

Nitro compounds containing an α-hydrogen can be reduced to oximes with zinc powder in acetic acid. Oximes can also obtained by the reduction of other reagents like alkandiamines, CS_2, Et_3N and $CaCl_2$ with Co-Cu(II) salts (Milios et al., 2006).

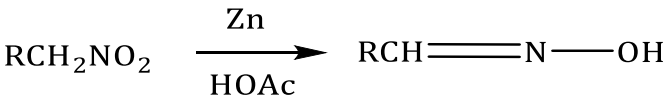

Figure 8. Reduction of Aliphatic Nitro Compounds

3.5. Oxidation of primary amines

If primary amines are oxidized with H_2O_2 or Caro's acid (H_2SO_5), as given in Figure 9, oximes are obtained. During the reaction, hydroxylamines are formed as intermediates and can be isolated if desired. However, they are mostly oxidized to nitroso compounds under reaction conditions. Nitroso compounds without α-hydrogen are stable, but if α-hydrogen is present, these compounds form the tautomer oxime (Kukushkin and Pombeiro, 1999; Constantinos et al., 2005).

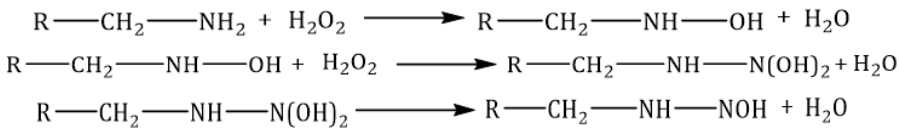

Figure 9. Oxime Production from Primary Amines

4. REACTIONS OF OXIMES

4.1. Reactions with heat and light

Although oximes are stable substances, some decomposition occurs when exposed to light and air for a long time. As a result of decomposition, the main carbonyl compound and some nitrogenous substances are formed. As an example, when benzophenoxime decomposes under the influence of heat, it yields ammonia, nitrogen, benzophenone and imine (Smith, 1966). If there are α-hydrogens in the oximine structure, degradation occurs in the form of alcohol and nitrile decomposition.

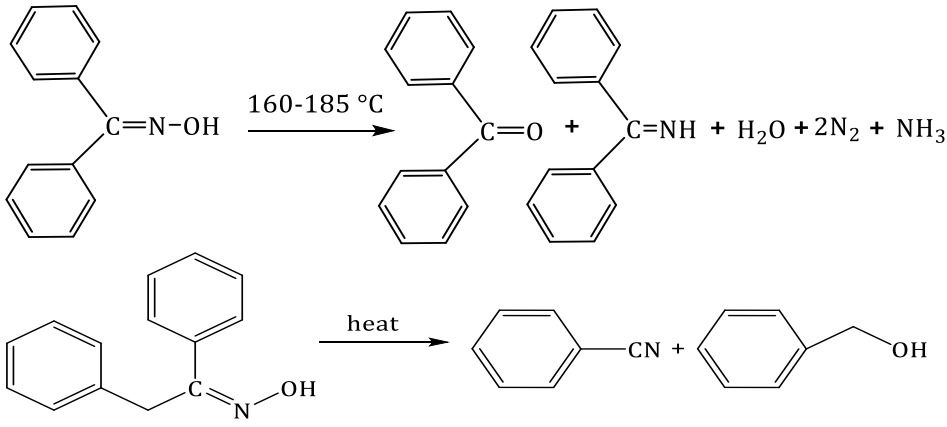

Figure 10. Decomposition Reactions of Oximes

4.2. Effect of acids

When oximes are interacted with strong mineral acids, they turn into salts. They also perform isomeric conversions. Syn- and amphi-isomers are converted to anti-isomers with HCl (Gök, 1981).

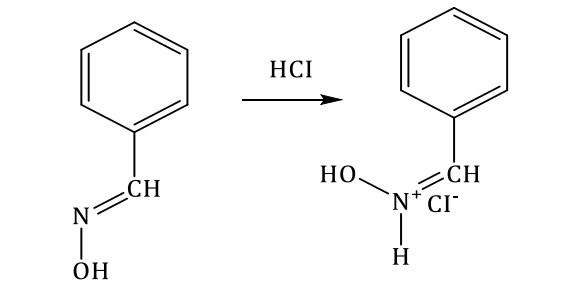

Figure 11. Exchange of Oximes with HCl

4.3. Oxidation of oximes

In aldoximes, different products are formed due to the oxidative instability of the C-H bond. When aldoximes are oxidized at -78 ^{o}C, they give nitrile oxides and *vic*-dioximes give furoxanes (Chakravorty, 1974).

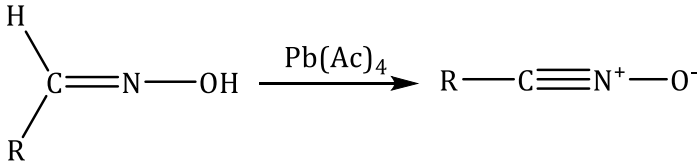

Figure 12. Formation of Nitrile Oxides from Oxidation of Oximes

4.4. Reduction reactions

The oximes are reduced with $ZnCl_2$ and dry HCl or with $LiAlH_4$ catalyzed by Ni or Pd. The reduction usually passes through the imine step to yield amines. Depending on the nature of the reducing agent, compounds containing –NH-OH, =NH or NH_2 groups are obtained (Özcan, 1985).

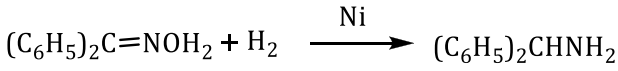

Figure 13. Reduction Reaction of Oximes

4.5. Reactions with acylation reagents

Oximes also react with acylation reagents to form acyl derivatives. All of the compounds that oximes give with acyls are in the *o*-acyl structure. Oximes with different geometric isomers give different

isomeric acyl derivatives. Although the acyl derivative of the syn-isomer converts back to the original oxime with the weak base, the acyl derivative of the anti-isomer forms nitrile (Smith, 1966). The general reaction for the acylation reaction of oximes is given in Figure 14.

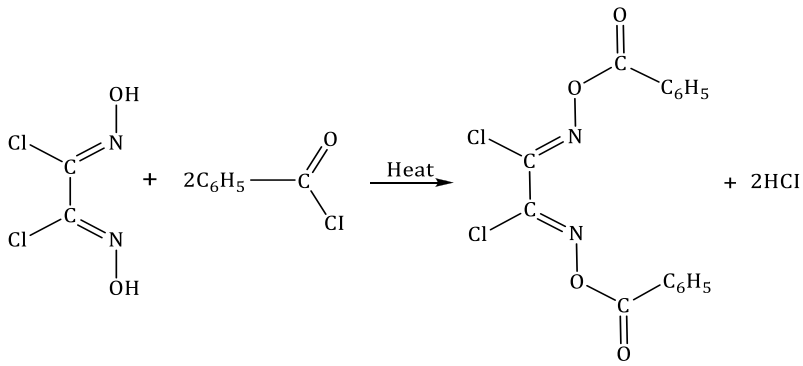

Figure 14. Reactions of Oximes with Acylation Reagents

4.6. Reactions with Grignard reagents

Oximes react with Grignard reagents as shown in Figure 15. Oximes yield aziridines with Grignard reagents and lithium aluminum hydride. As a result of the reaction of arylalkyloximes containing α-hydrogen with two moles of Grignard reagent, aziridines or α-aminoalcohol are formed instead of the expected product hydroxylamines. The formation of aziridine or α-aminoalcohol depends on the hydrolysis method. In this reaction, there is no participation in the carbon-nitrogen double bond, but the migration of nitrogen from the first carbon atom to the second carbon atom. Similar to the Grignard addition, oximes containing α-hydrogen react with lithium aluminum hydride and they form aziridines (Kurtoğlu and Serin, 2006).

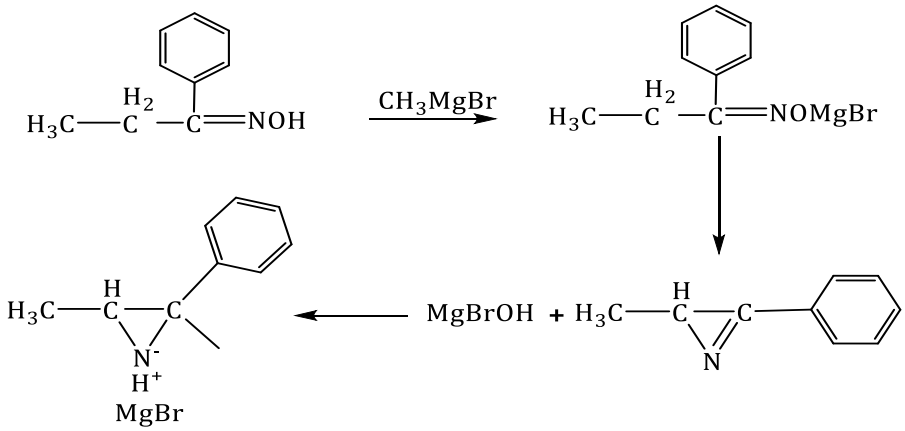

Figure 15. Reactions of Oximes with Grignard Compounds

4.7. Beckman conversion reactions

Ketoximes are converted to amides by the Beckman conversion reaction. For this, PCI_5 in ether with concentrated H_2SO_4 can be used. The alkyl or aryl group migrates onto the nitrogen atom to form N-substituted amides (Solomons and Fryhle, 2002).

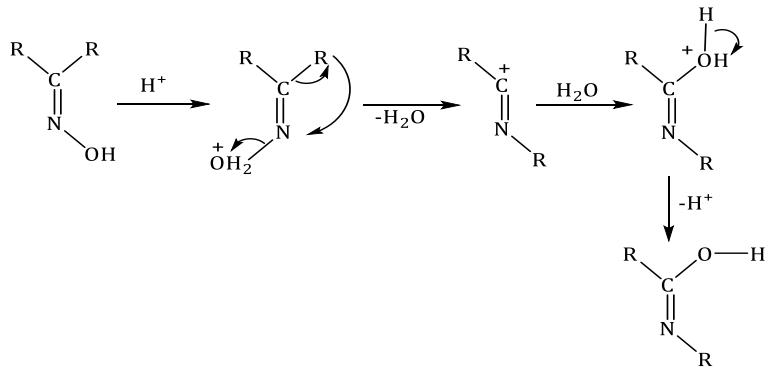

Figure 16. Beckman Conversion Reaction of Oximes

4.8. Diazonium coupling reaction

Diazonium compounds are stable in basic solution and they show some electrophilic behavior to oxime nitrogen. The diazonium coupling reaction is shown in Figure 17 (Macit, 1996).

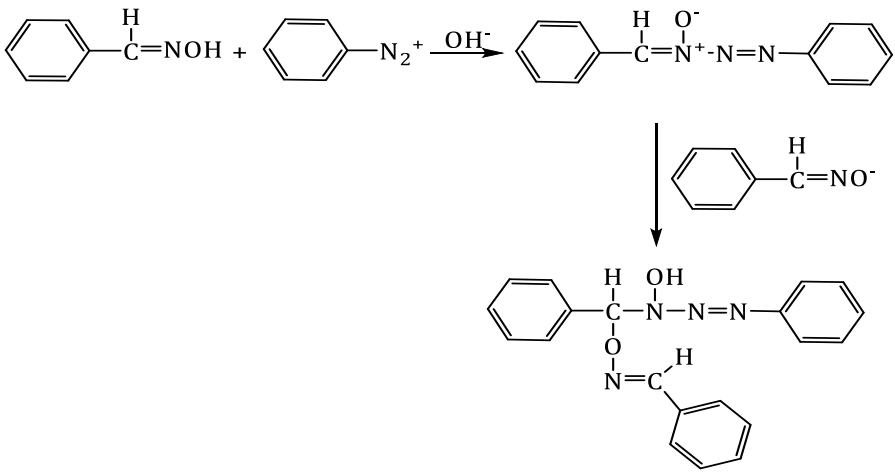

Figure 17. Diazonium Coupling Reaction

4.9. Halogenation reactions

In the reactions of oximes and halogens, halogens act directly on the oxime carbon and give hydroxamic acid chlorides at the end of the reaction which proceeds through ketoximes and halonitrozo, aldoximes and chlornitrozo compounds. If excess chlorine is used in the reaction, a deterioration will occur and manifested by yellowing. In this case, α,β-tetrachloro-α,β-dinitrozoethene type substances are formed. Hydrocyanic acid can easily join the carbon-nitrogen double bond in oximes forming α-hydroxyamino nitriles at the end of the

reaction (Kurtoğlu and Serin, 2006). The reaction of oximes with halogens is shown in Figure 18.

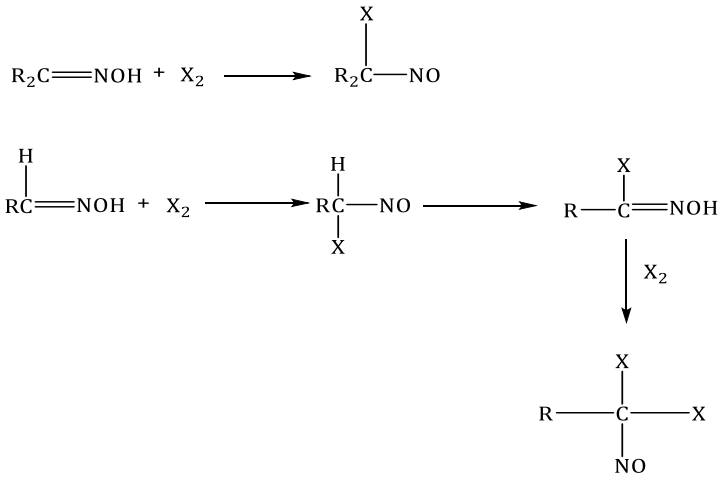

Figure 18. Reactions of Oximes with Halogens

4.10. Hydrolysis reactions

Oximes yield the appropriate aldehydes or ketones by hydrolysis from the double bond. Hydrolysis of the carbon-nitrogen double bond begins with the addition of water, as shown in Figure 19, which is followed by the elimination of the nitrogen group (Bischoff, 1980).

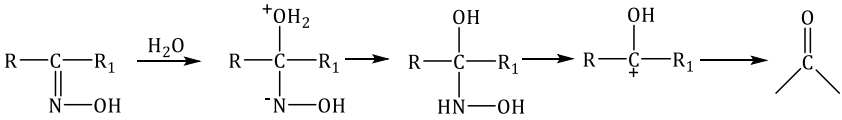

Figure 19. Hydrolysis of Oximes

In this reaction, the order of the reaction steps and rate-determining step depend on the pH of the medium or other conditions. In addition to acidic and basic catalysts, other chemicals such as thallium(III) nitrate, acetic acid/titan(III) chloride solution, sodium bisulfite solution, iron pentacarbonyl bortrifluoride, lead tetraacetate, cerium(IV) ions are also used in the hydrolysis of oximes to aldehydes and ketones (Bischoff, 1980).

5. SPECTROSCOPIC PROPERTIES OF OXIMES

With the development of spectroscopic techniques, more information has been gained about the structure of oximes, and the interconversions of isomers have been extensively studied. The structures of many oximines and their metal complexes have been determined precisely by X-ray diffraction studies. In addition, FT-IR and ^{1}H-NMR spectra are widely helpful in elucidating the structures of oximes.

When the FT-IR spectra of the oxime compounds were examined, it was observed that the bands of C=N stretching vibration were in the range of 1600-1665 cm^{-1}, the N-O vibrational bands were in the range of 940-885 cm^{-1} and the O-H vibrational bands were in the range of 3500-3200 cm^{-1}. In the case of metal bonding in complexes via oxime oxygens, there will be slight shifts in vibration frequency values. In the case of different functional groups on carbon and nitrogen, C=N stretching bands are observed in the range of 1610-1670 cm^{-1} with little shift due to conjugation (Keeney and Asare, 1984).

In monoximes, ^{1}H–NMR peaks of O-H protons are observed between approximately 9.00-13.00 ppm. In dioximes, on the other hand, ^{1}H–NMR peaks differ depending on the anti-, syn and amphi- geometric isomer states depending on the environment of the O-H protons. While a single peak over 10.00 ppm is observed for anti-isomers, two peaks close to each other are observed in amphi-isomers because one of the O-H groups forms a hydrogen bond with the other oxime nitrogen in the compound, and in syn-isomers, it interacts with the neighboring oxygen. These protons are replaced by deuterium in case of D_2O addition and the ^{1}H–NMR peaks disappear (Karatas, et al., 1991).

In the UV-Vis spectra of oximes, the most important and characteristic absorption band is the $\pi \rightarrow \pi^*$ electronic transition band of the C=N group is observed in the range of 250-300 nm. In the complexes formed by these compounds with transition metals, the bands of the $\pi \rightarrow \pi^*$ transition shift to a slightly longer wavelength. However, especially in compounds containing aromatic rings, the absorption bands of these transitions may interfere with the B bands of the aromatic ring. The low absorption intensities of d→d transitions, which provide useful clues in explaining their complex geometries with UV-Vis spectra, and the low solubility of oximes in organic solvents make it difficult to observe these transitions. In addition, since the bands of the d→d transitions can overlap with the bands of the ligands which makes it very difficult to distinguish these bands (Koçak and Bekaroğlu, 1984).

Although the υ(C=N) band is observed at 1685-1650 cm^{-1} in saturated, unconjugated oximes, the band in question may shift up to 1600 cm^{-1} in *vic*-dioximes. The fact that the υ(C=N) vibration is seen as a weak band around 1620 cm^{-1} in anti-glyoximes is due to their central symmetry structure.

The υ(N-O) band in *vic*-dioximes shows a strong absorption between 970-925 cm^{-1}. The N-O frequency does not change significantly depending on the conjugation, but changes according to the nature of the substituents attached to the oxime group. For example, it is 952 cm^{-1} in dimethylglyoximes, 978 cm^{-1} in anti-chloroglyoximes, 1000 cm^{-1} in anti-dichloroglyoximes (Avram and Mateescu, 1972).

^{1}H-NMR spectra are particularly useful in identifying stereoisomers in *vic*-dioximes. In anti-dioximes (O-H) the peak appears as a large singlet, while in amphi-dioximes (O-H·M) one of the protons shifts to the weaker field, the other emerges in its normal place, thus appearing as two singlets. In addition, in symmetrically unsubstituted vic-dioximes (O-H) protons are seen as two separate singlets (Avram and Mateescu, 1972).

6. VARIOUS OXIME LIGANDS

6.1. Monooximes

6.1.1. Carbonyl oximes

Carbonyl oximes are compounds containing oxime carbonyl on adjacent carbons as shown in Figure 20.

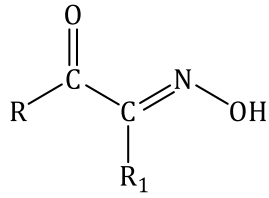

Figure 20. Carbonyl Oximes

Carbonyl oximes form complexes with transition metals Ni(II), Cu(II) and Co(II) in the form of $(HL)_2M$. The structures of these complexes are usually square plane or tetrahedral. The structure of these complexes is shown in Figure 21.

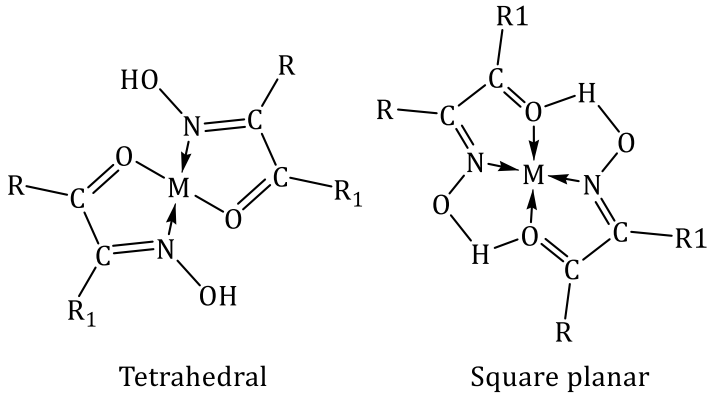

Figure 21. Tetrahedral and Square Planar Metal Complexes of Carbonyl Oximes

6.1.2. Nitrosophenols (Guinonemonoximes)

These compounds are in cyclic structure and form complexes with Cu(II) metal in tetrahedral geometry. However, in the presence of pyridine in the environment, it was determined by X-rays that the complexes were in a square pyramidal structure as shown in Figure 22 (Chakravorty, 1974).

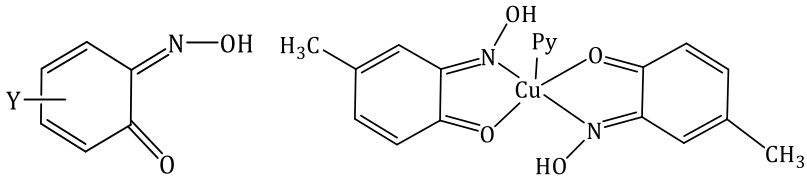

Figure 22. Nitrosophenols (Y: H, CH_3…)

The structure of the complex formed with nitrosophenols in the presence of Ni(II) metal in the environment is dimeric as in Figure 23.

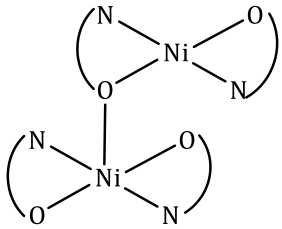

Figure 23. Nitrosophenol Ni(II) Complex

6.1.3. Imine oximes

Depending on the number of donor groups they contain, iminoximes form complexes by binding to metal ions as bi-, tri- or tetradentate

ligands (Fig. 24). Binding varies according to the Y group on the imine (Schmidt, 1984; Chakravorty, 1974).

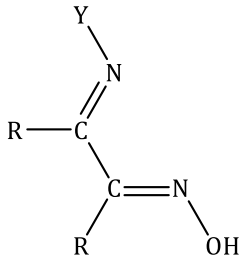

Figure 24. Iminoxime Ligand

If Y = CH_3 in the molecule, the ligand behaves as bidentate and attaches to the metal atom through N. (Fig. 25).

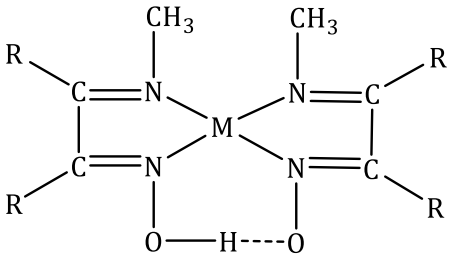

Figure 25. Iminoxime Complex

6.1.4. Pyridinoximes

In such ligands, bonding to the metal occurs through the nitrogens in the ring and oxime group (Fig. 26) (Schmidt, 1984).

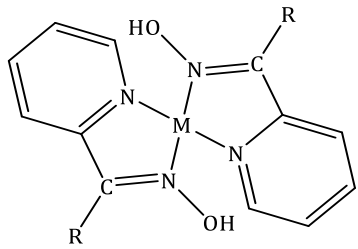

Figure 26. Pyridinoxime Complex

6.1.5. Hydroxyoximes

These oximes, which act as bidentate, bind to metals via oxygen and nitrogen atoms (Fig. 27).

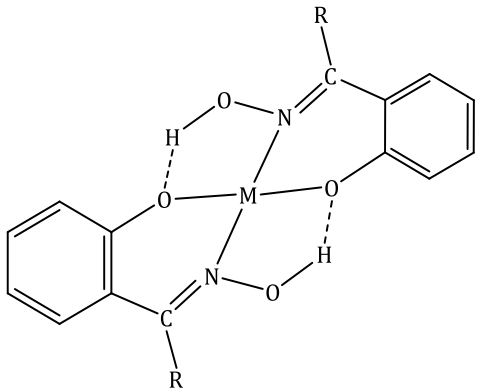

Figure 27. Hydroxyoxime Complex

6.2. Dioximes

Dioximes are compounds that contain two "-C=NOH" groups in their structure. Coordination of dioximes to metals can occur via different or same donor atoms, depending on whether the dioxime is in the anti or amphi state Ni(II) complexes synthesized from the anti-form of ligands are usually red in color and square plane. Ni(II) synthesized

from amphi-dioximes also binds to the metal via N and O atoms and forms a yellow-green complex. Studies on dioximes started with Tschugeff's synthesis of nickel dimethylglyoxime in 1905 (Fig. 28) (Gnichtel and Möller, 1981).

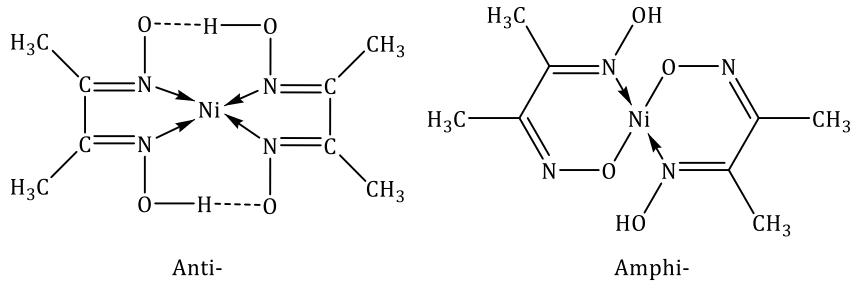

Figure 28. Nickeldimethylglyoxime Complexes

6.2.1. Cyclic Dioximes

They are compounds that contain two oxime groups directly adjacent to each other on the ring (Fig. 29).

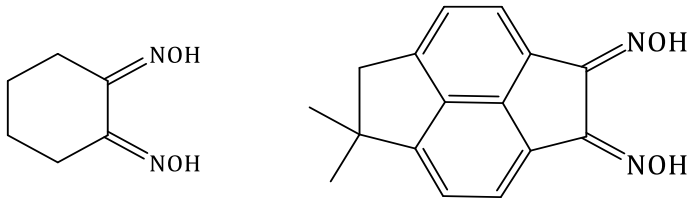

Figure 29. Cyclic Dioxime Ligands

6.2.2. Non-cyclic Dioximes

These compounds can be obtained from the interaction of monochloroglyoxime and dichloroglyoxime with compounds

containing groups such as NH_2 and SH. The oxime ligands obtained from dichloroglyoxime have a symmetrical structure. In addition, NH_2, SH groups containing compounds form symmetrical oximes by giving an additional reaction with cyanogen-di-N-oxide (Macit, 1996).

7. COMPLEXES OF OXIMES

As ligands, oximes form stable complexes with transition metals. Their stability depends on the oxime structure and cation. Oximes have two donor atoms, N and O. Oxime compounds coordinate to transition metals either over these two atoms or through one of these atoms and act as monodentate or bidentate ligands depending on the number of bonds. Mostly, this bonding takes place through the N atom. The bonding patterns made with metal in monoximes are shown in Figure 30 (Chakravorty, 1974).

Oximes form coordination with transition metals either directly or in the form of conjugated bases. In case B, one of the oximes behaves in its own structure and the other in its conjugate acid structure. The single hydrogen atom is used collectively in the O...H…O bridge. In Figure 30, A and B are the most well-known structures. C is generally observed in multi-core structures. In the D structure, the oximato anion is bonded to the metal atom through oxygen and is observed in very few complexes (Chakravorty, 1974; Kurtoğlu and Serin, 2006).

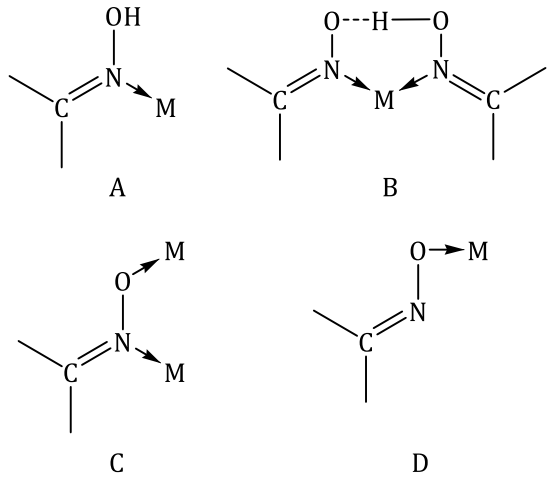

Figure 30. Coordination Modes of Oximes with Metal Atoms

The stereochemistry of the oxime is a determining factor in the structure of oxime complexes. The anti-complexes of oximes are more stable than the amphi- and syn-complexes. Especially, nickel complexes of anti-dioximes are red in color. Amphi-oxime complexes are less stable than anti and nickel complexes and yellowish green in color. Generally, amphi-oxime complexes are easily transformed into anti-oxime complexes under suitable conditions (Bekaroğlu and Sarısaban, 1978).

Today, the structure of many *vic*-dioxime metal complexes has been elucidated by single crystal X-ray analysis method. In these complexes, the metal ion and the four nitrogen atoms in the two dioxime molecules are in the same plane (Fig. 31). In the amphi- and anti- forms of *vic*-dioximes, intra-molecular hydrogen bridges are formed between oxygen atoms during the formation of complexes. Unpaired electrons on both nitrogen and oxygen are involved in this

type of complexation. The formed intermolecular hydrogen bridges increase the stability of the resulting complex and prevent their dissolution in water. Comparing the distances of the intramolecular hydrogen bridge (O…H…O) is an interesting application. The hydrogen bridge between the oxygen atoms is usually formed when the distances between the oxygens are greater than 2.44 Å. The distance of the hydrogen atom forming the bridge to the two oxygen atoms is equal to each other (Demetgül, 2008).

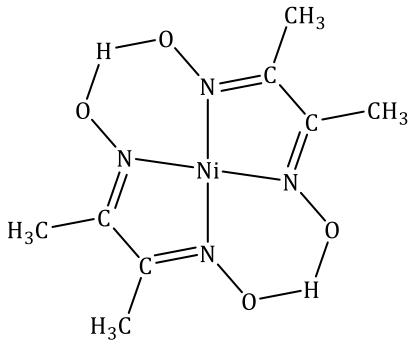

Figure 31. General Representation of *vic*-dioxime Metal Complexes

In the dimethyl glyoximine nickel complex, the distance between the two oxygens was found to be 2.44 Å by X-ray diffraction analysis. In this type of complex structure, C=N and N-O bond lengths were found to be 1.30 and 1.34 Å, respectively. When these values compared with free oxime ligands, it was observed that the N-O bond length was shortened at the end of the complex formation while the C=N bond did not change. Hydrogen bridge formation in anti-dioxime complexes causes a shift of the hydroxyl proton to approximately 16.8-18.3 ppm

in the ^{1}H-NMR spectrum (Pedersen and Larsen, 1973). Since the amphi forms of *vic*-dioximes are in coordination with transition metals over N and O atoms, the free –OH group shows a chemical shift close to that of ligands (Gül and Bekaroğlu, 1983).

In square planar *vic*-dioxime complexes, the distance between oxygens (O...H...O) connected by an intramolecular hydrogen bridge is 2.4 Å or more. When this distance is below 2.5 Å, the hydrogen atom is symmetrical between the oxygen atoms. Above 2.5 Å, H atom is located asymmetrically, the (O...H...O) bond angle is 175^{o} and the hydrogen atom is usually in an unsymmetrical bridge state (1 Å from one of the oxygens). Depending on the diameter of the metal ion forming the complex, this distance increases in the order Ni < Pd < Pt. The most important factor affecting the symmetry of the hydrogen bond formed is the state of the ligands. If the ligands forming the complex are symmetrical, the hydrogen bridge is formed in a symmetrical structure, otherwise it is mostly asymmetrical.

Numerous studies have been conducted on the complexes of α-dioximes and some metals. The isolation of dimethylglyoxime with Co(III) complex by L. Tschugaeff in 1907 was an important development in terms of being an approach model for elucidating biochemical mechanisms (Chin, 1950). The structure of the bis(dimethylglyoxymato) Ni(II) complex that dimethylglyoxime gives with the Ni(II) ion is shown in Figure 32.

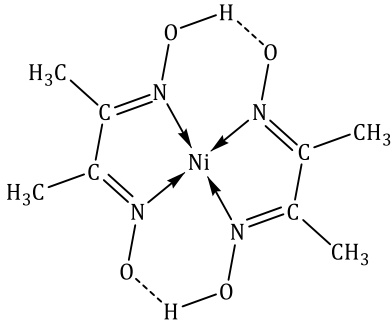

Figure 32. Bis(dimethylglyoxymato) Ni(II) Complex

Dimethylglyoxime, diaminoglyoxime and divalent cobalt ions react in various ways to give coordination compounds that differ from each other in terms of structure and magnetic properties. It is not possible to fully explain this situation with a theory. Although Co(II) gives octahedral complex with dimethylglyoxime (Fig. 33), while it gives a square plane complex with diaminoglyoxime.

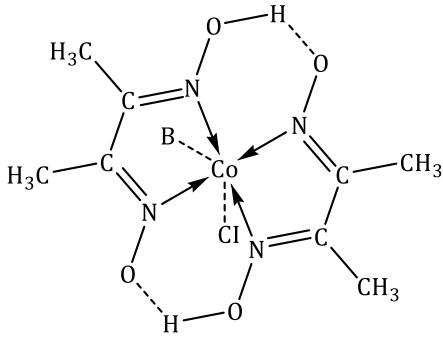

Figure 33. Co(II) Complex of Octahedral Dimethylglyoxime

The difference between these two structures is due to geometry and stability. The ability of the dimethylglyoxime cobalt complex to form cobalt-nitrogen bonds is of great importance in terms of biochemical reaction mechanisms. Because this complex shows properties to be the chemical model of vitamin B12 and its coenzymes (Yıldız, 1991).

8. USAGE AREAS OF OXIMES

Oxime is used in agriculture, pharmacy, fuel industry and many other fields. Oxime compounds are widely recognized due to their extraordinary effects in photochemical and biological reactions In addition to their properties such as chelating, oxygen retention, and biological self-degradation; they have new areas of use depending on the technological development as antioxidant and polymer initiator reagents, increasing the octane content in fuels, intermediate in dyestuffs, recovering precious metals, providing softness and waterproofing in leather and textile industry, pesticides, some antibiotic drugs (eg., cephalosporin), hormones, as additives in photography, in UV-stabilizers, flavorings and perfumes. The importance of coordination compounds in biological structures resulted with an increase in the rate and area of use in the industry each day. The recent anti-tumor effects in cancer research have led to intensification of research on complexes, "especially *vic*-dioxime complexes". Oximes are used for different purposes in many areas of organic, analytical, inorganic chemistry, industry and biochemistry. Some oximes and their various alkyl, oxy alkyl and amino derivatives have physiological and biological active properties. They are also

being used in motor oils, paints, epoxide resins as additives to improve some of their properties. Besides their use in laboratories, they are also used as rodentisit (Fessenden, 1993).

REFERENCES

Avram, M., Mateescu G.H.D., (1972). Infrared Spectroscopy (New York: Wiley–Interscience). *Applications in Organic Chemistry* pp 108-109.

Bekaroğlu Ö., Sarısaban S., Koray A.R., Ziegler, M.L, (1978). Molekul and kristall struktur von Bis(diaminoglyoximato) - kobalt(II) diaminoglyoxime. *Zeitschriftfür Naturforchung,* 32b, 387-392.

Bischoff, A.C., and Nastvogel, O., (1980). Diphenly α,γ- and α,β- diacipiperazin, *Dtsch. Chem. Ges*., 23, 2027-2037.

Chakravorty A., (1974). Structural chemistry of transition metal complexes of oximes, *Coordination Chemistry Reviews,* 13, 1-46.

Chaudhuri, P. (1999). *Proc. Indian. Acad. Sci. (Chem. Sci.)*, 111, 397-411.

Chin, C. (1950). *The Oximes of 1-(3-Methoxy-4-Agetoxyphenyl)-2,6-Dicarbethoxycyclohex-Anedione-3,5 and their Derivatives*, Doctoral Dissertation, Creighton University, Omaha, NE.

Constantinos, J. M., Stamatatos, T. C., Perlepes, S.P., (2005). The coordination chemistry of pyridyl oximes., *Polyhedron*, 25, 134-194.

Demetgül C., (2008). Synthesis and characterization of oxime compounds and metal complexes attached to solid support, Doctoral Dissertation, Çukurova University Institute of Natural and Applied Sciences, Adana.

Fessenden, R.J. and Fessenden. J.S., (1993). *Organic Chemistrty Solutions.* (Translation Ed.: Tahsin Uyar, Güneş Publishing House, Ankara.

Gnichtel, H and Möller, B., (1981). Synthese and reaktionen von 2-[α-(E)-(hydroxyimino)benzyl]3-imidazolin-3-oxiden., *Chem. Ber*., 3170-3175.

Gök, Y., (1981). Synthesis new α-dioxime, their Geometric Isomers and investigation of complex formations with some metals, Doctoral Dissertation, Karadeniz Technical University Institute of Natural and Applied Sciences, Trabzon.

Gül, A., Bekaroğlu Ö., (1983). Synthesis of N,N'-bis(4'- Benzo(15-crown-5) Diaminoglyoxime and ıts complexes with copper(II), nickel(II), cobalt(II), palladium(II) and uranyl(VI), *J. Chem. Soc., Dalton Trans*, 2537.

Karatas, İ., İrez, G., Sezgin, M., Uçan, H.İ. and Bedük, A.D., (1991). The Synthesis of some New Bis(1,2-dioximes) and Their Polymeric Metal Complexes. *Synth. React. Inorg. Met.-Org. Chem*., 21, 1031-1040.

Karipcin, F., (2001). Synthesis of bis(phenylglyoxime)methane derivatives and metal complexes, Doctoral Dissertation, Selçuk Üniversitesi, Selçuk University Institute of Natural and Applied Sciences, Konya.

Keeney, M.E, Asare, K.O., (1984). Transition Metal Hydroxyoxime Complexes. *Coordination Chemistry Reviews*, 59, 141-201.

Koçak, M,. and Bekaroğlu, Ö., (1984). Synthesis of ethane-1,2- bis(thioglyoxime) and its complexes with Nickel(II), Cobalt(III), Copper(II), Cadmium(II) and Uranyl(VI). *Synth. React. Inorg. Met.-Org. Chem.*, 14, 689-701.

Kukushkın, V.Y., Pombeıro, J.L., (1999). Oxime and oximate metal complexes: unconventional synthesis and reactivity. *Coordınatıon Chemıstry Revıews*. 181, 147-175.

Kurtoğlu, M., (1999). Synthesis and characterization of new oxime compounds containing nonionic groups and their metal complexes, Çukurova University Institute of Natural and Applied Sciences, Doctoral Dissertation, Adana

Kurtoğlu, M., Serin S., (2006). Oksimler; sentezi, reaksiyonları ve metal kompleksleri, *KSU Fen ve Mühendislik Dergisi*, 9(2), 25-32.

Macit, M., (1996). Synthesis of some new substituted glyoxime compounds and their complexes and spectrophotometric determination of nickel and copper using n-(2,6-dimethylphenyl)aminoglyoxime, Doctoral Dissertation, Ondokuzmayıs University, Samsun.

Migrdichian, V., (1957). *Organic Synthesis, Open-Chain Saturated Compounds*. Reinhold Pub., Corp. New York.

Milios, C.J., et al. Polyhedron 25 (2006) 134–194.

Ozcan, E., (1985). Synthesis of new vic-dioxime derivatives and investigation of complexes formed by the reaction with Ni(II), Cu(II), Co(II), Pd(II) Cl salts, Doctoral Dissertation, Selçuk University Institute of Natural and Applied Sciences, Konya

Pedersen, S.B., and Larsen, E., (1973). Anti-amphi and cis-trans isomerisms in some bis(dioximato) nickel(II) complexes. *Acta Chemica Scandinavica* 27, 3291-3301.

Schmidt, R., (1984). *Fhb-Berichte*, II. 1, 13.

Singh R.B., Garg B.S., Singh R.P., (1978). Oximes as spectrometric reagents: A Review, *Tetrahedron*, 25, 425-444.

Smith, P.A.S., (1966). *The Chemistry of Open-Chain Organic Nitrogen Compounds*. Benjamin, Newyork.

Solomon, T. W. G., Fryhle, C. B., & Snyder, S. A. (2014). *Organic Chemistry*. Hoboken.

Yıldız Z.S., (1991). Synthesis of new metal chelate compounds and characterization of their structures, Master Thesis, Karadeniz Technical University Institute of Natural and Applied Sciences, Trabzon.

CHAPTER 3

DYE DECOLORIZATION

Assoc. Prof. Dr. Güvenç GÖRGÜLÜ[1]

Prof. Dr. Bülent DEDE[2]

[1] Mehmet Akif Ersoy University, Faculty of Education, Department of Science Education, Burdur, Türkiye
guvencgorgulu@mehmetakif.edu.tr
[2] Süleyman Demirel University, Faculty of Arts and Science, Department of Chemistry, Isparta, Türkiye.bulentdede@sdu.edu.tr

INTRODUCTION

Light is the reason of existence of colors. Without light there would be no colors. Since our eyes are only sensitive to light, colors can be noticed only in the presence of light (Shevell, 2003). The relationship between the chemical structure of the matter and their color began to be investigated with the discovery of synthetic dyes (Seventekin, 1988).

In 1868, Graebe and Lieberman (Gräbe and Liebermann, 1868) realized that the reason why organic compounds are colored is related to their unsaturated character. In the experiments, it was observed that when hydrogen is added to colored organic compounds, the color disappears, and when hydrogen is removed from the same compounds, the color reappears. The thesis, which was put forward as a result of this experiment: "The color comes from the unsaturation in the molecule" is still among the basic conditions of color, along with other reasons.

Another color study that followed the work of Graebe and Lieberman is the theory of "chromophore groups" put forward by Witt in 1896 (Witt and Dedichen, 1896). According to Witt, the color of a compound is due to the presence of unsaturated groups such as nitroso or nitro, carbonyl and azo groups in the molecule and groups such as weakly acidic or weakly basic hydroxyl and amino in the molecule and their mutual interaction. This researcher stated that all hydrocarbons are colorless, but appear colored when unsaturated groups called chromophores are attached to them. Hydrocarbons with

a chromophore group are called chromogens. However, chromogens show dye properties. Witt suggested that in order for chromogens to acquire dye properties, the second series of molecules, which he called auxochrome, must be attached to the compound. In many cases, auxochrome groups not only complement the chromophore in color formation, but also cause the molecule to dissolve in water and have a certain affinity for the fiber (Gürses, 2019). With the binding of auxochrome groups to the chromogen, both color intensity and color depth increase (Baser and Inanıcı, 1990; Kurbanova *et al*., 1998).

DYES

The substances used to protect the surface of objects from external influences or to make them colorful in order to provide a beautiful appearance are called dyes. In spoken language, the words dye and dyestuff are often used interchangeably. However, these two words are not synonyms. Dyes do not make any changes to the areas they are applied to. They can be removed from the surface in large pieces by scraping. The substances applied to make the objects (fabric, fiber, etc.) colored themselves are called dyestuffs (Seventekin, 1988). In this review, we chose to use “dye” instead of both words as most of the recent publications do.

In addition to the definition of dye, another term essential colorants are yet to be defined. Essential colorants are generally commercial products which supply colouring by the addition of some other substances. These additives improve the product’s application properties like its dispersibility, flow or flocculation resistance.

Agreed definition of the essential colorant is a dye or pigment responsible for the colour of the product by itself.

A classification of dyes agreed upon was achieved nearly a hundred years ago by the Society of Dyers and Colourists. A 'Colour Index' book was produced to fulfill the need which provided certain information regarding the constitution and properties of the whole range of colours used in dyeing, printing and paint industries. Table 1 shows a list of colours with Colour Index Constitution Numbers (CICN). The colour index numbers are 5-digit numbers grouped into numerical ranges according to the chemical structure. The main categories used to classify colorants in Volume 4 (1971) are as follows:

Table 1. Colours with Colour Index Constitution Numbers (CICN)*

Structure	Range	Category
Nitroso	10000–10299	
Nitro	10300–10999	
Monoazo	11000–19999	Category:Azo dyes
Diazo	20000–39999	Category:Azo dyes
Triazo	30000–34999	Category:Azo dyes
Polyazo	35000–36999	Category:Azo dyes
Azoic	37000–39999	Category:Azo dyes
Stilbene	40000–40799	
Carotenoid	40800–40999	
Diarylmethane	41000–41999	Category:Diarylmethane dyes
Triarylmethane	42000–44999	Category:Triarylmethane dyes
Xanthene	45000–45999	
Acridine	46000–46999	Category:Acridine dyes
Quinoline	47000–47999	Category:Quinoline dyes
Methine	48000–48999	
Thiazole	49000–49399	Category:Thiazole dyes
Indamine	49400–49699	
Indophenol	49700–49999	Category:Indophenol dyes
Azine	50000–50999	Category:Azin dyes
Oxazine	51000–51999	Category:Oxazine dyes
Thiazine	52000–52999	Category:Thiazine dyes
Sulfur	53000–54999	
Lactone	55000–55999	
Aminoketone	56000–56999	
Anthraquinone	58000–72999	Category:Anthraquinone dyes
Indigoid	73000–73999	
Phthalocyanine	74000–74999	Category:Phthalocyanines
Natural dyes	75000–75999	Category:Natural dyes
Oxidation bases	76000–76999	
Inorganic pigments	77000–77999	Category:Inorganic pigments

***(The Colour Index™)

Classification of dyes

Hence, there is a broad spectrum of dye users and manufacturers, an unambiguous classification for all type of dye related people is an important matter. The classification of dyes may be designed considering the target group like the textile industry, manufacturers, students and researchers. Dyes are mainly classified according to their water-solubilities, chemical structures, dyeing properties and places of use (Clark, 2011; Gordon & Gregory, 2012). Here we have chosen a type of classification for students and researchers. The types of dyes are briefly explained in line with the aim of this review which is primarily focused on the dye decolorization.

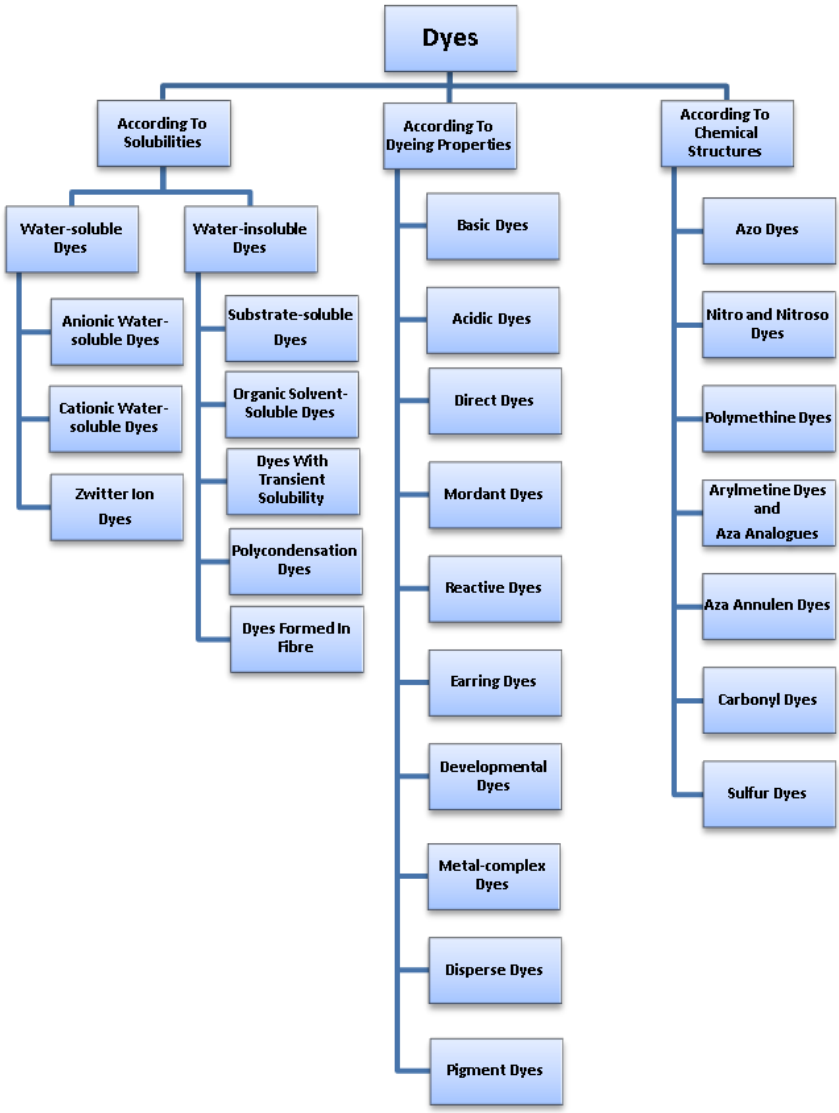

Figure 1. Classification of Dyes

1. ACCORDING TO SOLUBILITIES IN WATER

1.1. Water-Soluble Dyes

The dye molecule carries at least one salt-forming group. If the starting materials used do not contain a water-soluble group, solubility can be achieved by adding a salt-forming group to the dye molecule afterwards. Dyes in water-soluble class are examined in 3 stages (Baser and Inanıcı, 1990) as *anionic*, *cationic* and *zwitter ion water-soluble dyes*. Na^+ salts of acidic ($-SO_3^-$, $-COO^-$), basic (like; $-NH_2$), or both groups are added to the medium, respectively forming an internal salt. During dyeing, zwitter ion dyes behave like anionic dyes in basic or neutral environments (Chavan, 2011).

1.2. Water-Insoluble Dyes

It is possible to divide the dyes that are used in textile and other fields and that do not dissolve in water into various groups according to their solubility mediums. Dyes insoluble in water but soluble in all kinds of organic solvents are called *solvent dyes* which are applicable as sprays or lacquer. Also another group of dyes named *substrate soluble dyes* are dispersion dyes and can be applied especially on synthetic fibres. *Dyes with transient water-solubility* are obtained by various reduction agents to make them absorbed by the fibers. By a consequent oxidation, absorbed dye becomes water-insoluble.

Earrings and sulfur dyes are applied according to this principle. Some water-insoluble dyes are condensing with each other or with other molecules forming large molecules while being applied to the fiber or

after being applied. This group is called *polycondensation dyes*. Water-insoluble pigments are also classified in this group. Pigments with their structural difference have no affinity to the substances that affect fiber and other enzymes. Pigments are frequently applied in suspensions of drying oils and resins (Hunger, 2003).

2. ACCORDING TO DYEING PROPERTIES

Generally, dyeing practitioners do not consider the chemical structure of the dye which is an important factor in determining the method of dyeing the fiber. According to dyeing properties, dyes may be classified in ten groups as shown in Figure 1 (Baser and Inanıcı, 1990).

Basic dyes are in the form of hydrochlorides of organic bases and carry the cationic group in the colored part. They contain N or S atoms as positive charge carriers. Due to their structure, they are bonded with fibers containing anionic groups because they act as basic. They are mainly used for dyeing polyacrylonitrile, partially wool and cotton fibers.

The second group is called *acidic dyes,* due to making the applications in acidic baths and almost all of them are salts of organic acids.

Direct dyes form the largest group of dyes. They generally contain sodium salts of sulfonic and sometimes carboxylic acids. Direct dyes, do not require electrolytes as reactive dyes do. Their exhaustion rate is higher compared to other dyes. Most of the dyes in this class are

polyazo compounds, along with some stilbenes, phthalocyanines, and oxazines (Hunger, 2003).

Mordant dyes are characterized by carrying of a hydroxyl group ortho to the azo-group. They also require a mordant metal like chromium to form an insoluble compound for the fixation of the color on fabric properly. Many natural and synthetic dyes fall into this class. They contain acidic or basic functional groups (Cardon, 2007).

Reactive dyes containing reactive groups that can form true covalent bonds with functional groups in the fiber structure. After the treatment applied they eventually will have a reactive group which enables them to react with the OH- group of cellulose. A sulphonic group is added to the reactive dye to make solubility possible. Depending on the application method reactive dyes may be classified as alkali-controllable, salt-controllable and temperature-controllable dyes. (Basar and Inanici, 1990; Gürses *et al*., 2016).

Earring dyes that contain carbonyl groups and are insoluble in water. They are made water-soluble by reduction and in this state they are drawn to the fiber. As a reducing agent, sodium dithionite, ($Na_2S_2O_4$), air oxygen is used for oxidation. As a result of the reduction, the keto group in the dyestuff molecule turns into an enol group.

All dyes that can be formed on the fiber and converted into their final form are included in *developmental dyes*. Naphtol-AS dyes and phthalocyanine dyes, called azo dyes, are in this class. In this type of dyes, the component with fiber affinity is the first absorbed by the fiber, then it is reacted with the second component and converted into

a water-insoluble form. Almost all color variations are obtained with this process.

Metal complex dyes may be divided into two classes: 1:1 metal complexes and 1:2 metal complexes. The dye molecule will typically be a monoazo structure with functional groups as hydroxyl, carboxyl or amino groups which form strong coordination complexes with transition metal ions. Cr, Co, Ni and Cu are frequently used metal ions. Application of metal-complex dyes to protein fibers gave good results. However, the negative effects of metal-complex dyes to the environment is intensively concerned (Dede *et al*., 2016)

Dispersion dyes can dissolve in water in trace amounts and therefore can be applied as dispersions in water. Disperse dyes are characterized by the absence of solubilizing groups and low molecular weight (Figure 2). More than 50% disperse dyes are simple azo compounds, about 25% are anthraquinones and the rest are methine, nitro or naphthoquinone dyes. Disperse dyes, which are mainly used for polyester, are also used for cellulose acetate and triacetate, polyamide and acrylic fibers. Disperse dyes are supplied as powder and liquid form. (Clark, 2011)

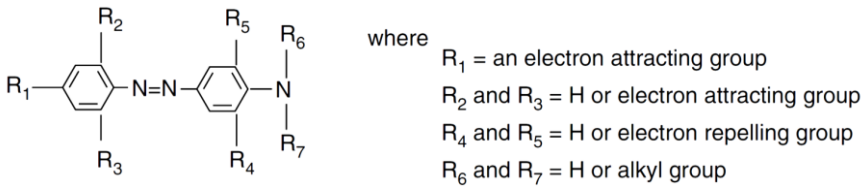

Figure 2. Generalized Structure of a Dispersion Dye

Textile fibers can also be combined with inorganic and mostly preferred organic pigments (Figure 3).

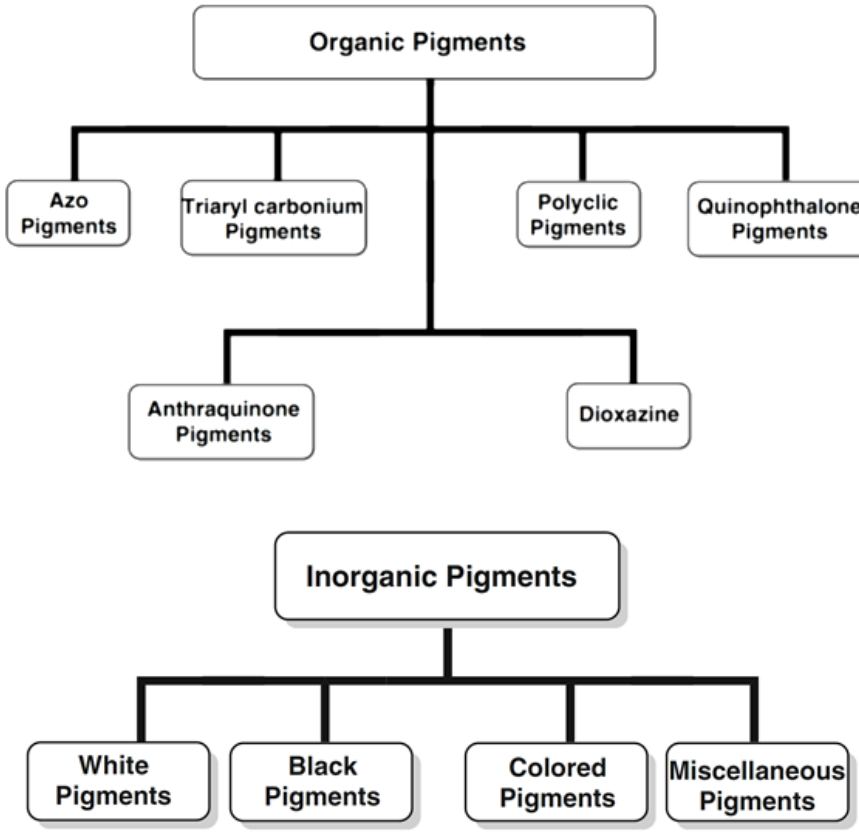

Figure 3. The Types of Organic and Inorganic Pigments

(Gürses *et al*., 2016)

Pigment dyes do not have affinity to the fiber themselves unless they adducted on a synthetic resin called binder molecule as shown in Figure 4. They are used as finely dispersed water-in-oil emulsions. Emulsion deteriorates after being impregnated with fiber or fabric. Disintegration and hardening of the binder to the fabric are its undesirable properties. There has been progress on these undesirable issues recently.

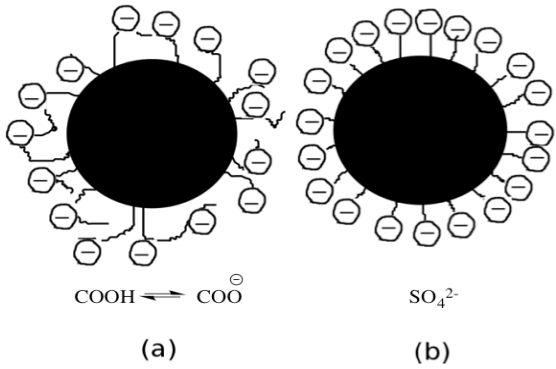

Figure 4. Binder Spheres Coated with Acrylic Acid (a) and Anionic Surfactant (b)

3. ACCORDING TO THEIR CHEMICAL STRUCTURES

Dyes are basically the organic chemical structures with three important groups as (a) chromophore, (b) auxochrome, and (c) matrix in the molecular structure (Figure 5). A chemical classification based on the synthesis and practical applications of dyes is given below (Maheshwari *et al*., 2021).

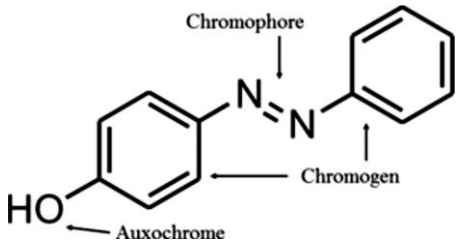

Figure 5. Auxochrome, Chromophore and Chromogen Parts of 4-Hydroxyazobenzene

Azo dyes are characterized by the existence of a chromophore azo (-N=N-) group in their structure. Nitrogen atoms in this group are bonded to carbon atoms by sp^2 hybridization forming σ bonds. One of the carbon atoms attached to the azo group may be an aromatic or heterocyclic ring and the other may be an aliphatic chain-linked group. Since the color intensities of aliphatic azo compounds are low, azo dyes are generally formed with aromatic azo compounds. Azo dyes are represented by the formulas Ar1-N=N-Ar2 (aromatic azo compounds), R1-N=N-R2 (aliphatic azo compounds), R-N=N-Ar (aliphatic-aromatic azo compounds).

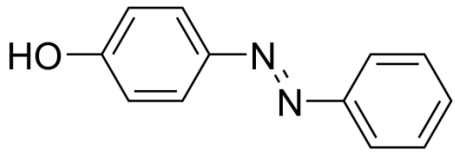

Figure 6. Chemical Structure of an Orange Colored Azo Dye

Nitro and nitroso dyes contain electron donor groups in *-ortho* position with nitro and nitroso groups in their chemical structures.

Nitroso compounds are mostly used in the synthesis of other dyes. They do not have any dye properties unless they formed complexes with heavy metal salts. While o*rtho*-nitroso compounds have complex forming characteristics, technically important nitro dyes have an electrodonor group in -*o* position (Figure 7). Picric acid is the oldest known synthetic nitro dye (Püntener, 2000).

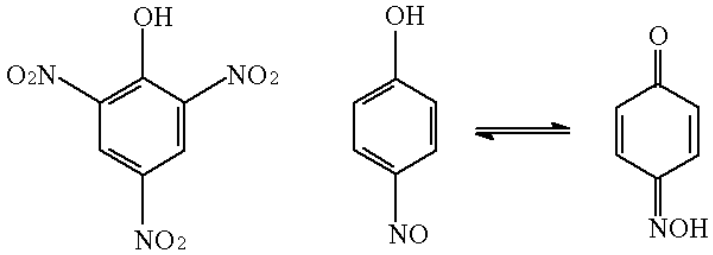

Figure 7. Nitro Dye Picric Acid (left) and *p*-Nitrosophenol and *p*-Benzoquinone Monooxime (right)

Polymethine dyes form a large group of colored compounds. They are compounds with polymethine $(\text{-CH=})_n$ and heteroatoms in their structure as shown in Figure 8. Polymethine dyes are the cation dyes currently used for dyeing polyacrylonitrile fibers.

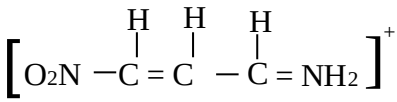

Figure 8. Polymethine Dye

Arylmethane and poly(aza) dyes have the general formula of (Ar-X=Ar) in which X; can be -CH= (diarylcarbonium) or –N=. Compounds in which X is in the form of -CH= are called

diarylcarbonium, and compounds in the form of -C(Ar)= are called triarylcarbonium. If this group is –N=, it is the aza derivative which is the basic part of the analog absorption system.

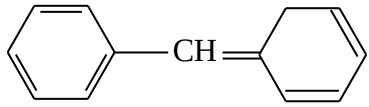

Figure 9. Arylmethane Dyes

Aza annulene dye class has a cyclic colorant structure with 18 π electrons and double bonds in the conjugated state. Whether a closed system has an aromatic structure is determined by the number of (4n+2)π electrons according to Huckel's rule. If n=1,2,3,… is an integer number, 6, 10, 14, 18, 22, systems can be aromatic. However, for aromaticity to occur, this number of electrons must be in a plane and be delocalized. A monocyclic ring consisting of successive C=C and C-C bonds may also be referred to as [n]annulen (Chaudhary & Violet, 2020).

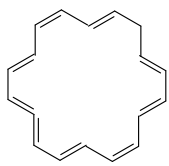

Figure 10. Aza [18] Annulene Dye

Carbonyl dyes are characterized with a **c**onjugated double bonds and at least two carbonyl groups again conjugated state to these in their molecular structure (Figure 11). It is divided into two subclasses as indigo and anthraquinone structure.

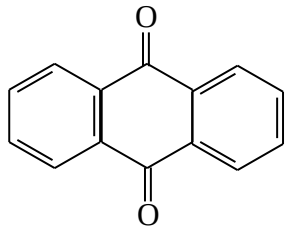

Figure 11. Carbonyl Dye

Sulfur dyes are called water-insoluble, macromolecular, colored organic compounds formed by the reaction of aromatic amines, phenols, sulfur and sodium sulfide or sodium polysulfide (Figure 12). It can be symbolized as Bm-S-S-Bm (Chaudhary & Violet, 2020).

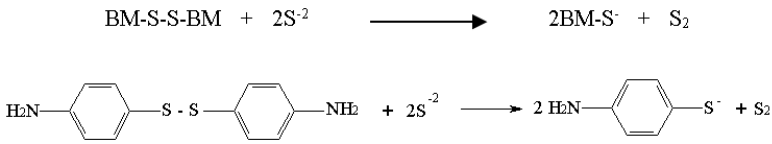

Figure 12. Sulfur Dye

Dye Removal Methods

Dyes are widely used in many fields as textile, leather, cosmetics and food industry. These dyes or pigments are added to the wastewater stream and cause harmful effects for the environment. Colored wastewater discharged to the receiving waters reduces the light

transmittance in the aquatic environment causing an adverse effect on the rate of photosynthetic activity which leads to the depletion of oxygen and eventually threaten the life in the aquatic ecosystem. Also, discharged dyes cause the rise of some aquatic organisms which brings the accumulation risk of toxic and carcinogenic products. In this context, the color removal processes of industrial wastewater containing dyes become crucial (Moussavi and Mahmoudi, 2009). Removal of dyes from wastewater can be divided into three main categories as physical, chemical and biological methods.

1. PHYSICAL TREATMENT METHODS

A. Adsorption

Adsorption is an effective method to remove waste color, toxic substances and organic solvents. Activated carbon is the most widely used and effective adsorbent for dyes. The molecular structure of a compound has a determining effect on adsorption. Adsorption improves with increasing molecule size and factors such as aromaticity, polarity and C-chain branching. High molecular weight dyes have difficulty passing through the pores of an activated carbon, while low molecular weight dyes are dispersed within the micropores (Jayswal, 2007).

While decolorization with activated carbon is particularly effective for cationic, mordant and acid dyes, there is less decolorization for disperse, direct, vat, pigment and reactive dyes. The performance of the method depends on the type of carbon used and the characteristics

of the wastewater. While regeneration and reuse cause a decrease in performance, this disadvantage can be eliminated by using an excessive amount of activated carbon which is an expensive material (Kocaer and Alkan, 2002).

B. Membrane filtration

It is possible to continuously purify, concentrate and most importantly separate the dye from the wastewater with membrane filtration. The most important advantage of the membrane filtration to other methods is that the system is resistant to temperature, an unexpected chemical environment and microbial activity. Reverse osmosis membranes yield over 90% for most ionic species and provide a high quality permeate. Dyes and auxiliary chemicals in dye bath effluent are removed in a single step (Kocaer and Alkan, 2002).

C. Ion Exchange

The ion exchange method is a widely used and preferred method in the industry for removing anions and cations from the solution and softening the water. Organic substances that dissolve in water and contain ion-forming groups are removed by this method (Jayswal, 2007).

The advantages of ion exchange are its high water treatment capacity and high efficiency in removing metal ion contaminants. Factors such as pH, temperature, metal concentration, ionic charge and contact time allow us to understand and manage heavy metal ions (Göde and Pehlivan, 2006).

2. CHEMICAL TREATMENT METHODS

A. Coagulation and flocculation

Coagulation is the name given to the disorder of colloidal particles in an aqueous solution and flocculation is a term used to separate solid particles from aqueous solution by aggregation of colloidal particles of an organic polymer.

Both inorganic and organic polymers are used in the removal of dyes from wastewater. Coagulation and flocculation are often used as a pretreatment step before using other techniques (Jiang, 1997). Inorganic coagulants, lime (CaO), alum ($AI_2(SO_4)_3$), iron and ferrous sulfate $Fe_2(SO_4)_3$ and $FeSO_4$ are widely used in the treatment of wastewater containing dyes separately or in combination (Germirli *et al*., 1990).

Organic polymers are used as flocculating agents for color removal treatment. Generally, it offers more advantages than inorganic coagulants hence, the volume of sludge it produces is less and it significantly increases color removal. However, the color removal efficiency using flocculation alone was found to be unsatisfactory (Hazel, 1995).

B. Electrochemical method

Electrochemical methods have been successfully tested for various industrial wastewaters. Electrochemical removal of dye containing wastewaters is a relatively new technique and was developed in the early seventies. Organic and toxic pollutants such as dyes and phenols

in wastewater are removed by anodic processes that enable the formation of strong oxidants such as $OH^{\bullet}$ radical and ozone. This method has been applied to many other related sectors in wastewater originating from the paint manufacturing industry. Generally, during electrochemical treatment, contaminants can be removed either by direct or indirect oxidation process. When compared to other aqueous processes, the electrochemical mechanism seems quite complex (Brillas & Martínez-Huitle, 2015).

C. Chemical oxidation method

Among all chemical methods, oxidation is one of the most powerful method for the removal of various refractory compounds from stabilized leachate (Parsons and William, 2004).

The efficiency of chemical oxidation is attributed to the power of highly concentrated radicals such as free hydroxy radical ($OH^{\bullet}$) as an oxidant. These radicals can be produced exposing the potential oxidant to UV light. Some of these oxidant couples are UV/O_3, UV/H_2O_2, O_3/H_2O, UV/TiO_2, Fe_2^{+}/H_2O_2 (Fenton oxidation) (Gogate and Pandit, 2004). The kinetics of the advanced oxidation process depends on the concentration of radicals and pollutants (Murray and Parsons, 2004).

D. Chlorination

Chlorine is added to the solution to oxidize the molecules. Chlorination has been found to be an effective method for COD reduction and decolorization of wastewater containing azo dyes. The

most important factor regarding chlorination is the potential to form toxic organic compounds as a result of chemical reaction. Chlorination is a process that uses chlorine (Cl), hypochlorite (HOCl) and chlorine dioxide (ClO_2) as strong oxidizing reagents. Although the chlorination is an efficient and lower cost method compared to other methods, its application is not common due to the concerns about the safety of the method (Bafana *et al*., 2011). Excess chlorine forms adsorbed organohalides. Trihalomethane is one of the end products occurs during chlorination process which is listed among the carcinogen organic chemicals. Therefore, chlorination is not considered a safe method for waste color removal. On the other hand, chlorine dioxide (ClO_2) is less reactive and causes fewer side reactions. However, it cannot show effective color removal in colored wastewater (Waterick, 1988).

E. Ozonation

Ozonation is not only used commonly to decolorize but also to disinfect wastewaters. The interest in ozone oxidation among the color removal methods from wastewater is still in tendency to increase probably due to its effective color removal, as well as the treatment of COD (chemical oxygen demand), not forming AOX (adsorbable organic halogen), not causing treatment sludge or concentrated waste problems. One of the biggest problems with ozone formation is that its formation has high energy costs. In addition, ozone decomposition produces free radicals and oxygen (Chhaya *et al*., 2020).

This formed free radical and oxygen atom react with the dye and break up the chromophore group in its structure and remove it. When dissolved in water, the oxidizer reacts with a large number of non-biodegradable compounds. In this case, the nature of the compounds in the wastewater will determine the degree of reaction with ozone and the efficiency of ozonation. As a result of the tendency of compounds with special functional groups such as aromatic ring and C=C double bond to react with ozone, carbonyl compounds are formed (Westerhoff *et al*., 1999).

Ozone oxidation follows two main pathways: After the ozone molecule decomposes, either the ozone molecule makes a direct electrophilic attack on the pollutants or it produces OH radicals and this allows the radicals it produces to react with pollutants (Steensen, 1997).

F. Fenton reaction

Briefly, this method is the production of OH radical with a mixture of hydrogen peroxide and Fe^{2+} salt (Spetch *et al*., 1996). Today, this method is used effectively in reducing toxicity, destruction of organic pollutants, increasing biodegradability, BOD/COD, odor and color removal (Bishop, 1968).

The advantages of the Fenton method are that the mechanical part is simple, it allows working in a wide temperature range, it consists of a combination of oxidation and coagulation processes, and it increases the oxygen concentration in the water. Since it is ecologically safe, it is anticipated that this method will be used effectively in the treatment

of all colored wastewater in the future. In addition, it is widely used as a pretreatment reagent in H_2O_2 dyeing processes which makes the Fenton method more economical (Bautista *et al.*, 2008).

H_2O_2 and Fe^{2+} ions are generally more stable in a strongly acidic environment. If H_2O_2 and Fe^{2+} ions are added to a water system containing organic matter, they will form complex redox reactions in a strongly acidic environment (Eq. 1.1-1.4) (Kang and Hwang, 2000; Külünk, 2000; Matavos-Aramyan & Moussavi, 2017).

$$H_2O_2 + Fe^{2+} \longrightarrow Fe^{3+} + HO^- + HO^\bullet \quad (1.1)$$

$$HO^\bullet + RH \longrightarrow H_2O + R^\bullet \quad (1.2)$$

$$R^\bullet + Fe^{3+} \longrightarrow R^+ + Fe^{2+} \quad (1.3)$$

$$R^+ + H_2O \longrightarrow ROH + H^+ \quad (1.4)$$

The $OH^\bullet$ radicals formed react with organic substances such as RH (example: unsaturated dye molecules). Thus, the chromophore and chromogens of the dye molecule are damaged and their colors are removed.

Fenton oxidation is still being used to remove the wastewater by textile, olive-oil, paper and wine industries. It is also effective to remove the toxic/organic wastes from landfill leachate, sludge waste,

contaminated soil and refinery effluents (Matavos-Aramyan & Moussavi, 2017).

3. BIOLOGICAL TREATMENT METHODS

A. Aerobic method

Aerobic system is the process of using free oxygen dissolved in wastewater to reduce organic waste components in the presence of microorganisms. The traditional aerobic biological process is also not very successful in the treatment of dyes. Because paints are designed to be durable (Stern *et al*., 2003).

The basic mechanism of decolorization in aerobic processes is through adsorption by biomass. These reactions are continuous reactions. However, the rate of reaction is limited by parameters such as dissolved oxygen (DO), concentration, mixing, nutrients, and concentration of micro-bacteria.

B. Anaerobic method

The anaerobic method occurs in the absence of free oxygen and converts the components in organic wastewater into methane and carbon dioxide. Anaerobic biological treatment technologies have proven to be effective tools to treat various industrial wastewaters.

It has been proven that a large number of biooxidation-resistant dyes can initiate removal studies in an anaerobic environment through the degradation of a chromophore (Field *et al*., 1995; Rai *et al*., 2005). The suitability of anaerobic technology in color removal has been an area where intensive studies are carried out today. Figure 13 shows the

advantages of applying the biological techniques compared to conventional physical and chemical ones.

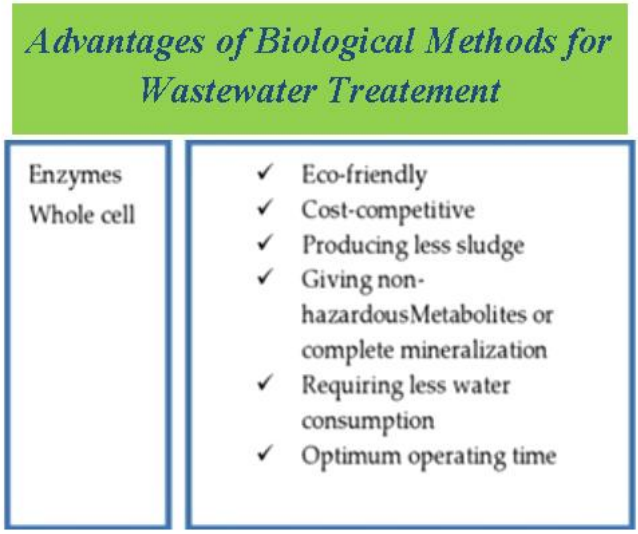

Figure 13. Advantages of Biological Techniques in Wastewater Treatment. (modified from Sghaier *et al*., 2019).

REFERENCES

Bafana, A., Devi, S. S., & Chakrabarti, T. (2011). Azo dyes: past, present and the future. *Environmental Reviews*, *19*(NA), 350-371.

Baser, I., & Inanici, Y. (1990). *Dyestuff Chemistry*. Marmara University Pub., Istanbul.

Bautista, P., Mohedano, A. F., Casas, J. A., Zazo, J. A., & Rodriguez, J. J. (2008). An overview of the application of Fenton oxidation to industrial wastewaters treatment. *Journal of Chemical Technology & Biotechnology: International Research in Process, Environmental & Clean Technology*, *83*(10), 1323-1338.

Bishop, D. F., Stern, G., Fleischman, M., & Marshall, L. S. (1968). Hydrogen peroxide catalytic oxidation of refractory organics in municipal waste waters. *Industrial & Engineering Chemistry Process Design and Development*, *7*(1), 110-117.

Brillas, E., & Martínez-Huitle, C. A. (2015). Decontamination of wastewaters containing synthetic organic dyes by electrochemical methods. An updated review. *Applied Catalysis B: Environmental*, *166*, 603-643.

Bruna de Campos Ventura-Camargo, B., & Marin-Morales, M. A. (2013). Azo dyes: characterization and toxicity-A review. *Textiles and Light Industrial Science and Technology*, 2(2), 85-103.

Cardon, D. (2007). *Natural dyes. Sources, Tradition, Technology and Science*, 268.

Chaudhary, B. & Violet, T. (2020). Chemistry of synthetic dyes: A review. *J. Interdiscipl. Cycle Res*, 12(390), 390-396.

Chavan, R. B. (2011). Environmentally friendly dyes. *Handbook of Textile and Industrial Dyeing*, 515-561.

Chhaya V. Rekhate & J.K. Shrivastava (2020) Decolorization of Azo Dye Solution by Ozone Based Advanced Oxidation Processes: Optimization Using Response Surface Methodology and Neural Network, *Ozone: Science & Engineering*, 42:6, 492-506

Clark, M. (Ed.). (2011). *Handbook of Textile and Industrial Dyeing: Principles, Processes and Types of Dyes*. Elsevier.

Field, J. A., Stams, A. J., Kato, M., & Schraa, G. (1995). Enhanced biodegradation of aromatic pollutants in cocultures of anaerobic and aerobic bacterial consortia. *Antonie Van Leeuwenhoek*, *67*(1), 47-77.

Germirli, F., Tünay, O., & Orhon, D. (1990). An overview of the textile industry in Turkey–pollution profiles and treatability characteristics. *Water Science and Technology*, *22*(9), 265-274.

Gogate, P. R., & Pandit, A. B. (2004). A review of imperative technologies for wastewater treatment I: oxidation technologies at ambient conditions. *Advances in Environmental Research*, *8*(3-4), 501-551.

Gordon, P. F. & Gregory, P. (2012). *Organic Chemistry in Colour*. Springer Science & Business Media.

Göde, F., & Pehlivan, E. (2006). Removal of chromium (III) from aqueous solutions using Lewatit S 100: the effect of pH, time, metal concentration and temperature. *Journal of Hazardous Materials*, *136*(2), 330-337.

Gräbe, C. & Liebermann, C. (1868). Ueber farbstoffe aus der anthracengruppe. *Berichte Der Deutschen Chemischen Gesellschaft*, 1(1), 104-106.

Gürses, A. (2019). Sustainable colorants. In *The Impact and Prospects of Green Chemistry for Textile Technology* (pp. 21-55). Woodhead Publishing.

Gürses, A., Açıkyıldız, M., Güneş, K., & Gürses, M. S. (2016). *Dyes and Pigments*. Springer, Cham.

Hazel, B. G. (1995). Industry evaluation of colour reduction and removal–the DEMOS project. *Colour in Dyehouse Effluent*, 59-72. http://hdl.handle.net/10603/58839

Hunger, K. (2003). *Industrial Dyes: Chemistry, Properties, Applications.* Wiley-VCH, Weinheim.

Jayswal, A.S. (2007). *Treatment of waste water containing dyes organic and metal pollutants by sorption ion exchange methods using inorganic materials.* Doctoral Dissertation, Maharaja Sayajirao University of Baroda. India.

Jiang, C. (1997). *Color and organic pollutant removal from industrial dye wastewaters*. (Doctoral Dissertation, University of Kentucky). USA.

Karakaya, C. Dede, B., & Cicek, E. (2016). Novel metal(II) complexes with bidentate Schiff base ligand: synthesis, spectroscopic properties and dye decolorization functions. *Acta Phys Pol A*, *129*(2), 208-212.

Kocaer, F.O., Alkan, U., (2002). Boyarmadde içeren tekstil atıksularının arıtım alternatifleri, *Uludağ Üniversitesi Mühendislik-Mimarlık Fakültesi Dergisi*, 7(1), 47-55.

Kurbanova, R. Mirzaoğlu, R., Ahmedova, G., Şeker, R., & Özcan, E. (1998). *Boya ve Tekstil Kimyası ve Teknolojisi.* Baskı, Konya.

Maheshwari K. Agrawal M., Gupta A.B. (2021) *Dye Pollution in Water and Wastewater.* In Muthu S.S., Khadir A. (Eds). *Novel Materials for Dye-containing Wastewater Treatment. Sustainable Textiles: Production, Processing, Manufacturing & Chemistry*. Springer, Singapore.

Matavos-Aramyan, S., & Moussavi, M. (2017). Advances in Fenton and Fenton based oxidation processes for industrial effluent contaminants control-a review. *Int. J. Environ. Sci. Nat. Resour*, *2*(4), 1-18.

Moussavi, G., & Mahmoudi, M. (2009). Degradation and biodegradability improvement of the reactive red 198 azo dye using catalytic ozonation with MgO nanocrystals. *Chemical Engineering Journal*, *152*(1), 1-7.

Murray, C. A., & Parsons, S. A. (2004). Advanced oxidation processes: flowsheet options for bulk natural organic matter removal. *Water Science and Technology: Water Supply*, *4*(4), 113-119.

Parsons SA., Williams M., 2004. Introduction. In S.A. Parsons (Ed.), Advanced Oxidation Process for Water and Wastewater Treatment. London: IWA Publishing, pp. 1-6.

Püntener, A. G. (2000). *Leather dyes.* In H.S. Freeman & A.T. Peters, (Eds). *Colorants for Non-Textile Applications* (pp. 478-557). Elsevier Science.

Rai, H. S., Bhattacharyya, M. S., Singh, J., Bansal, T. K., Vats, P., & Banerjee, U. C. (2005). Removal of dyes from the effluent of textile and dyestuff manufacturing industry: a review of emerging techniques with reference to biological treatment. *Critical Reviews in Environmental Science and Technology*, *35*(3), 219-238.

Seventekin, N. (1988). *Boyarmadde Kimyasına Giriş*. EÜ.

Shevell, S. K. (Ed.). (2003). *The Science of Color*. Elsevier.

Sghaier, I., Guembri, M., Chouchane, H., Mosbah, A., Ouzari, H. I., Jaouani, A., Cherif, A. & Neifar, M. (2019). Recent advances in textile wastewater treatment using microbial consortia. *J. Text. Eng. Fash. Technol*, *5*(3), 134-146.

Spetch, O., Wurdack, I., & Wabner, D. (1996). Fenton's reagent in der abwasserreinigung. *Entsorga-Magazin Entsorgungswirtschaft, Technische Universitäet München*, *11*, 96.

Steensen, M. (1997). Chemical oxidation for the treatment of leachate-process comparison and results from full-scale plants. *Water Science and Technology*, *35*(4), 249-256.

Stern, S. R., Szpyrkowicz, L., & Rodighiero, I. (2003). Anaerobic treatment of textile dyeing wastewater. *Water science and technology*, *47*(10), 55-59.

The Colour Index™ colour-index.com published online by Society of Dyers and Colourists and American Association of Textile Chemists and Colorists.

Tünay, O., Kabdasli, I., Eremektar, G., & Orhon, D. (1996). Color removal from textile wastewaters. *Water Science and Technology*, *34*(11), 9-16.

Walterick Jr, G. C. (1988). *U.S. Patent No. 4,765,923*. Washington, DC: U.S. Patent and Trademark Office.

Westerhoff, P., Aiken, G., Amy, G., & Debroux, J. (1999). Relationships between the structure of natural organic matter and its reactivity towards molecular ozone and hydroxyl radicals. *Water research*, *33*(10), 2265-2276.

Witt, O. N. & Dedichen, J. (1896). Ueber Naphtacetol. *Berichte Der Deutschen Chemischen Gesellschaft*, *29*(3), 2945-2954.

CHAPTER 4

ASSESSING THE FRACTAL CHARACTERISTICS OF PRECIPITATION SERIES

Dr. Eng. Cristian Ștefan DUMITRIU[1]

[1] Department of Installations for Constructions,Transilvania University of Brasov,5 Turnului Str, 900152, Brasov, Romania.e-mail cristian.dumitriu@unitbv.ro

INTRODUCTION

The hydro-meteorological conditions are essential factors that determine the anthropic activities, especially in agricultural field and the management of the water resources. Last decade the climate change impact the hydrological processes. Extreme events, as drought and flood are more frequent than before all over.

Water availability is another issue that population is facing in different countries, especially in arid zones. The variation of precipitation significantly influences the water supply, the vegetation growth and the ecosystems' equilibrium.

Analysing the precipitation and temperature evolution at different scales help to forecast and prevent the effects of extreme events on the economy and households, by making decisions on the water resources allocation and use and taking measure to prevent floods.

Most spatio-temporal analyses are based on testing the existence of a monotonic trend. Here, after a short statistical analysis, we adopt – the fractal technique to characterized the series evolution.

Different researchers searched the fractal characteristics of precipitation and temperature series (Hubert, 1992; Bărbulescu *et al.*, 2010; Bărbulescu, and Deguenon, 2015; Bărbulescu and Șerban, 2012) or its multifractal structure (Venogupal *et al*., 2006; Veneziano, 2006; Deidda *et al.,* 2006). Even if this approach is not new, it can

help obtaining a throughout image of the hydro-meteorological series of interest, emphasizing the existence of a pattern of the series at hand.

Here we apply this methodology to study the precipitation series recorded at Constanta hydro-meteorological station located in the Dobrogea region, Romania (Figure 1).

Figure 1. The Romanian map and Constanța city

The complexity and variety of the region's characteristics results from the soil, relief, vegetation and hydrographical network and the climate factors (Brânză, 2005)

The mean annual temperature is about 11°C, higher on the North and North – East. In the summer temperatures are about 22^{o} - 23^{o}C. The thermic gradients decrease on the direction North - South.

The variation of average annual temperature is inversely proportional with the continental influence, inside Dobrogea. The minimum thermic was registered in January and the maximum, in July. The highest thermic winter potential has been registered at the South of Cape Midia.

The mean annual precipitations are in the interval 350-450 mm, the 400 mm isohyet being, parallel to the seashore. Years with precipitation in the interval 200-250 are also noticed.

2. METHODOLOGY

2.1. Statistical analysis

Normality, homoscedasticity, autocorrelation tests have been performed for each series, using the Shapiro – Wilks (Shapiro and Wilk, 1965), Levene (Levene, 1960) and Box-Ljung tests (Box and Ljung, 1978).

The **change points** presence has been checked by the Hubert segmentation (Hubert *et al.*, 1989; Hubert and Charbonnel, 1993).

The existence of the **anomalies** has been assessed by the IQR and Local Outlier Factor (LOF) methods.

In the IQR method, the aberrant values are those values of the series situated outside the interval [Q_1-1.5*IQR, Q_3+1.5*IQR], where Q_1 and Q_3 are the first and third quartiles, and IQR the interquartile range.

In the local outlier factor (LOF) method (Alghushairy *et al.*, 2021; Breuning *et al.*, 2000), the outliers are selected based on a score.

The outlier is 'local' because only a neighborhood situated at a k-distance from the analyzed object is considered. Therefore, for a value x_i in a time series, its local outlier factor, LOF_{x_i}, is calculated by

$$LOF_{x_i} = \frac{1}{N_{x_i} lrd_{x_i}} \sum_{x_j \in N_{x_i}} lrd_{x_j},$$

where N_{x_i} is the number of neighbors of x_i and lrd_{x_j} is the local reachability density of x_j, defined as the maximum between the k -distance to x_j and the distance between any p and x_j (Knorr and Ng, 1998, 1999; Ramaswamy *et al.*, 2000).

The Mann-Kendall (MK) test is utilized for verifying the hypothesis of a monotonic trend existence. With the values increasingly ordered, the test statistic S is computed by (Mann, 1945; Kendall, 1975):

$$S = \sum_{i=1}^{n-1} \sum_{j=i+1}^{n} sign(x_j - x_i) ,$$

where $sign$ is the sign function.

For n >11, S is approximately Gaussian, with a variance that depends on the tied values and zero mean. When there are no such values, the variance is:

$$\sigma^2 = \frac{1}{18} n(n-1)(2n+5).$$

The existence of a monotonic trend cannot be rejected if $|z_S| > z_{\alpha/2}$, where z_S is the test statistics and $z_{\alpha/2}$ is the critical value at a significance level α.

The **seasonal version of the Mann-Kendall** test is employed for checking same hypothesis as for the Mann-Kendall test but for seasonal data. After applying the Mann-Kendall series on each season, the mean and variances of these seasons are summed up for computing the Seasonal Mann-Kendall statistics (Kulkami and Von Storch, 1995).

Since the series autocorrelation may influence the test's results, the series' preprocessing may be utilized (von Storch and Navarra, 1999).

When the hypothesis that there is a monotonic trend is not rejected, the Sen's slope (Sen, 1968) is calculated using the medians.

The KPSS test was applied to test the series stationarity against its nonstationarity (Kwiatkowski *et al*., 1992).

2.2. Fractal analysis

Mandelbrot (1982) defined a fractal by comparing the topological and the Hausdorff–Besicovitch dimensions. If the first one is lower than the second one, the set is called **fractal**.

Leibovitch (1998) refers to fractals as objects for which '*the shapes of the smaller features are kind of the shapes of larges features*.

The properties of invariance of different processes at different scales can be analyzed with the fractal and multifractal tools. In the fractal approach (Mandelbrot, 1977) the evolution (or behavior) is defined by a single parameter, the **fractal dimension**, which can be evaluated by box-counting methods.

To determine the fractal dimension, the scaling exponent is computed as a linear function of the fractal dimension (*d)*; *d* is determined from the linear regression fitted for log Q(*d*) as a function of log(*d*), where Q is the studied characteristic.

Here, the fractality is assessed by the box-count (Falconer, 1990), and Hall-Wood dimension (Hall and Wood, 1993), variogram, and variation estimators.

The box-count dimension of a curve in R^2 is defined by

$$D_{BC} = \lim_{\varepsilon \to o} N(\varepsilon)/\log(1/\varepsilon)$$

where $N(\varepsilon)$ ($\varepsilon>0$) is the smallest number of squares with the side ε in $\mathbf{R}^2$ that can cover the curve (Falconer, 1990).

The Hall – Wood dimension is a version of box-count dimension, defined by

$$D_{HW} = 2 - \lim_{\varepsilon \to o} A(\varepsilon)/\log(\varepsilon),$$

where $N(\varepsilon)$ is the sum of the areas of all boxes with the side ε intersecting the curve obtained by the linear interpolation of the graph of the data (Hall and Wood, 1993).

Davies and Hall (1998) introduced **the variogram estimator,** while Genton (1999) proposed a robust version of this method.

The **dimension estimator**, D_G is determined by plotting log(d) against log($\widehat{V}(d)$), where

$$\widehat{V}(d) = 4.924405\{U_i(d) - U_j(d): i < j\}^2_{(k)},$$

$$U_i(d) = X_{i/n} - X_{(i-d)/n},$$

d is the lag and $k = C^2_{[(n-d)/2]+1}$.

The **variation estimator** (*Gneiting et al.*, 2012) is a generalized version if the variogram estimator, which relies on

$$\gamma_p(t) = 1/2E|X_u - X_{u+t}|^p.$$

Particular cases are the madogram (p = 1), and variogram (p = 2).

2.2. Data series

The studied series are maximum monthly precipitation and maximum annual precipitation series collected between January 1961 and December 2009 (Figure 2).

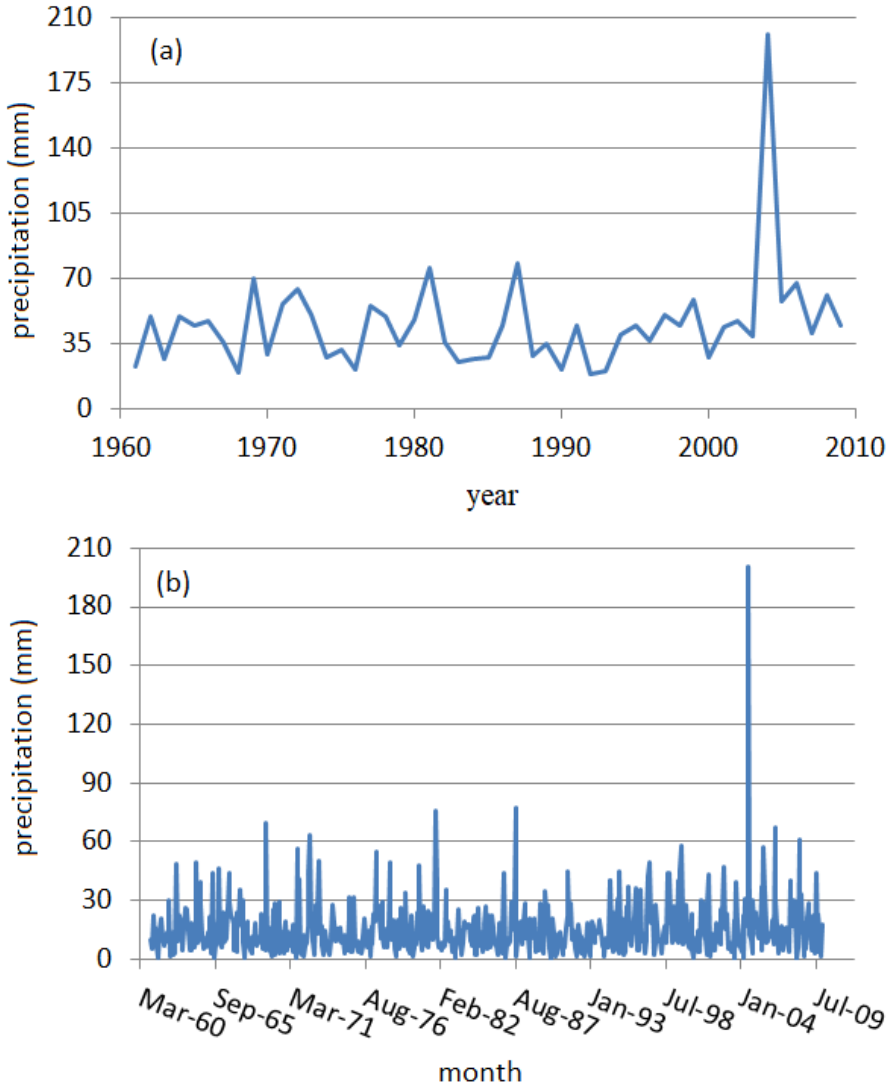

Figure 2. Annual and monthly maximum precipitation series

3. RESULTS AND DISCUSSION

The histogram and the correlogram of the maximum monthly series are presented in Figures 3 and 4. The histogram is right skewed, so the data series is not Gaussian.

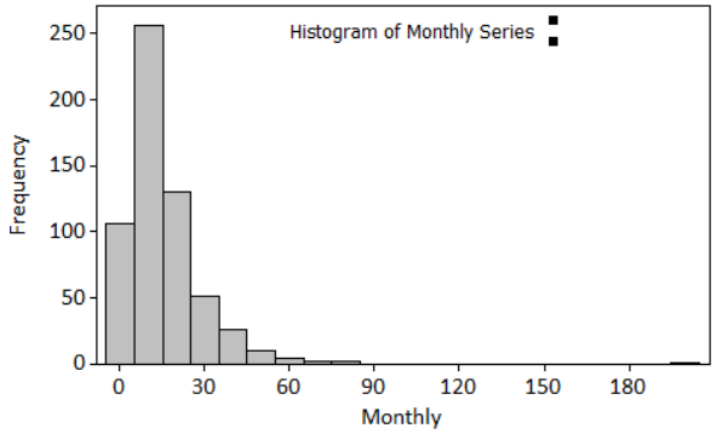

Figure 3. The histogram of the monthly maximum precipitation series

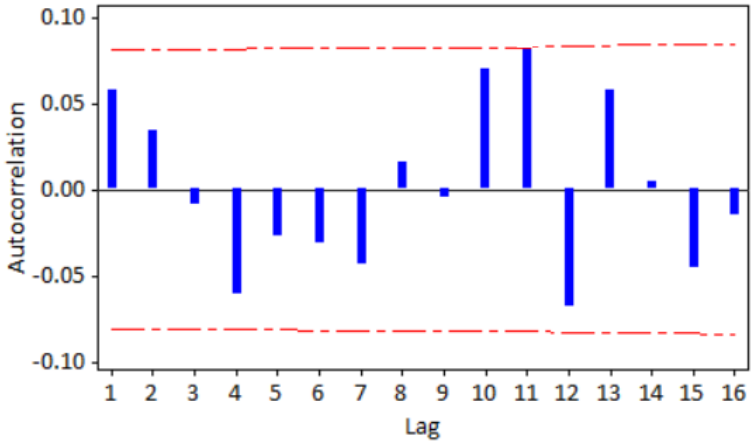

Figure 4. The autocorrelation function (and 95% confidence level- dotted lines) of the monthly maximum precipitation series

Similar shape has the annual precipitation series. From Figure 4 it results that there is no correlation of the monthly data series. There same is true for the annual series.

The Box-Ljung method rejected the autocorrelation hypothesis for both annual and monthly series. The Hubert segmentation procedure

detected a change point in August 2005 (with a maximum precipitation of 201 mm).

The only outlier detected by IQR method for the annual data was 201. For the monthly data, 34 outliers were found to be outliers.

The LOF method selected the same outlier for the annual series and only 27 for the monthly one (Figure 5). 4.05% of monthly values are aberrant values (at 95% confidence level).

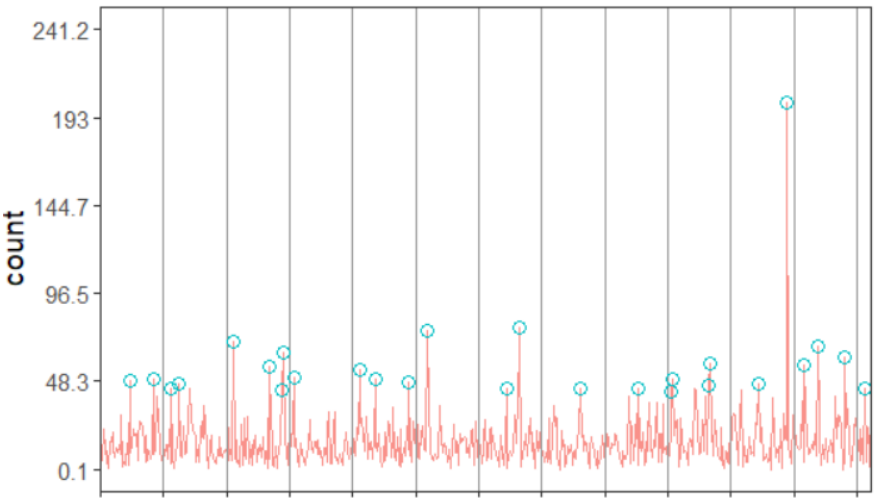

Figure 5. Outliers detected for monthly data (represented by dots)

The Mann – Kendall test rejected the hypothesis that there is a trend of the annual series.

The same test and its seasonal version on the monthly series rejected the same hypothesis as well.

The only p-value less than 0.05 in the KPSS test corresponds to the test for stationarity in level on the monthly series. So, the nonstationarity in level cannot be rejected for this series.

The fractal dimensions for the annual series are presented in Figures 6 and 7.

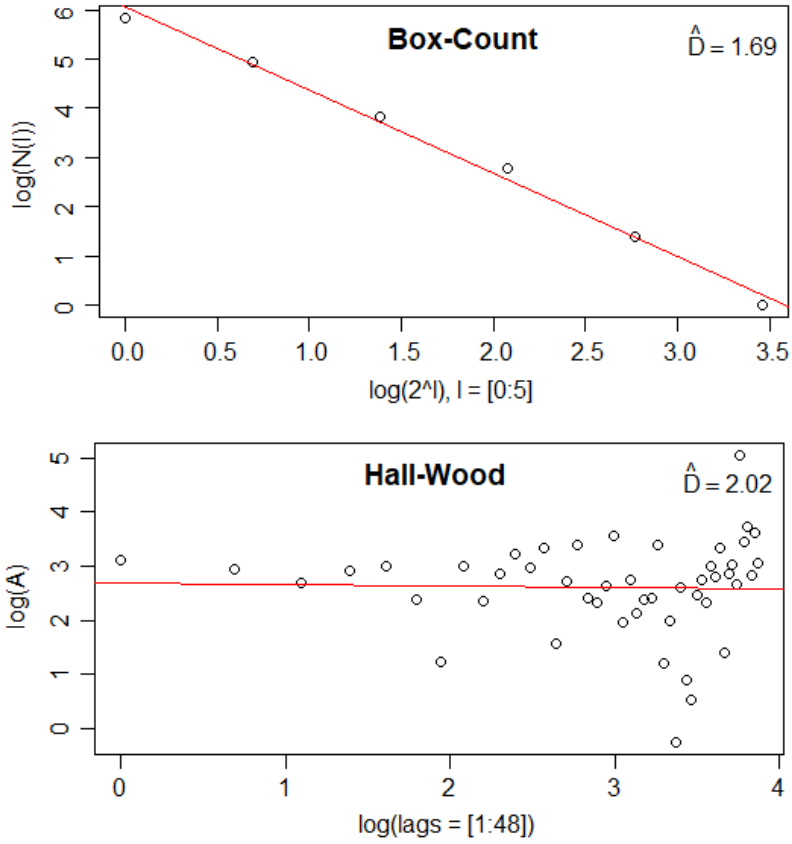

Figure 6. Box count and Hall-Wood dimensions for the annual series

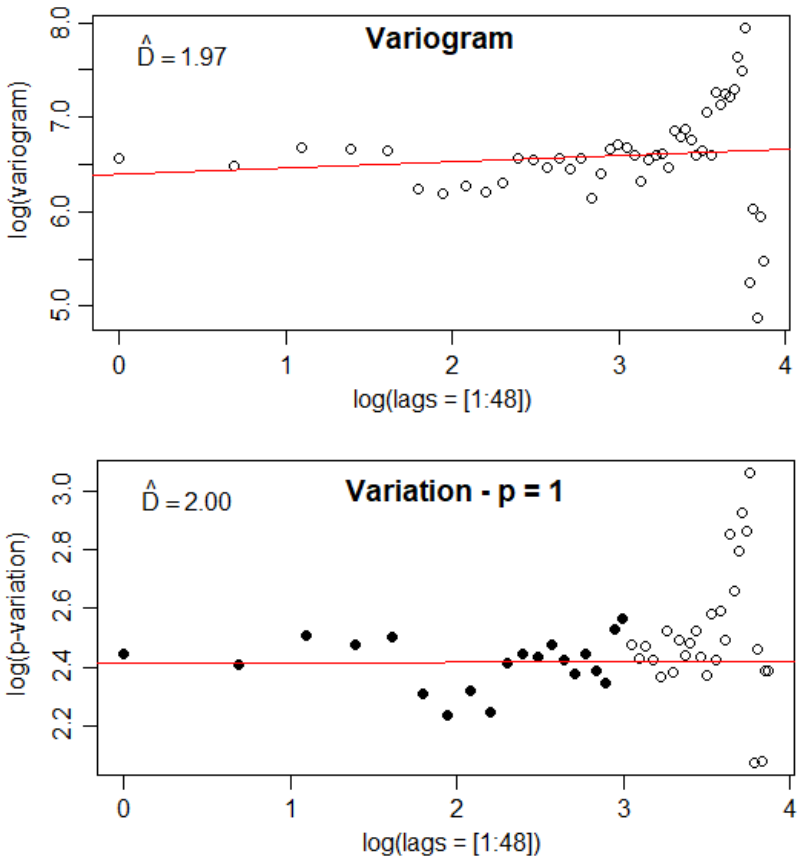

Figure 7. Variogram and variation estimators for the annual series

There is a concordance of the values given by the Hall-Wood dimension, and the values of the variation and variogram estimators, which are approximately 2. A lower value was returned by the box-count dimension, 1.69.

The corresponding dimensions for the monthly series are presented in Figures 8 and 9. The Box dimension, the variogram and variation estimators are approximately the same as for the annual series.

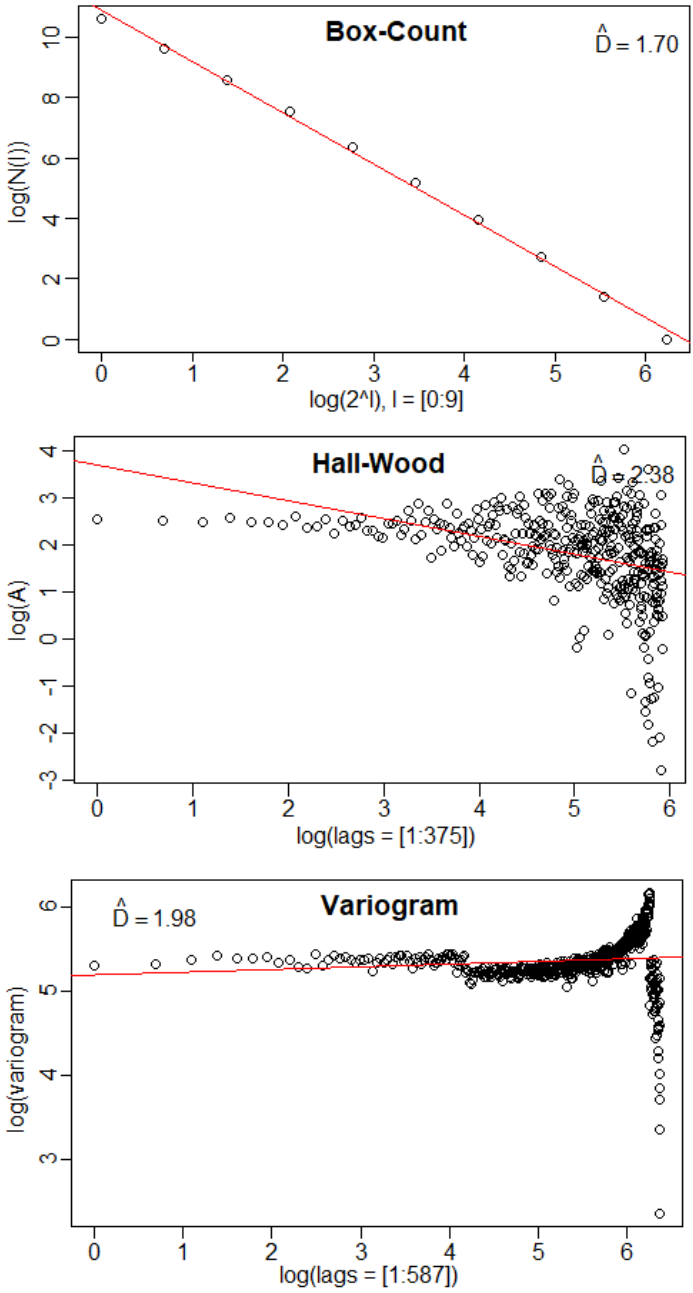

Figure 8. Box count, Hall-Wood dimensions and the variogram for the monthly series

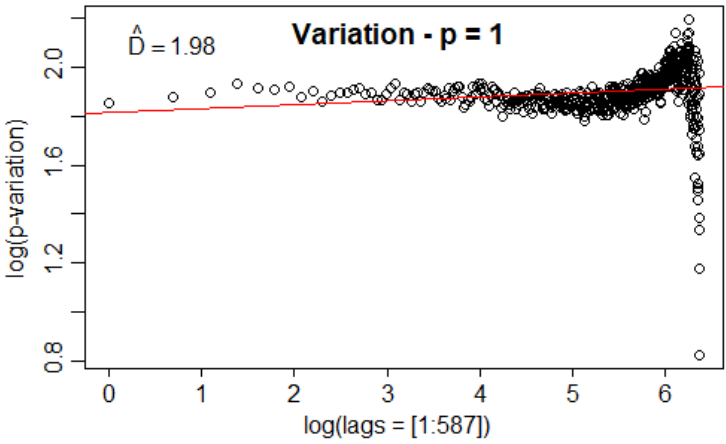

Figure 8. Variation estimator for the monthly series

The value of the Hall-Wood estimator is higher (2.38) for the monthly series. All these values show the fractal character of the maximum annual and monthly series.

9. CONCLUSIONS

In this article we addressed the fractal character of the maximum annual and monthly precipitation series recorded at Constanta, Romania.

Compared to the results for the annual precipitation series (Bărbulescu et al., 2010), show a more accentuated fractal behavior of these series.

In a future study, we would be interesting to estimate the multifractal characteristics of the same series and to compare with the results from the literature.

REFERENCES

Alghushairy, O., Alsini, R., Soule, T., Ma, X. A Review of Local Outlier Factor Algorithms for Outlier Detection in Big Data Streams, Big Data and Cognitive Computing, vol. **5(1)** (2021), 1, https://doi.org/10.3390/bdcc5010001.

Bărbulescu, A., Deguenon, J. About the variations of precipitation and temperature evolution in the Romanian Black Sea Littoral, *Romanian Reports in Physics,* vol. **67(2**) (2015), pp. 625 – 637.

Bărbulescu, A., Șerban, C. Statistical and multifractal analysis of rainfall of Romania, *International Journal of Ecological Economics & Statistics*, vol.**25**(**2**) (2012), pp. 1-11.

Bărbulescu, A., Șerban, C., Maftei, C., Statistical analysis and evaluation of Hurst coefficient for annual and monthly precipitation time series, *WSEAS Transactions on Mathematics*, vol. **9(10)** (2010), 791 – 800.

Brânză, D. (2005) The influence of the meteo-climatic conditions and the pollution of the marine environment on the navigation, maneuvering the ship and the ecosystems in the area of the Romanian Black Sea coast, Ex Ponto, Constanţa (in Romanian)

Breunig, M. M., Kriegel, H. P., Ng, R.T., Sander, J. LOF: Identifying density-based local outliers, Proceedings of the 2000 ACM SIGMOD international conference on Management of data—SIGMOD '00, Dallas, TX, USA, 16–18 May 2000.

Davies, S., Hall, P. Fractal analysis of surface roughness by using spatial data, *Journal of the Royal Statistical Society, Series B,* vol. **61** (1999), pp. 3–37.

Deidda, R., Badas, M.G., Puliga, E., Space - time multifractality of remotely sensed rainfall fields, *Journal of Hydrology*, vol. **322** (2006), pp. 2–13.

Falconer, K. J. (1990) *Fractal Geometry: Mathematical Foundations and Application*s, Wiley, New York.

Genton, M G. Highly robust variogram estimation, *Mathematical Geology*, vol. **30**, (1998), pp. 213–221.

Gneiting, T. Sevcikova, H., Percival, D. B. Estimators of fractal dimension: Assessing the smoothness of time series and spatial data, Stat. Sci., vol. **27(2)** (2012), pp. 247-277.

Grassberger, P., Generalized dimensions of strange attractors. *Physics Letters A.*, vol. **97(6)** (1983), pp. 227 – 230.

Hall, P., Wood, A. On the performance of box-counting estimators of fractal dimension, *Biometrika*, vol. **80** (1993), pp. 246–252

Hubert, P., Carbonnel, J.P., Chaouche, A., Segmentation des séries hydrométéorologiques. Application à des séries de précipitations et de débits de l'Afrique de l'Ouest, *Journal of Hydrology*, vol. **110** (1989), pp. 349 – 367.

Hubert, P., Analyse multifractale de champs temporels d'intensité des précipitations. In: Proceedings of Rencontres hydrologiques Franco Roumaines, UNESCO, Paris, 3–6 September 1991, SC/92/WS/48, 1992, pp. 379–386.

Hubert, P., Carbonnel, J.P., Segmentation des séries annuelles de débits de grands fleuves africains. *Bulletin de liaison du CIEH*, vol. **92** (1993), pp. 3 – 10.

Kendall, M. G. (1975) *Rank correlation methods*, Griffin, London.

Knorr, E.M., Ng, R.T., Algorithms for Mining Distance-Based Outliers in Large Datasets, Proc. 24th Int. Conf. on Very Large Data Bases, New York, NY, 1998, pp. 392-403.

Knorr, E. M., Ng, R.T. Finding Intensional Knowledge of Distance-based Outliers, Proc. 25th Int. Conf. on Very Large Data Bases, Edinburgh, Scotland, 1999, pp. 211-222.

Kulkami, A., Von Storch, H. Monte Carlo Experiments on the Effect of Serial Correlation on the Mann-Kendall Test of Trend, *Meteorologische Zeitschrift*, vol. **4**(**2**) (1995), pp. 82-85.

Kwiatkowski, D., Phillips, P.C.B., Schmidt, P., Shin, Y., Testing the null hypothesis of stationarity against the alternative of a unit root, *Journal of Econometrics*, vol. **54(**1–3) (1992), pp. 159–178.

Leibovitch, L.S. (1998) *Fractal and Chaos Simplified for Life Sciences*, Oxford University Press, New York.

Levene, H., 1960, Robust tests for equality of variances. In: Olkin I. et al. ed., Contributions to Probability and Statistics: Essays in Honor of Harold Hotelling, Stanford University Press, Palo Alto, 1960, pp. 278-292.

Ljung, G.M., Box, G.E.P., On a Measure of a Lack of Fit in Time Series Models, *Biometrika*, vol. **65(2)** (1978), pp. 297–303.

Mandelbrot, B. (1977) *Fractals: form, chance and dimension*, W.H. Freeman and co., San Francisco.

Mandelbrot, B. (1982) *The fractal geometry of nature*, W.H. Freeman and co., San Francisco.

Mann, H. B., Nonparametric tests against trend, vol. **13(3)** (1945), pp. 245-259.

Ramaswamy S., Rastogi R., Kyuseok, S., Efficient Algorithms for Mining Outliers from Large Data Sets, ACM SIDMOD, vol. **29(2) (**2000**)**, pp. 427 -438, https://doi.org/10.1145/335191.335437.

Shapiro, S., Wilk, M. B., An Analysis of Variance Test for Normality (Complete Samples), *Biometrika*, vol. **52(3/4)** (1965), pp. 591 – 611.

Veneziano, D., Furcolo, P., Iacobellis, V., Imperfect scaling of time and space-time rainfall, *Journal of Hydrology*, vol. **322** (2006), pp. 105 – 119.

Venugopal, V., Roux, S.G., Foufoula-Georgiou, E., Arneodo, A. Revisiting multifractality of high resolution temporal rainfall using a wavelet-based formalism, *Water Resources Research*, vol. **42** (2006), W06D14, doi: 10.1029/2005WR004489.

von Storch, H. Navarra, A. (1999), *Analysis of Climate Variability: Applications of Statistical Techniques Proceedings of an Autumn School Organized by the Commission of the European Community on Elba from October 30 to November 6, 1993*, 2nd ed. Berlin Heidelberg: Springer-Verlag (1999)

Sen, P. K. Estimates of the Regression Coefficient Based on Kendall's Tau, *Journal of the American Statistical Association*, vol. **63(324)** (1968). 1379–1389, https://doi.org/10.1080/01621459.1968.10480934.

CHAPTER 5

THE EFFECT OF Gd ON THE STRUCTURAL AND OPTICAL PROPERTIES OF TETRAHEDRAL BINARY $Zn_{0.95}Er_{0.05}O$ SEMICONDUCTING NANO THIN FILMS

Assoc. Prof. Dr. Elif AŞIKUZUN[1]

[1] Kastamonu University, Faculty of Engineering and Architecture, Department of Metallurgical and Materials Engineering, Kastamonu, Turkey.
easikuzun@kastamonu.edu.tr, https://orcid.org/0000-0003-1850-7080

INTRODUCTION

Semiconductors are materials whose resistivity varies between ρ=10 ohm.cm and 10 ohm.cm at room temperature. The electrical properties of semiconductors can be changed by methods such as optical excitation, doping, and heat treatment. For this reason, semiconductor materials are used in many devices such as transistors, switches, diodes, detectors, thermistors and sensors. Zinc oxide is a semiconductor compound from group II B-VI A of the periodic table. Considering the recent increase in research on zinc oxide, it is seen that there is an intense interest in this field. In recent years, considering the increase in research on zinc oxide, it is seen that there is an intense interest in this field.

ZnO has a direct band structure and is a semiconductor that has a very wide band gap (~3.3 eV) [1-4]. Due to its wide band gap, it is considered as a suitable material for making LEDs in the blue and ultraviolet region of the electromagnetic wave spectrum.

The photoelectric, piezoelectric and thermoelectric properties of the ZnO semiconductor are quite good and are used in many applications due to these properties. These applications are; gas sensors, thin film transistors, photoelectric devices, optoelectronic devices, solar cells, UV detectors, piezoelectric transducers, surface acoustic circuits, thermoelectric devices, pH sensors, biosensors [5-8]. In addition, ZnO absorbs UV light and performs band transitions. Due to this feature, zinc oxide is widely used as a transparent conductive oxide thin film [9].

In this study, undoped and Er/Gd doped ZnO nano thin films are prepared by using dip coating method with sol-gel method. Sol-gel method, which is one of the thin film forming techniques, has a wide area of use in terms of easily covering of large areas and creating homogeneous multi-layered films. Sol-gel method can be used in the production of single-component or multi-component oxide films [10,11]. The binary structure system ($Zn_{0.95}Er_{0.05}O$) are transformed into ternary structure ($Zn_{0.95-x}Er_{0.05}Gd_xO$) with 5% Er and 1%, 2%, 3%, 4% and 5% Gd doping rate. The effects of Gd doping on the characterization of ZnO thin films are investigated. X-ray diffraction pattern results show that the films have a hexagonal structure and a c-axis (002) orientation. This trend emerges as the dominant peak at approximately $2\theta=34.38^{o}$. According to the grain size results calculated from the X-ray diffraction peaks, it is observed that the grain sizes decreased with the increasing Gd doping.

The transmittance and energy band gap are determined by making UV measurements of undoped and Gd-doped ZnO thin films. The basic absorption spectra of the semiconductor samples produced by the sol-gel method are obtained in the 190-1100 nm scanning region at room temperature. It is observed from the results of UV measurements that the transmittance values of the films decreased with increasing Gd doping, and accordingly, there is a large defect in the material.

1. EXPERIMENTAL DETAILS

In the preparation of the solution, % 98,0 − % 101,0 purity ZnO (zinc oxide), 99.9% purity $Gd(OOCCH_3)_3.xH_2O$ (Gadolinium (III) acetate hydrate) and 99.9% purity $C_{15}H_{21}ErO_6$ (Erbium (III) 2,4-pentandione) powder is used. 0.6 ml methanolamine and 50 ml methanol are added as solvent. x values are determined as 0.01, 0.02, 0.03, 0.04 and 0.05 % in the $Zn_{1-x}Er_{0,05}Gd_xO$ compound. The solutions prepared in the beakers are covered and stirred for at least 5 hours in a heated magnetic stirrer until it became a transparent solution. The most important point at this stage is that the solution is transparent and no precipitation or granulation appears in the solution. After mixing, the sol is prepared for film formation. The films are coated in a vertical furnace at 400°C using the dip coating method. The coating process is repeated 20 times for each sample. This situation is expressed as 20 dipped of the film are covered. Then, the Gd-doped ZnO thin films are heat treated at 600°C for 30 minutes.

2. RESULT AND DISCUSSIONS

2.1. X-Ray Diffraction (XRD) Measurements

In this thesis, XRD measurements are performed by Bruker D8 Advance X-ray powder diffractometer using Cu−Kα radiation in the range of $3^o \leq 2\theta \leq 90^o$. The phase structures and lattice parameters of samples are determined by Bruker-EVA 10.0.1.0 analysis program and ICDD PDF2-2002 data cards.

All of the samples have hexagonal wurtzite crystal structure that is specific structure of ZnO. Bragg angle and full width half maximum (FWHM) values are found from X-ray diffraction pattern results and grain size is calculated for each sample using Warren-Scherrer method [12].

$$D=0,941\lambda/Bcos\theta \quad (1)$$

where, D denotes the grain size, λ presents the wavelength of the X-ray used and B depicts the full width half of the maximum (FWHM) peak intensity.

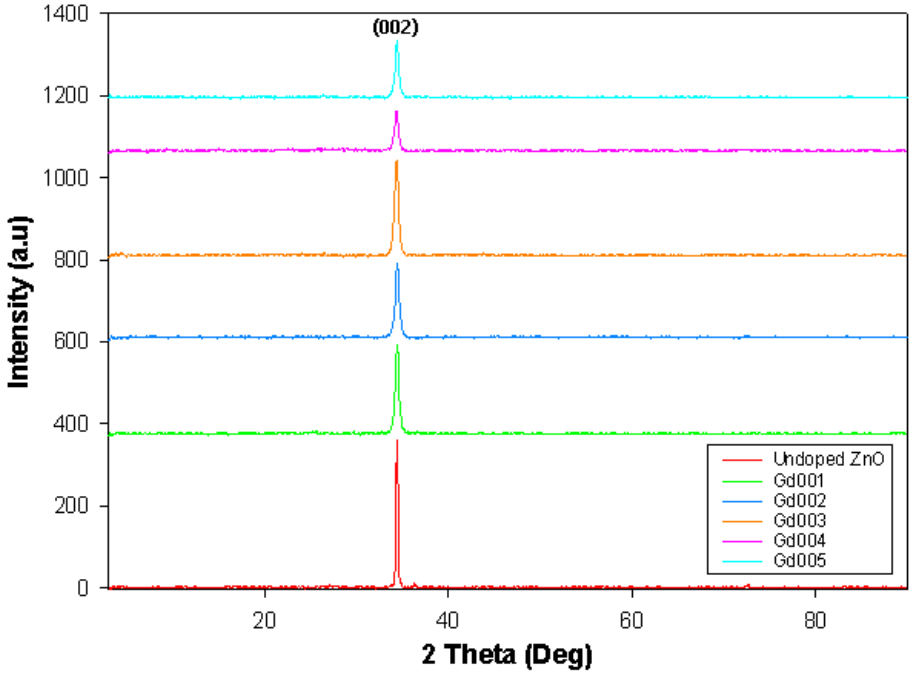

Figure 1: XRD images of doped and undoped thin films.

According to the XRD results of doped and undoped ZnO thin films, no secondary phase is found that caused a remarkable change in the

obtained diffraction patterns (Fig.1). This means that the presence of Er+2 and Gd+2 ions in the ZnO lattice affects crystal structure. The reason of that is the small amount of Er and Gd enters into the structure in grain boundary of the lattice.

The dominant peak is (002) oriented zinc oxide. This orientation is along the c axis. The calculated c lattice parameters are given in Table 1. The grain size value decreases with increasing the Gd ions in the ZnO based material. The smallest value is 17.56 nm for the Gd003.

Table 1: d, 2θ, FWHM, c and D values of doped and undoped thin films.

Samples	d (m)	2θ (Degree)	FWHM	Lattice Parameters (Å)	Grain Size (nm)
				c (Å)	
Undoped ZnO	2.606	34.38	0.253	5.21	34.36
Gd001	2.601	34.44	0.446	5.20	19.49
Gd002	2.599	34.46	0.464	5.19	18.74
Gd003	2.608	34.35	0.495	5.21	17.56
Gd004	2.608	34.35	0.467	5.21	18.61
Gd005	2.604	34.41	0.410	5.20	21.20

2.2. Optical Measurements

The transmittance values and energy band gaps of undoped and Gd doped ZnO thin films are determined by using UV-VIS measurements [13-15]. The basic absorption spectra of the semiconductor thin films produced using the dip coating method with the sol-gel method are

obtained in the 190-1100 nm scanning region at room temperature (Fig. 2).

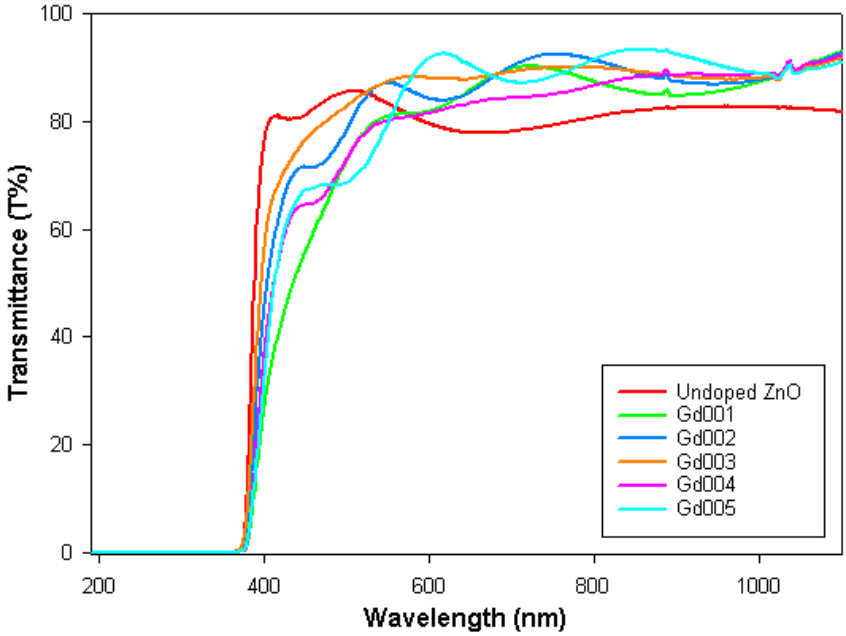

Figure 2: Optical transmittance spectra of ZnO-based nano-thin films.

It is determined that the films were quite transparent (approx. 75%) in the visible region (400-700nm). The band-gap energy (E_g) of the films are determined using $(\alpha hv)^2$) versus (hv) graph (Kubelka–Munk function versus energy) in the Fig.3. The obtained values are given in Table 2.

Discrete Photon Energy

$$\alpha h\nu = \mathrm{A}\left(h\nu - E_g\right)^n \quad (2)$$

Absorption Coefficient — Constant — Band-Gap Energy

n is associated with type of optical transmission in the band gap.

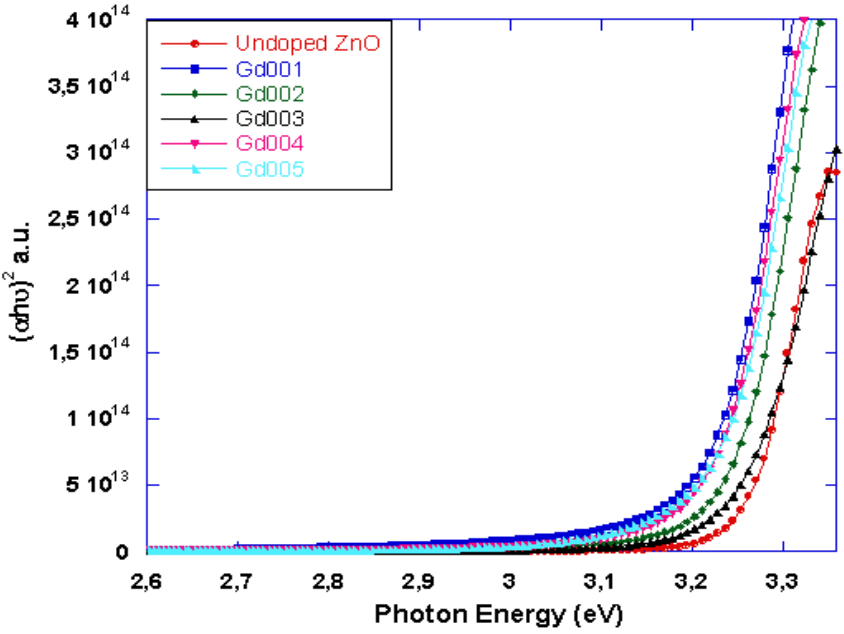

Figure 3: Energy band gaps of optical transmittance spectra of ZnO-based nano-thin films.

The optical band-gap energy of the undoped ZnO film is approximately 3.27 eV. Energy band gaps of the Gd-doped thin films vary between 3.23-3.25eV as shown in Fig. 3 and Table 2. As can see, the undoped ZnO exhibits a larger band-gap energy [16,17].

Table 2: Film thickness, dislocation density, micro-strain, transmittance and energy gap values for thin films.

Samples	Film Thickness (nm)	Dislocation Density (δ)	Micro Strain (ε)	Average Transmittance (%)	Band-Gap Energy (eV)
Undoped ZnO	339	0.800	0.0010	81.12	3.27
Gd001	335	2.266	0.0017	80.84	3.23
Gd002	182	2.332	0.0017	71.32	3.24
Gd003	550	2.608	0.0018	87.22	3.25
Gd004	108	2.223	0.0017	64.52	3.23
Gd005	147	1.528	0.0014	67.01	3.23

CONCLUSIONS

As seen from the XRD pattern, the (002) plane is the dominant orientation plane of ZnO and Gd-Er doped ZnO thin films. The ZnO structure with Gd-Er dopant element is possess hexagonal wurtzite type structure. It is seen that the c lattice parameters of the samples decreased until the Gd002 doping and the values increased after this rate. Grain sizes decreased until the Gd003 doping, then increased. According to this result, we can say that 002-003 doping rates are a threshold value. The grain sizes are reduced with increasing Gd doping. Transmittance values decreased with increasing Gd doping. Poor transmittance shows great defect in the material. More defects increase absorption. Optical analysis revealed that the films are quite transparent (approx. 75%) in the visible region (400-700nm). Obtained energy gaps show that conduction band and valence band

converged and thus energy band gap decreased. It is seen that the energy range of the Gd003 doping, which has the highest transmittance value among the samples, the energy band gap of the Gd003 doping is closest to the energy band gap of undoped zinc oxide.

REFERENCES

Salam, S. (2013). Sol–gel synthesis of intrinsic and aluminum-doped zinc oxide thin films as transparent conducting oxides for thin film solar cells, Thin Solid Films, Vol. 529, pp 242-247.

Saleh, R., Prakoso, S.P., Fishli A. (2012). The influence of Fe doping on the structural, magnetic and optical properties of nanocrystalline ZnO particles, Journal of Magnetism and Magnetic Materials, Vol. 324, pp 665-670.

Arda, L., Ozturk, O., Asikuzun, E., Ataoglu, S. (2013). Structural and mechanical properties of transition metals doped $ZnMgO$ nanoparticles, Powder Technology, Vol. 235, pp 479–484.

Ohyama, M., Kouzuka, H., Yoko, T. (1997). Sol-gel preparation of ZnO films with extremely preferred orientation along (002) plane from zinc acetate solution, Thin Solid Films, Vol. 306, pp 78-85.

Tsay, C., Fan, K., Chen, S., Tsai, C. (2010). Preparation and characterization of ZnO transparent semiconductor thin films by sol–gel method, Journal of Alloys and Compounds, Vol. 495, pp 126–130.

Caglar, Y., Caglar, M., Ilican, S. (2012). Microstructural, optical and electrical studies on sol gel derived ZnO and ZnO: Al films, Current Applied Physics, Vol. 12, pp 963-968.

Asikuzun, E., Ozturk, O., Arda, L., Akcan, D., Senol, S.D., Terzioglu, C. (2015). Preparation, structural and micromechanical properties of (Al/Mg) co-doped ZnO nanoparticles by sol–gel process, Journal of Materials Science: Materials in Electronics, Vol. 26, pp 8147–8159.

Ohyama, M., Kouzuka, H., Yoko, T. (1997). Sol-gel preparation of ZnO films with extremely preferred orientation along (002) plane from zinc acetate solution, Thin Solid Films, Vol. 306, pp 78-85.

Ashour, M.A., Kaid, N.Z., El-Sayed and Ibrahim, A.A. (2006). Physical properties of ZnO thin films deposited by spray pyrolysis technique, Applied Surface Science, Vol. 252, pp 7844-7848.

Uhlmann, D.R., Suratwala, T., Davidson, K., Boulton, J.M., Teowee, G. (1997). Sol-gel derived coatings on glass, Journal of Non- Crystalline Solids, Vol. 218, pp 113-122.

Yuonesi, M., Pakdel, A. (2010). Effect of low concentration of nickel on structural and optical properties of ZnO nanofilms, Physica B,Vol. 405, pp 2083–2087.

Ozturk, O, Cetinkara, H.A., Asikuzun, E., Akdogan, M., Yilmazlar, M., Terzioglu, C. (2011). Investigation of mechanical and superconducting properties of iron diffusion-doped Bi-2223 superconductors, Journal of Materials Science: Materials in Electronics, Vol. 22, pp 1501-1508.

Ilican, S., Caglar, M., Caglar, Y. (2010). Sn doping effects on the electro-optical properties of sol gel derived transparent ZnO films, Applied Surface Science, Vol. 256, pp 7204-7210.

Dimova-Malinovska, D., Nichev, H., Angelov, O. (2008). Correlation between the stress in ZnO nano thin films and the Urbach band tail width, Physica Status Solidi (C), Vol. 5, pp 3353-3357.

Lu, J.G., Ye, Z.Z., Zeng, Y.J., Zhu, L.P., Wang, L., Yuan, J., Liang, Q.L. (2006). Structural, optical and electrical properties of (Zn, Al) films over a wide range of compositions, Journal of Applied Physics, Vol. 100, pp 073714.

Rai, R.C. (2013). Analysis of the Urbach tails in absorption spectra of undoped ZnO nano thin films, Journal of Applied Physics, Vol. 113, pp 153508.

Senol, S.D., Ozturk, O., Terzioğlu, C. (2015). Effect of boron doping on the structural, optical and electrical properties of ZnO nanoparticles produced by the hydrothermal method, Ceramics International, Vol. 41, pp 11194–11201.

CHAPTER 6

PREPARATION METHODS AND APPLICATIONS OF METAL OXIDE/CLAY AND METAL OXIDE/GRAPHENE OXIDE NANOCOMPOSITES

Asst. Prof. Dr. Murat KIRANŞAN[1*]

[1] *University of Gumushane, Vocational School of Gumushane, Department of Chemistry and Chemical Processing Technologies, 29100-Gümüşhane, TURKEY.
*murat.kiransan@gumushane.edu.tr (*Corresponding Author)
ORCID ID : 0000-0002-8520-6563

INTRODUCTION

Composite material is a group of materials formed by the combination of at least two different materials for a specific purpose. The purpose of composite material synthesis is to obtain a property that does not exist in any of the components alone (Kathiryelu et al., 2008). Nanocomposites are defined as composites be formed of particles synthesized in at least one dimension at the nanometer scale. Nanocomposite material synthesis is a subject that has attracted a lot of attention in recent years (Alexandre and Dubois, 2000). According to their composition nanocomposites; it can be classified in different categories as polymeric, ceramic, metallic and metal oxide (Gao, 2004). Clay minerals are used in agriculture, ceramics, construction and chemical catalysts. Clays have a very important feature due to their intercalation, two dimensional semi-magnetism, structural phase transition, fractal properties and mixed crystal behavior (Dintcheva et al., 2009). In recent years, natural clay minerals such as montmorillonite, kaolinite, bentonite, zeolite and polygorskite have been used in catalyst synthesis, preparation of nanocomposites, sensors, electrodes, as antibacterial agents and nuclear waste storage (Arora et al., 2011). Chemical analysis, the water holding and ion exchange properties of clays they are composed of aluminum silicate compounds (Auta and Hameed, 2013). The color of natural clays is available in various colors such as white, gray, pink and brown depending on the mineral structure and chemical composition of the minerals (Chang et al., 2016). Because the clay particles are very small and form permanent suspensions in water, clays can be easily

separated from their great impurities (Shaban et al., 2017). Clay minerals are essentially aluminum hydrosilicates. In some minerals, aluminum is completely or partially change by Fe or Mg (Zhang et al., 2013a). Alkali minerals or alkali metals form the main components of clay structures. Clays consist of a single clay mineral. But most are mixtures of several minerals (Dogan et al., 2006). Clays are substances that can become plastic when mixed with water at a certain rate. The plasticity property is lost when the adsorbed water moves away from the clay (Zahedi et al., 2013). Particle size of clay; it depends on factors such as adsorbed ions, the type of clay, the organic substances it contains and the formation of the clay ground (Tyagi et al., 2006).

Graphene, which is one of the honeycomb lattice structures of the carbon atom, has gained great importance recently due to it is thermal, mechanical and electronic properties (Song et al., 2014). Due to the unique properties of graphene, it is use as an inorganic filler is preferred to improve the electrical, thermal and mechanical properties of graphene derived nanocomposite materials (Liu et al., 2015). Graphene is a two-dimensional nanomaterial with a length of 0.142 nm between covalent bonds of carbon atoms (Meng et al., 2016). Due to the electrons in it is structure, it moves as massless relativistic particles in a unique way in the quantum vacuum and can be used in many areas due to it is superior properties (Hanifah et al., 2015). The areas where graphene is used can be listed as specific electrodes, transistors, sensors, clean energy devices, organic photovoltaic devices and nanocomposites (Chen et al., 2012). Graphene oxide is a

single layer graphite oxide that can be obtained by reducing graphite into layered layers by sonication or mechanical mixing (Park and Ruoff, 2009). Graphene oxide, on the other contains more functional groups in its structure than graphene (Singh et al., 2016). These functional groups increase the interaction at the interface and provide the homogeneous distribution of the support material in the matrix (Stankovich et al., 2007). However, the presence of oxygen containing functional groups causes graphene oxide to display non-conductive properties. To increase the electrical and thermal conductivity of graphene oxide reduction is done and reduced graphene oxide (rGO) is obtained (Yasin et al., 2018).

Also graphene; it is composed of zero-dimensional fullerenes, one-dimensional carbon nanotubes and three-dimensional graphite (Yun et al., 2013). Graphene is one atom thick nanoparticle in a hexagonal structure in which carbon atoms are sp^2 hybridized. Due to it is many uses, it is one of the most popular and most researched materials in recent years (Kim et al., 2012). Because of the strong covalent bonds between the C-C bonds of graphene it has important mechanical properties. Single layer graphene has a Young's modulus of about 1100 GPa and a tensile strength of 130 GPa (Thema et al., 2013). However, it has high conductivity at room temperature and has a very large surface area (Potts et al., 2011). Considering that a single layer of graphene is 0.42 nm, it is impressive that it is 30 times stronger than steel. Graphene can conductive electric current at the speed of light due to it is high carrier concentration and mobility (Cao et al., 2015).

1. METAL OXIDE/CLAY AND METAL OXIDE/GRAPHENE OXIDE NANOCOMPOSITES

1.1. Metal Oxide/Clay Nanocomposites

Clays have been widely used in industry as they are inexpensive and easily available materials (Neaman and Singer, 2000). The properties of clay minerals such as high cation exchange, pH, interaction with water were investigated and their structures were tried to be developed by modified them according to these properties (Zhang et al., 2019). Clay minerals are naturally heterogeneous substances. There are many minerals such as quartz, calcite and pyrite in their structures (Ning et al., 2007). Clays are found in many different colors in nature depending on the ratio and chemical composition of these mineral contents (Huang et al., 2004). The most important feature that distinguishes clays from stones is that the clays have a very small size and large surface area even in one size (Mishra et al., 2018). In addition to these properties, it is physical adsorption properties are rather high. Clay minerals, which have a layered structure, are composed of two different structures tetrahedral and octahedral units (Kuang et al., 2019).

A tetrahedral structure is a unit with a silicon atom in the center and equidistant from the central atom with oxygen or hydroxyl ions at the corners. It is geometric shape is regular tetrahedron (Yu et al., 2011). An octahedral structure is a geometric structure with aluminum ions at its center and oxygen or hydroxyl ions at its corners. It is geometric shape is regular octahedron (Powell and Beall, 2006). The structures

of clay minerals are formed by the overlapping of different combinations of lattice layers formed by tetrahedral and octahedral units. Clay minerals are classified according to these formations (Marcussen et al., 2009). The resulting layers are named to 1:1 layered if they formed of one octahedral, 2:1 layered if they formed of two tetrahedrals and one octahedral (Nathaniel et al., 2011). The clay minerals with a 1:1 (TO) layer formed by a tetrahedral layer and an octahedral layer form the kaolinite clay group. Clay minerals with a 2:1 (TOT) layer with an octahedral layer between two tetrahedral layers contain the group of sepiolite, smectite, vermiculite, chlorite and montmorillonite (Sari and Tuzen, 2014).

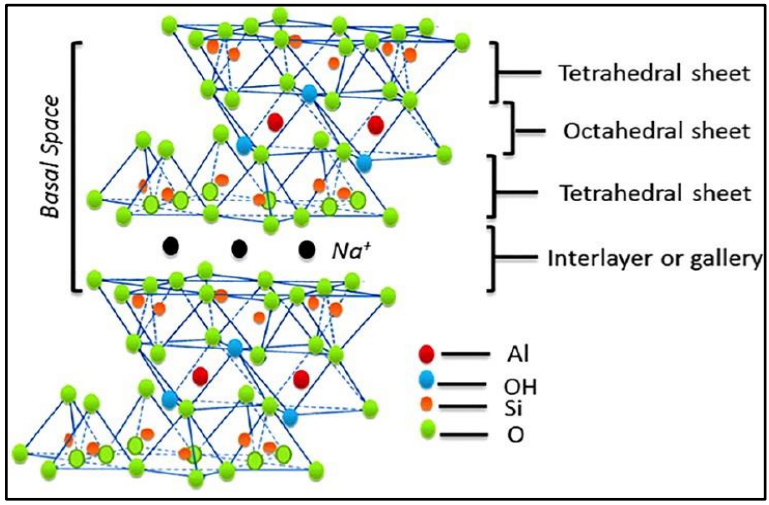

Figure 1. Structure of 2:1 layered clay minerals (Zanetti et al., 2000; Zhao et al., 2010)

The change of cations (Al and Si) in clay minerals with each other is called isomorphic change (Zhao et al., 2010). As a result of these change, due to the different charge amounts of the cations, the

electrical charge balances are disturbed in the structures they are and positive charge excesses occur (Wang et al., 2014). Therefore, the surface of the clay layers is negatively charged. Negative charges adsorb the cations around them. These cations provide electrical neutralization and are held by ineffectual electrical forces (Ma et al., 2017).

Sepiolite, natural magnesium hydrasilicate, belonging to the paligorskite family it is a clay mineral. It has a fibrous structure formed as a result of the stacking of tetrahedral and octahedral oxide layers and has channel spaces that continue along the fiber (Hu et al., 2020). Sepiolite is the most widely used clay mineral among adsorbent clays due to its fibrous and porous structure, as well as its high surface area and effective physicochemical properties (Zhou et al., 2019). In recent years, it has been observed that the use of sepiolite clay in the environmental applications has increased (Liu et al., 2018a; Zhou et al., 2018).

Montmorillonite clay has a 2:1 layered structure, which is from the smectite clay class. It has the properties of being a unit with an octahedral layer between two tetrahedral layers (Na et al., 2010). Montmorillonite is a clay mineral whose chemical structure occurs of aluminum hydrosilicates, formed by the penetration of the aluminum layer between two silicon layers and occur of a TOT layer (Wu et al., 2011). Octahedrals of aluminum in montmorilonite clay it is sandwiched by silicon tetrahedral layers on both sides. The layers are connected to each other by weak Van der Waals bonds the separation

of the layers is easier compared to other clay minerals (Varadwaj et al., 2014).

Table.1 Properties and applications of montmorillonite (Kıranşan, 2015)

Physical Properties	Value	Applications
Unit cell molecular wt. (g/mol)	540.46 g/mol	To slow down water flow through soil
Density (g/ml)	2.5-2.5 to 3.0	To produce Nanocomposites
Moh hardness (20°C)	1.5-2.0	As filler for paper or rubber
Crystal system and d-spacing (nm)	Monoclinic; 1.47x0.442x0.149	To de-colour & purify liquids, wines, juices, etc.
Characteristic	H_2O its volume expands up to 30-fold	As a base for pesticides and herbicides
Appearance	White, Yellow, or Brown with dull luster	In drilling muds to give the water greater viscosity
DSC endothermic peaks, T (°C)	140; 700; 875°C	For thickening of lubricating oils and greases
DSC exothermic peak T (°C)	920°C	For binding foundry sands
MMT swells in water more than any other mineral	Largest for Na-MMT smaller for multivalent counter-ions	Absorption of ammonia, proteins, dyes and other polar, aromatic or ionic compounds
Cleavage	Perfect in on direction, lamellar	As an absorbent

The most important features that distinguish montmorillonite clay from other clay groups are that it has a layered structure and swelling with water at a high ratio. The reason for this is the adsorption of water between the layers (Kalantari et al., 2015). Due to this properties of clay, it is widely preferred especially in chemistry, industry, agriculture, environment and engineering applications. In

addition, it is a highly studied mineral due to its high plasticity, abundance in nature and low cost (Bhattacharyya and Gupta, 2008). Vermiculite clay is a 2:1 layered phyllosilical mineral, usually formed as a result of the change of mica minerals or chlorite. This clay with high plasticity and colloidal structure was named vermiculite (Dos Anjos et al., 2014). Although the use of pure clay in industry is limited, processed vermiculites are widely used especially for thermal and insulation purposes (Marcussen et al., 2009).

Metal oxide nanostructures are one of the raw materials of advanced technological products and their application areas are extended over many different sectors (Lyons et al., 2013). It has important application areas such as automotive, informatics and communication, chemistry, biology, genetic engineering, electronic technology, energy, environment and defense industries (Wu et al., 2010). If the sizes, shapes and atomic regulations of metal oxide semiconductors on the surface are formation at the nanoscale, they turn into effective materials with superior electronic, magnetic, optical, chemical and catalytic properties (Beura et al., 2017). In order to development and improve some properties of metal oxide structures, different atoms consisting of cations or anions must be doped by entering into the crystal lattice. This process affects the properties of metal oxides such as semiconductivity, surface structure and optical transmittance (Kim et al., 2016).

Table.2 Chemical structures of some commonly used clay silicates and some characteristic parameters (Morgan and Gilman, 2003; Ray and Okamoto, 2003; Bergaya et al., 2006; Açışlı, 2014).

Silicates	Chemical Formula	CEC (meq/100g)	Width Layer (nm)
Montmorillonite	$M_x(Al_{4x}Mg_x)Si_8O_{20}(OH)_4$	110	100 -150
Hektorite	$M_x(Mg_{6x}Li_x)Si_8O_{20}(OH)_4$	120	200 - 300
Saponite	$M_xMg_6(Si_{8x}Al_x)Si_8O_{20}(OH)_4$	86,6	50 - 60

Chemical structures and some characteristic properties of some commonly used clay silicates are given in Table 2. A schematic representation of clay modification with various quaternary ammonium surfactants is shown in Fig. 2.

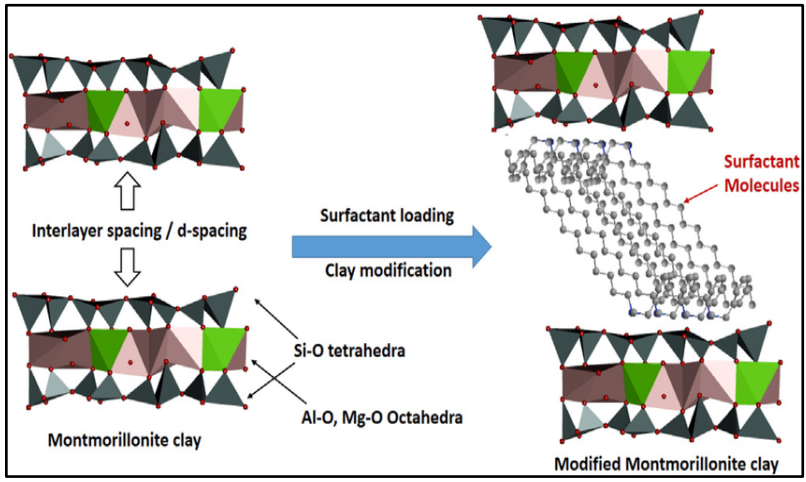

Figure 2. Schematic representation of clay modification with various quaternary ammonium surfactants (Ray and Okamoto, 2003; Stodghill et al., 2004; Shah et al., 2016).

Metal oxides with different structures are used alone as chemical catalysts. Because they have higher oxidizing power compared to other materials, metal oxide such as titanium dioxide (TiO_2), zinc oxide (ZnO), iron(III) oxide (Fe_2O_3), tungsten oxide (WO_3), tin dioxide (SnO_2), nickel (II) oxide (NiO), manganese dioxide (MnO_2) nanostructures are the main materials preferred and used as chemical catalysts (Mori, 2004; Pfitzner et al., 2013).

Metal oxide nanostructures; nanocomposites with more effective surface area can be synthesized by immobilized them between the layers of clays such as bentonite, montmorillonite and sepiolite with different methods (Araujo et al., 2013). In the literature, metal oxide/clay nanocomposites synthesized by different methods are Fe_3O_4/bentonite (Hashemian et al., 2015), MMT/kaolinite/TiO_2 (Dukic et al., 2015), Fe_3O_4/montmorillonite (Kalantari et al., 2015), ZrO_2/kaolinite (Bhattacharyya and Gupta, 2006), $CoFe_2O_4$/montmorillonite (Ai et al., 2011), structures with different properties such as were synthesized. As a result of the modified of metal oxide nanoparticles between the clay layers, nanocomposites with different synergetic properties containing the properties of both metal oxide and clay are obtained (Meshram et al., 2011). Metal oxide/clay nanocomposites preparation with different methods have conductivity, nanosize effect and catalyst properties of metal oxide. These structures have properties of clay such as surface area, micropore area and total pore volume (Miao et al., 2006).

1.2. Metal Oxide/Graphene Oxide Nanocomposites

Graphene is a single layered, atomic thick particle that formation the main class of carbon allotropes in which the regular carbon atoms in its hexagonal particle structure are sp^2 hybridized (Chowdhury et al., 2014). Graphene is one of the most important materials researched today regarding it is application areas. Graphene has very good electrical, electrochemical, thermal and mechanical properties due to its two dimensional, single atom thickness and strong bonding structure (Hibino et al., 2010; Sun et al., 2015). Two dimensional tight lattice of graphene that does not pass even the smallest atom due to its structure, it is theoretically preferred to be used as a very effective sensor (Xia et al., 2015). Since the carbon atoms in the layers of graphene are at different distances from each other, it causes the formation of carbon allotropes in the graphene structure (Novoselov et al., 2005; Mao et al., 2012).

Hummers method is preferred for graphene oxide synthesis. The advantages of the Hummers method are it is ease of synthesis, low cost and ability to produce great quantities of products (Yang et al., 2012; Zan et al., 2013). The synthesis of graphene oxide is based on the oxidation of graphite with an oxidant and strong acid. Oxidation reactions change according to the applied method, experimental conditions and graphite properties (Sengupta et al., 2011). Graphene oxide is defined as heavily oxygenated because it contains many oxygen containing functional groups such as epoxy, hydroxyl, carbonyl and carboxyl groups in the basal plane (Wu et al., 2013;

Istrate et al., 2016). Graphene oxide large surface area, functional groups (hydroxyl and carboxyl groups), water dispersing properties and easy modified, it has some effective adsorption properties against toxic ions (Novoselov et al., 2004; Xia et al., 2015). The structures of graphene oxide (GO) and reduced graphene oxide (rGO) are shown in Fig. 3.

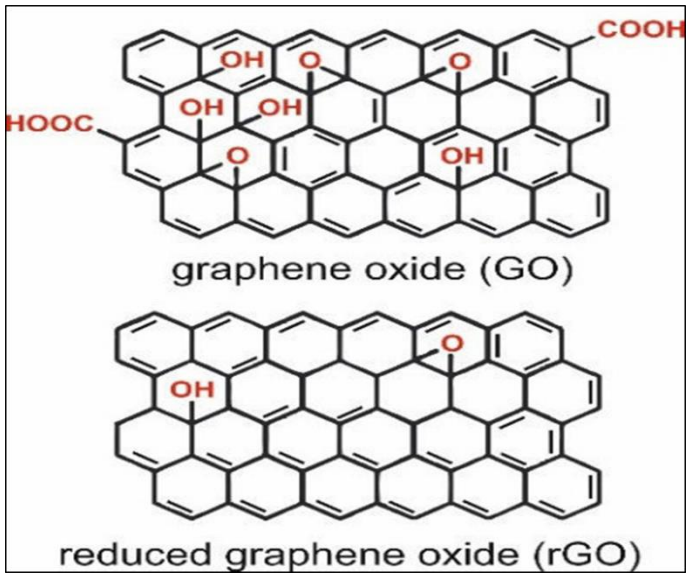

Figure 3. Molecular structures of graphene oxide (GO) and reduced graphene oxide (rGO) (Tadyszak et al., 2018; Carneiro et al., 2019; Raffone et al., 2019).

Toxic chemicals are used in the production of graphene oxide and toxic gases are produced during the experiment (Marcano et al., 2010). In the Hummers method, graphite is subjected to a reaction with chemicals such as potassium permanganate, which has strong oxidation properties and concentrated sulfuric acid (Guo et al., 2011; Yoon et al., 2017). The Hummers method is the most extensive method used in the preparation of graphene oxide.

A standard graphene oxide (GO) product preparation by this method, on average 1 nm thick and lateral dimensions on the other hand, it consists of thin graphene oxide flakes of 1 μm (Platero et al., 2017). When graphite layers are oxidized, graphene layers are opened with the effect of oxide derivatives and these layers are separated from each other by sonication (Zeng et al., 2019). With this method, non-hydrophilic graphite is converted into hydrophilic and dispersed graphene oxide (Ensafi et al., 2016; Wang et al., 2018). The physical and chemical methods used in graphene synthesis are shown in Fig. 4.

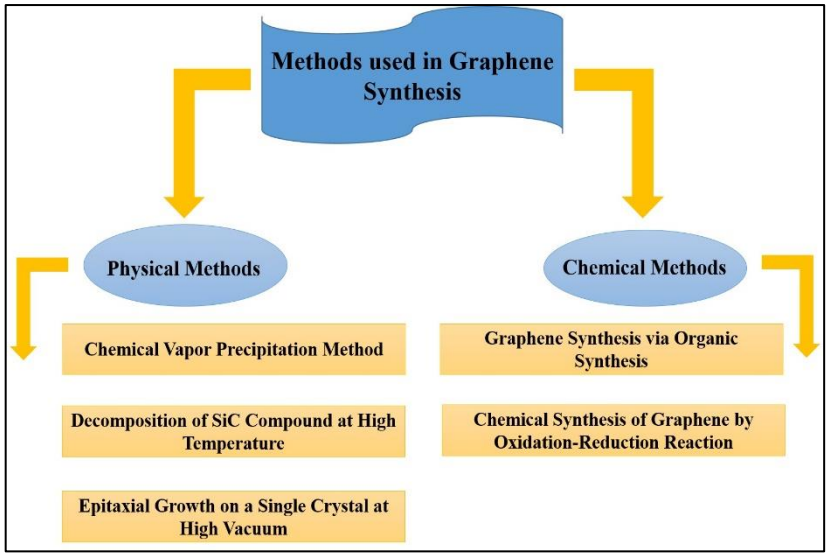

Figure 4. Physical and chemical methods used in graphene synthesis (Pei et al., 2010; Wakeland et al., 2010; Konios et al., 2014).

Graphene oxide has some hydrophilic properties due to the functional groups in its structure. These properties reduce the conductivity of graphene oxide, thus causing limitations in electronic applications (Chen et al., 2019a). Therefore, the functional groups of graphene

oxide are reduced it must be removed by reduction to produce reduced graphene oxide (You et al., 2020). Reduced graphene oxide (rGO) structures are obtained by reducing the different functional groups in the structure of graphene oxide using chemical, photochemical, photothermal and electrochemical methods (Zou et al., 2020). The reduced graphene oxide has different electronic and interface properties and the C/O ratio increases with the reduction of graphene oxide (Guruprasad et al., 2019). The stages of the synthesis of graphene oxide and reduced graphene oxide from graphite by Hummers method are shown in Fig. 5.

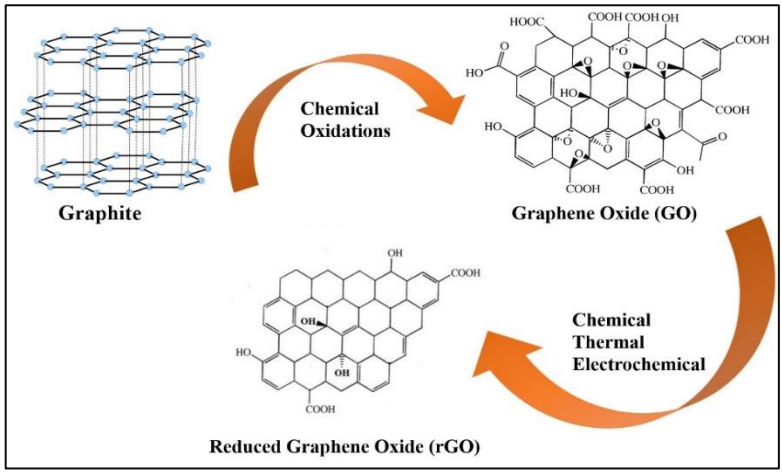

Figure 5. Stages of synthesis of graphene oxide and reduced graphene oxide from graphite by Hummers method (Ramesha et al., 2011; Erçarıkcı et al., 2014; Dağcı and Alanyalıoğlu, 2016).

Increasing the C/O ratio causes the bandgap of the graphene oxide to decrease and increases the conductivity of the sample (Cheng et al., 2018). The new nanocomposite structure formed as a result of the interaction of metal oxide structures with graphene oxide has the

properties of both metal oxide and graphene oxide (Silva et al., 2017; Vilian et al., 2018). Chemical catalysts, sensors, biosensors, super capacitors, effective electrodes and new alternative nanotechnological produces can be obtained by synthesize metal oxide/graphene oxide nanocomposites with different methods (Yan et al., 2010; Lin et al., 2018).

There are metal oxide/graphene oxide nanocomposite structures synthesized by different chemical processes in the literature. These nanocomposite structures are MoO_2/GO (Chen et al., 2019b), MnO_2/GO (Liu et al., 2021), Fe_3O_4/GO (Chien et al., 2020), CeO_2/rGO (Yao et al., 2016), MoS_2/rGO (Pytlakowska et al., 2020), $MgFe_2O_4$/GO (Hwa et al., 2020), Cu_2O/PANI/rGO (Liu et al., 2018b).

2. PREPARATION METHODS OF METAL OXIDE/CLAY AND METAL OXIDE/GRAPHENE OXIDE NANOCOMPOSITES

2.1. Sol-Gel Method

In general definition, the sol-gel method is the synthesis of an inorganic complex by a chemical reaction at a low temperature in a suitable solvent. Inorganic complex can also be formed by vapor phase or high temperature processes such as melting (Shao et al., 2014). The sol-gel process is the process by which organometal compounds, usually alkoxides form the final solid produce in solution. The resulting produce may be a high surface area aerogel or nanoparticle (Choi et al., 2013). An advantage of the sol-gel method is that the process can be carried out at room conditions. This advantage

of the process is that it allows the synthesis of materials with different functional properties (Athanassiou et al., 2010).

The sol-gel process also to the formation of an amorphous complex in contrast to the crystallization process from a solution. In this method, it includes all the methods that the gelation of colloidal solutions and the formation of a solid phase (Pappas et al., 2008). Sol-gel method is mostly used in the synthesis of oxide gels. In this process, one or more compositions must have the effective properties of the sol or gel (Chandradass and Balasubramanian, 2006). Sol is a stable suspension of colloidal solid particles in a liquid. These solid particles must be small enough when moving from dispersion forces greater than gravity (Randall et al., 2011).

The dispersion state of colloidal particles in a liquid consisting of solid particles with a diameter between 1-100 nm is named to "sol". In the same solution, substances with a complex structure with submicron size pores and an average length of more than 1 μm are named to "gels" (Nistico et al., 2017). The molecules that make up the gel are connected to each other by weak or strong bonds, forming complex textures that contain liquid between the spaces (Puetz and Aegerter, 2004). Therefore, a non-aqueous phase is formed which is formation by the combination of molecules in the liquid medium (Gill et al., 2018). The different chemical structures of the reaction starting materials determine the type of solvent to be used in the Sol-Gel process (Silahua-Pavon et al., 2019). These solvents may be water, alcohol or alkyl halides. In the production of metal oxides, water is

used as a solvent and in metal alkoxides, alcohols are used as a solvent (Lepry and Nazhat, 2015).

The gel formation of the alkoxide precursor as a result of a series of hydrolysis and condensation reactions forms the basis of the chemistry of the sol-gel process (Lukowiak et al., 2013). By supporting this process with acid or base catalysts, products with different physical properties of hydrolysis kinetics are obtained. The selection of starting material and catalyst varies according to the effective properties of the final produce (Fan et al., 2014). In the sol-gel process, a solution is obtained by mixing the starting gel materials (nitrates or hydroxides) with a certain concentration of catalyst and solvent for the synthesis of metal powder (Delben et al., 2013).

By mixing the synthesized solution, cross bonds are formed between the polymer chains. As a result of the reactions, a complex molecular structure is formed (Maeda et al., 2013). The formation of various complex structures by the sol-gel process is shown in Fig. 6.

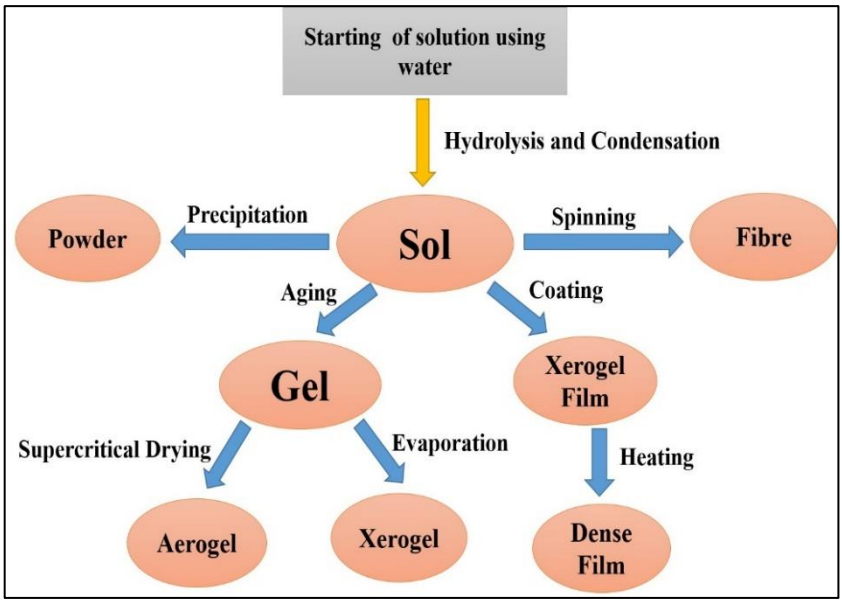

Figure 6. Diagram showing the formation of various complex structures by the sol-gel process (Yea et al., 2017; Sharma et al., 2018).

Silicon alkoxides have a very weak tendency to reaction and reaction very slowly. Therefore, the hydrolysis and condensation reaction rates of silicon alkoxides should be increased with the supporting of an acid or base catalyst (Cotolan et al., 2016). Transition metal alkoxides are generally more reactive than silicon. In order to slow and control the speedy condensation of transition metal alkoxides, they must be complexed with a suitable organic ligand before sol-gel reactions (Astinchap et al., 2016). Theoretically, almost all of the porous metal oxides used in the heterogeneous catalysis such as SiO_2, Al_2O_3, TiO_2, ZrO_2 can be synthesized by the sol-gel process (Sreethawong et al., 2013). Initiator salts generally used in the preparation of metal oxides

by the sol-gel method are metal-organic compounds known as metal alkoxides (Danks et al., 2016).

2.1.1. The Phases of the Sol-Gel Method

Sol-Gel process consists of alkoxide hydrolysis, peptidization and polymerization, gel synthesis and calcination/sintering phases. The reaction stages of sol-gel chemistry are to preparation the solution of the starting material in a certain solution and to obtained a homogeneous mixture as a result of the reaction of the necessary chemicals according to the synthesized material (Debecker et al., 2013; Brinker and Scherer, 2013). In addition, it is the conversion of the solution into gel as a result of hydrolysis and condensation reactions and the conversion of the gel formed into the desired produced with appropriate processes (Yu et al., 2012). A metal alkoxide, which is a starting material, reaction with tetra ethoxysilane and water to hydrolysis. As a result of hydrolysis, silanol and ethyl alcohol are formation (Song et al., 2018). Four moles of water are consumed in the all reaction for hydrolysis to occur in all alkoxy groups. The formed tetrahedral silica [$Si(OH)_4$] gives condensation reaction siloxane bonds are formed. The condensation reaction happens as water or alcohol condensation (Zhang et al., 2016). Colloidal particles behavior as ‘sol’ when sufficient Si-O-Si bonds are formation during simultaneous hydrolysis and polycondensation reactions. The size of the particles in the sol and the degree of cross bonds between the particles primarily depend on the water/alkoxide ratio and the temperature and mixing rate in the reaction medium

(Ogawa et al., 2003). Colloidal particles and condensed silica species in the reaction medium are effectively bonded to form a three dimensional complex (Wu et al., 2017). The physical properties of this complex structure depending on the size of the particles and the degree of cross bonds that be formed between the particles. During gelation, the viscosity of the gel increases rapidly (Lichtenberger and Schubert, 2010). The phases of the gel formation process are shown in Fig. 7.

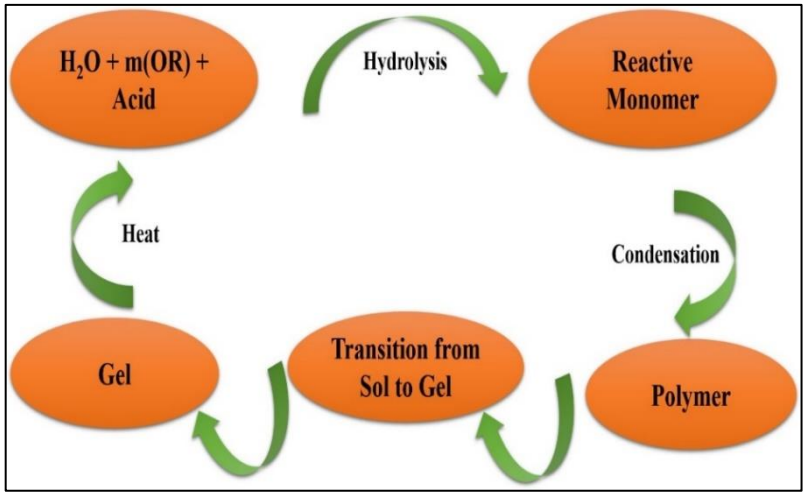

Figure 7. The phases of the gel formation process (Livage and Sanchez, 1992; Chen and Mao, 2007; Sharma et al., 2018).

Peptidization is the dispersion of precipitation substances under the action of a solvent. A sol is prepared by dispersing these residues. Preferred substances in peptidization are electrolytes (Kurajica, 2019). Electrolytes make the colloidal particles ion-charged. The reason for charging is that colloidal particles can be found stable once they become charged (Mandic and Kurajica, 2015). During the drying

process of the gels, the liquid phase between the pores is separated. In this process, high capillary stress occurs and an undesirable in this way cracks and cleavages occur, which will disrupt the porous structure of the gel (Dalvandi and Ghasemi, 2013). Surfactants are preferred to decrease capillary stress. With the effect of the surfactants used the volume of the pores can be increased or the hyper critical drying method can be applied (Bagheri et al., 2013).

During the dehydration of the gel, the gel formed is heated to a certain temperature under vacuum to removal non-reaction free silanol (Si-OH) groups in the pores. In this case, stable gels with chemical properties can be synthesized (Kakihana, 1996). During the condensation of the gels, the porous structure of the gel, which is kept at high temperatures, decreases and a complex gel structure is formed (Alvarez et al., 2017). The condensation temperature depends on the three-dimensional complex structure and surface area of the gel. Alkoxide gels can be condensation at temperatures such as 1000 ^{o}C (Dave and Chaturvedi, 2011).

2.1.2. Advantages and Disadvantages of the Sol-Gel Method

The structures synthesized by the Sol-Gel process method should be of high homogeneity, nm size and the crystal structure should be symmetrical (Akia et al., 2009). Although these properties have an effect on the heat treatment made as a result of Sol-Gel application, the synthesis parameters applied during the direct gel produced also have an effect (Malengreaux et al., 2017).

Among the advantages of the sol-gel process, the chemical reactions of the method can be controlled, sol-gel products are more homogeneous according to pure substances. Nanosized powder particles can be synthesized and it is also a basic process (Cecilio et al., 2004). Sol-Gel method is an energy saving process. With this method, low temperatures can be processed and materials with new properties can be obtained (Dumeignil et al., 2003). Other advantages of the sol-gel method are that special materials such as thin films can be synthesized less pollution the air (Kim et al., 2005). The disadvantages of the Sol-Gel method are that the starting materials are expensive substance loss is high during application and the chemicals used are harmful to health (Nguyen et al., 2012). In addition, the formation of carbon and hydroxyl residues in complex structures during sol-gel synthesis is an undesirable disadvantage (Tokudome et al., 2007).

2.2. Hydrothermal Method

The basis of the hydrothermal method depends on geological studies. The term "hydrothermal" was first used in the mid-19th century by the English geologist Roderick Murchison (1792-1871) to describe the formation of minerals in thermal water solutions arising from cold magma (Alshammari and Hellgardt, 2017). In recent years, extensive studies have been carried out to examine the synthesis of hybrid materials, the development of new hydrothermal processes and the reaction mechanism (Biller et al., 2015). The hydrothermal process is defined as a heterogeneous reaction that occurs to ensure the

dissolution and recrystallization of materials that cannot be dissolved under normal conditions with the support of high pressure and temperature controlled aqueous solutions (Danso-Boateng et al., 2015; Elliott et al., 2015).

The hydrothermal method is carried out by placing the starting materials and solvents in a closed container and heating them to the determined pressure and desired temperatures (Alper et al., 2019; Azzaz et al., 2020). If water is preferred as the solvent it is named the hydrothermal method, if alcohol or another organic solvent is preferred it is named the solvothermal method (Berge et al., 2015). Hydrothermal process is the crystallization of reagents in aqueous solution at high pressure (>1 atm) and high temperature (>100 ^{o}C) in a closed system (Libra et al., 2011; Zhuang et al., 2017). A different definition of the hydrothermal synthesis method is the crystal synthesis process, depending on the solubility of substances in high pressure and high temperature water (Tay et al., 2009; He et al., 2013). The initial reagents do not fully dissolve in the solution, it is possible to make the experiments by controlling different parameters such as temperature and pH (Passos et al., 2015; Obeid et al., 2019).

The need for expensive autoclave systems in the hydrothermal method is an important disadvantage for this process (Tran, 2016; Bhuvaneshwari and Gopalakrishnan, 2016). However, controlling the chemical mechanism of this process, providing better homogeneity compared to the reagents, not requiring high temperatures and processes such as calcination are among the important advantages

(Kannaki et al., 2012; Hussain et al., 2019). The diagram of the parts of the autoclave used in the hydrothermal process is given in Fig. 8.

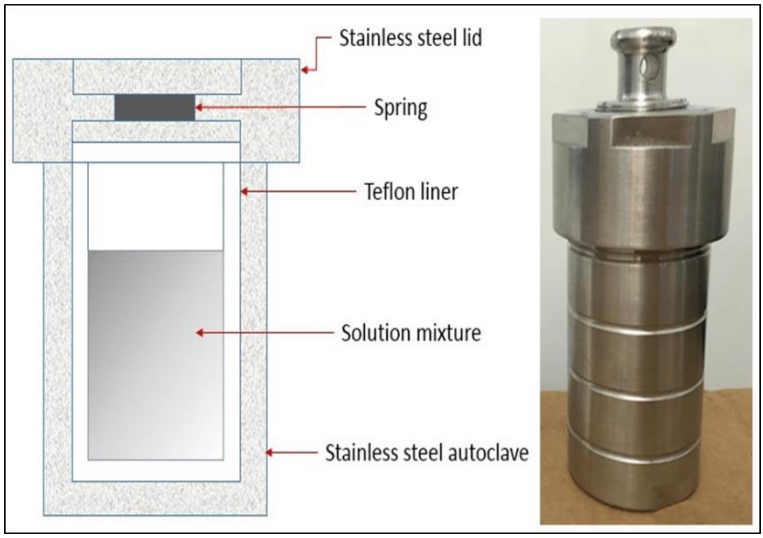

Figure 8. Diagram representation of autoclave used in hydrothermal process (Byrappa and Yoshimura, 2001; Zou et al., 2006; Asim et al., 2014).

The hydrothermal method is a very interesting method for the synthesis of nanomaterials with perfect crystal structure, since the reaction temperature is lower than 200 ^{o}C (Sim et al., 2007; Huang et al., 2010). The synthesis method carried out in solution allows obtaining a very high quality product without impurities (Sui et al., 2013). In the hydrothermal method, the particle size and morphology of the obtained product can be controlled by change the experimental conditions (Peterson et al., 2008; Reza et al., 2014). This process allows the material to be synthesized in the desired crystal structure it is a convenient method (Qi et al., 2014). The schematic representation of the stages of the hydrothermal synthesis method is shown in Fig. 9.

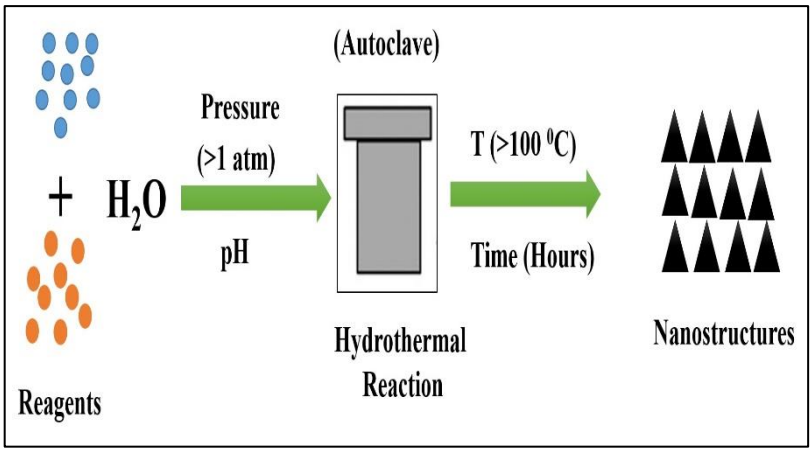

Figure 9. Schematic representation of the stages of the hydrothermal synthesis method (Yu et al., 2014; Kesavan et al., 2020).

In addition, the synthesis of nano sized particles in a completely closed system prevents the decrease in the amount of solvents over time (Escala et al., 2013).

In the hydrothermal process, the synthesis temperature is very important to control the chemical reaction. Because the temperature increase can increase the number of collisions in the solution (Chang and Hu, 2006; Khaleed et al., 2016).

2.3. Microemulsion Method

Systems with dispersion of a liquid in another liquid and containing micelles are named emulsions. Microemulsions, which are a special type of emulsions, have a thermodynamically stable structure (Eastoe et al., 2006; Chu et al., 2013). Microemulsion system, dispersed liquid droplets inside they are systems with a diameter of less than 100 nm and a homogeneous appearance in structure (Capek, 2004).

In general, the particles in the microemulsion show spherical or spherical like precipitation (Lin and Yates, 2005). Unlike these structures, in elliptical, hexagonal or cylindrical structures obtaining is possible (Li et al., 2009; Abazari et al., 2014). The shape of the micelle formed depends on the molecular geometry of the surfactants, their polarity, their concentration in the solution, parameters such as temperature and pH (Bai et al., 2013). When the forces in the formation of micelle are examined, micelles can only form if the surfactant concentration is above the critical micelle concentration and the ambient temperature is above the critical micelle temperature (Sanchez-Dominguez et al., 2015). When micelles are examined thermodynamically, they are systems that form spontaneously as a result of the equilibrium between entropy and enthalpy (Bai et al., 2013).

2.4. Microwave Heating Method

Microwave heating is emerging as one of the most attractive alternative technologies in the pyrolysis process (Gerbec et al., 2005). Microwave pyrolysis not only overcomes the disadvantages of traditional pyrolysis methods such as slow heating, but also improves the quality of pyrolysis end products (Maitani et al., 2016). The microwave heating process provides important savings in processing time and energy (Xia et al., 2009).

To start heating the material in microwave heating is at a higher temperature than the surrounding area, unlike the conventional heating process, where the conventional furnace space must reach it is

operating temperature (Tong et al., 2013; Gao et al., 2017). As a result, microwave heating facilitates reactions involving solid reagents and increases the efficiency of reactions occurring in the environment, such as homogeneous reactions in the gas phase, compared to conventional heating (Mushtaq et al., 2014; Mao et al., 2018). In addition, low temperatures in the microwave space can be useful for condensing the final pyrolysis vapors (Xie et al., 2016; Zhang et al., 2017). Microwave heating is the transfer of microwave energy to an electromagnetic field it exhibits higher heating rates because it is transmitted directly to the material through molecular interaction and does not take time to heat the ambient space (Lidstrom et al., 2001; Bu et al., 2013).

2.5. Electrochemical Synthesis Method

The electrochemical synthesis method is formed by passing an electric current between two or more electrodes separated by an electrolyte. Synthesis occurs at the electrolyte-electrode interface (Therese and Kamath, 2000; Pang et al., 2005). Electrochemical synthesis occurs within the electric double layer, which has a very high potential gradient and near the electrode (Buama et al., 2017). Under electrochemical conditions, reactions often synthesize products that cannot be obtained by a chemical synthesis. The resulting product is formed on the electrode surface as a thin film or a coating (Avramova et al., 2006; Casella and Di Fonzo, 2011).

Electrochemical synthesis is a technique limited by the boiling point of the electrolyte. The boiling point of the electrolyte can be increased

by the addition of dissolved salt (Kang et al., 2015). Electrochemical synthesis is an oxidation or reduction reaction. By fine calibration the applied cell potential, the oxidizing or reducing power is constantly changed, bringing advantages that cannot be achieved by chemical synthesis (Chen et al., 2006; Han et al., 2014). However, this process has some disadvantages. Electrochemical synthesis can often produce amorphous solid products whose structural characterization is imprecise (Zhang et al., 2001; Karuppuchamy et al., 2006). Therefore, electrodeposition can only be performed on conductive and semiconductor substrates. In a general electrochemical synthesis, the reactants dissolved in the electrolyte are deposited as a solid product (Marchesi et al., 2015; Oliveira et al., 2016). Therefore, the effect of the reactant decreases as the reaction progresses. Two important parameters that determine the synthesis products of the electrochemical reaction are the deposition current and the cell potential (Wessels et al., 2006; Peng et al., 2012; Yang et al., 2013).

2.6. Sonochemical Synthesis Method

In high energy sonochemical reactions, nanostructures are formed by the collapse, growth and shaping of chemical components in a liquid by ultrasonic effect without molecular reaction (Gedanken et al., 2004; Suslick and Bang, 2010). It has acoustic cavitation with a temperature of 5000°C and a pressure of 1700 atm formed in the liquid (Yayapao et al., 2013). In structures formed as a result of the sonochemical synthesis, the liquid film at low pressure has a

temperature of about 2000°C (Abulizi et al., 2014; Anandan et al., 2014).

Under the influence of this temperature, nanostructured deposition of chemicals in the liquid film occurs (Ullah et al., 2017). Nanostructured particles for catalytic applications are sonochemically synthesized using volatile organometallic starting reagents (Jamshidi et al., 2016; Mosleh et al., 2018). Although these nanostructured particles have a surface area, they are more precious than commercial powders. Sonochemical synthesis is generally carried out in an inert gas atmosphere (Thompson and Doraiswamy, 1999; Jiang et al., 2004).

3. APPLICATIONS OF METAL OXIDE/CLAY AND METAL OXIDE/GRAPHENE OXIDE NANOCOMPOSITES

Semiconductor metal oxide technologies are of great importance to solve the world's energy needs and environmental problems caused by the intense consumption of non-renewable fossil fuels (Chae et al., 2003; Akhavan and Ghaderi, 2009). Therefore, hybrid nanocomposite structures synthesized with metal oxide support have gained great popularity in recent years (Sakaushi et al., 2010; Gordon et al., 2012). These hybrid nanocomposite structures are preferred because of their low cost, chemical stability, high catalytic activity and biocompatibility (Vinodgopal et al., 2010; Morales-Torres et al., 2012).

Metal oxide/graphene oxide nanocomposites are being investigated for applications such as solar cells, lithium-ion batteries, sensors,

photocatalytic reduction of carbon dioxide, development of self-cleaning surfaces and antibacterial activities (Zhang et al., 2013b; Taheriniya and Behboodi, 2016). Hybrid metal oxide nanostructures have been intensively investigated in recent years due to their various application areas such as optics, electronics, magnetic devices, catalysts, adsorbent and sensors (Lambert et al., 2009; Jadhav et al., 2013). Metal oxide/clay nanocomposites are becoming attractive as chemical catalysts because they have large surface areas (Badre et al., 2007; Fterich et al., 2016). In addition, metal oxide hybrid structures are frequently preferred in degradation processes with the effect of light according to their semi conductivity status (Titirici et al., 2006; Duo et al., 2017).

4. CONCLUSION

Modified clay, metal oxide/clay and metal oxide/graphene oxide nanocomposites have been used as composite materials efficiently and effectively to removal harmful pollutants from wastewater. However, there are certain disadvantages in terms of minimum amount of harmful pollutants removal, cost effect and efficiency of nanocomposite materials.

Therefore, advanced research has been carried out to development effective and complex composites for wastewater treatment. Recently, researchers have begun to produce new nano sized composite materials with different properties, large surface area and multi-functional. New materials have begun to be synthesized by using

materials such as clay, metal oxide and reduced graphene oxide with effective properties.

ACKNOWLEDGEMENTS

The authors would like to express special thanks to the University of Gumushane for supports.

REFERENCES

Abazari, R., Mahjoub, A. R., Saghatforoush, L. A., Sanati, S. (2014). Characterization and optical properties of spherical WO_3 nanoparticles synthesized via the reverse microemulsion process and their photocatalytic behavior. Materials Letters, Vol. 133, pp 208-211.

Abulizi, A., Yang, G. H., Zhu, J. J. (2014). One-step simple sonochemical fabrication and photocatalytic properties of Cu_2O-rGO composites. Ultrasonics Sonochemistry, Vol. 21, pp 129-135.

Açışlı, Ö. (2014). Monomeric and micellar adsorption of quaternary ammonium salts. Doctoral Thesis, Institute of Science and Technology, Erzurum.

Ai, L., Zhou, Y., Jiang, J. (2011). Removal of methylene blue from aqueous solution by montmorillonite/$CoFe_2O_4$ composite with magnetic separation performance. Desalination, Vol. 266, pp 72-77.

Akhavan, O. and Ghaderi, E. (2009). Photocatalytic reduction of graphene oxide nanosheets on TiO_2 thin film for photo inactivation of bacteria in solar light irradiation. The Journal of Physical Chemistry C, Vol. 113, pp 20214-20220.

Akia, M., Alavi, S. M., Rezaei, M., Yan, Z. (2009). Optimizing the sol-gel parameters on the synthesis of mesostructure nanocrystalline γ-Al_2O_3. Microporous and Mesoporous Materials, Vol. 122, pp 72-78.

Alexandre, M. and Dubois, P. (2000). Polymer layered silicate nanocomposites: Preparation properties and uses of new class of materials. Materials Science Engineering, Vol. 28, pp 1-63.

Alper, K., Tekin, K., Karagoz, S. (2019). Hydrothermal liquefaction of lignocellulosic biomass using potassium fluoride-doped alumina. Energy Fuels, Vol. 33, pp 3248-3256.

Alshammari, Y. M. and Hellgardt, K. (2017). CFD analysis of hydrothermal conversion of heavy oil in continuous flow reactor. Chemical Engineering Research and Design, Vol. 117, pp 250-264.

Alvarez, S. Y. M., Mar, J. L. G., Palomino, G. T., Alejandro, F. M., Ramirez, A. H., Reyes, L. H. (2017). UV and visible activation of Cr (III)-doped TiO_2 catalyst prepared by a microwave-assisted sol-gel method during MCPA degradation. Environmental Science and Pollution Research, Vol. 24, pp 12673-12682.

Anandan, S., Sivasankar, T., Lana-Villarreal, T. (2014). Synthesis of TiO_2/WO_3 nanoparticles via sonochemical approach for the photocatalytic degradation of methylene blue under visible light illumination. Ultrasonics Sonochemistry, Vol. 21, pp 1964-1968.

Araujo, A. L. P. D., Gimenes, M. L., Barros, M. A. S. D. D., Silva, M. G. C. D. (2013). A kinetic and equilibrium study of zinc removal by Brazilian bentonite clay. Materials Research, Vol. 16, No. 1, pp 128-136.

Arora, A., Choudhary, V., Sharma, D. K. (2011). Effect of clay content and clay/surfactant on the mechanical, thermal and barrier properties of polystyrene/organoclay nanocomposites. Journal of Polymer Research, Vol. 18, pp 843-857.

Asim, N., Ahmadi, S., Alghoul, M. A., Hammadi, F. Y., Saeedfar, K., Sopian, K. (2014). Research and development aspects on chemical preparation techniques of photoanodes for dye sensitized solar cells. International Journal of Photoenergy, https://doi.org/10.1155/2014/518156.

Astinchap, B., Moradian, R., Nasseri-Tekyeh M. (2016). Investigating the optical properties of synthesized ZnO nanostructures by sol-gel: The role of zinc precursors and annealing time. Optik-International Journal for Light and Electron Optics, Vol. 127, pp 9871-9877.

Athanassiou, E. K., Grass, R. N., Stark W. J. (2010). Chemical aerosol engineering as a novel tool for material science: from oxides to salt and metal nanoparticles. Aerosol Science and Technology, Vol. 44, pp 161-172.

Auta, M. and Hameed, B. H. (2013). Acid modified local clay beads as effective low-cost adsorbent for dynamic adsorption of methylene blue. Journal of Industrial and Engineering Chemistry, Vol. 19, pp 1153-1161.

Avramova, I., Stoychev, D., Marinova, T. (2006). Characterization of a thin CeO_2-ZrO_2-Y_2O_3 films electrochemical deposited on stainless steel. Applied Surface Science, Vol. 253, pp 1365-1370.

Azzaz, A. A., Jeguirim, M., Kinigopoulou, V., Doulgeris, C., Goddard, M. L., Jellali, S., Matei Ghimbeu, C. (2020). Olive mill wastewater: from a pollutant to green fuels, agricultural and water source and bio-fertilizer e hydrothermal carbonization. Science of the Total Environment, Vol. 733, pp 139314.

Badre, C., Pauporte, T., Turmine, M., Lincot, D. (2007). A ZnO nanowire array film with stable highly water-repellent properties. Nanotechnology, Vol. 18, pp 365705.

Bagheri, S., Shameli, K., Hamid, S. B. A. (2013). Synthesis and characterization of anatase titanium dioxide nanoparticles using egg white solution via sol-gel method. Journal of Chemistry, Vol. 848205, pp 5-10.

Bai, G., Dai, H., Deng, J., Liu, Y., Qiu, W., Zhao, Z., Li, X., Yang, H. (2013). The microemulsion preparation and high catalytic performance of mesoporous NiO nanorods and nanocubes for toluene combustion. Chemical Engineering Journal, Vol. 219, pp 200-208.

Bergaya, F., Theng, B. K. G., Lagaly, G. (2006). Handbook of Clay Science, First Edition. Elsevier.

Berge, N. D., Li, L., Flora, J. R. V., Ro, K. S. (2015). Assessing the environmental impact of energy production from hydrochar generated via hydrothermal carbonization of food wastes. Waste Management, Vol. 43, pp 203-217.

Beura, R. and Thangadurai, P. (2017). Structural, optical and photocatalytic properties of graphene-ZnO nanocomposites for varied compositions. Journal of Physics and Chemistry of Solids, Vol. 102, pp 168-177.

Bhattacharyya, K. G. and Gupta, S. S. (2006). Kaolinite, montmorillonite and their modified derivatives as adsorbents for removal of Cu (II) from aqueous solution. Separation and Purification Technology, Vol. 50, No. 3, pp 388-397.

Bhattacharyya, K. G. and Gupta, S. S. (2008). Kaolinite and montmorillonite as adsorbents for Fe (III), Co (II) and Ni (II) in aqueous medium. Applied Clay Science, Vol. 41, No. 1, pp 1-9.

Bhuvaneshwari, S. and Gopalakrishnan, N. (2016). Hydrothermally synthesized Copper Oxide (CuO) super structures for ammonia sensing. Journal of Colloid and Interface Science, Vol. 480, pp 76-84.

Biller, P., Sharma, B. K., Kunwar, B., Ross, A. B. (2015). Hydroprocessing of bio-crude from continuous hydrothermal liquefaction of microalgae. Fuel, Vol. 159, pp 197-205.

Brinker, C. J., Scherer, G. W. (2013). Sol-gel Science: The physics and chemistry of sol-gel processing. Academic press.

Bu, I. Y. Y. (2013). Rapid synthesis of ZnO nanostructures through microwave heating process. Ceramics International, Vol. 39, pp 1189-1194.

Buama, S., Junsukhon, A., Ngaotrakanwiwat, P., Rangsunvigit, P. (2017). Validation of energy storage of TiO_2NiO/TiO_2 film by electrochemical process and photocatalytic activity. Chemical Engineering Journal, Vol. 309, pp 866-872.

Byrappa, K. and Yoshimura, M. (2001). Handbook of hydrothermal technology, A technology for crystal growth and material processing. New Jersey, Noyes.

Cao, Y. C., Fu, Z., Wei, W., Zou, L., Mi, T., He, D., Yan, C., Liu, X., Zhu, Y., Chen, L., Sun, Y. (2015). Reduced graphene oxide supported titanium dioxide nanomaterials for the photocatalysis with long cycling life. Applied Surface Science, Vol. 355, pp 1289-1294.

Capek, I. (2004). Preparation of metal nanoparticles in water-in-oil (w/o) microemulsions. Advances in Colloid and Interface Science, Vol. 110, pp 49-74.

Carneiro, P., Morais, S., Pereira, M. C. (2019). Nanomaterials towards biosensing of alzheimer's disease biomarkers. Nanomaterials, Vol. 9, pp 1663.

Casella, I.G. and Di Fonzo, D.A. (2011). Anodic electrodeposition of cobalt oxides from an alkaline bath containing Co-gluconate complexes on glassy carbon.

An electro analytical investigation. Electrochimica Acta, Vol. 56, pp 7536-7540.

Cecilio, A. A., Pulcinelli, S. H., Santilli, C. V., Maniette, Y. (2004). Improvement of the Mo/TiO_2-Al_2O_3 catalyst by the control of the Sol-Gel synthesis. Journal of Sol-gel Science and Technology, Vol. 31, pp 87-93.

Chae, S. Y., Park, M. K., Lee, S. K., Kim, T. Y., Kim, S. K., Lee, W. I. (2003). Preparation of size-controlled TiO_2 nanoparticles and derivation of optically transparent photocatalytic films. Chemistry of Materials, Vol. 225, pp 34-51.

Chandradass, J. and Balasubramanian, M. (2006). Effect of magnesium oxide on sol-gel spun alumina and alumina-zirconia fibres. Journal of the European Ceramic Society, Vol. 26, pp 2611-2617.

Chang, K. H. and Hu, C. C. (2006). Coalescence inhibition of hydrous RuO_2 crystallites prepared by a hydrothermal method. Applied Physics Letters, Vol. 88, No. 19, pp 193102.

Chang, J., Ma, J., Ma, Q., Zhang, D., Qiao, N., Hu, M., Ma, H. (2016). Adsorption of methylene blue onto Fe_3O_4/activated montmorillonite nanocomposite. Applied Clay Science, Vol. 119, pp 132-140.

Chen, S., Paulose, M., Ruan, C., Mor, G. K., Varghese, O. K., Kouzoudis, D., Grimes, C. A. (2006). Electrochemically synthesized CdS nanoparticle-modified TiO_2 nanotube-array photoelectrodes: Preparation, characterization, and application to photoelectrochemical cells. Journal of Photochemistry and Photobiology A: Chemistry, Vol. 177, pp 177-184.

Chen, X. and Mao, S. S. (2007). Titanium dioxide nanomaterials: synthesis, properties, modifications and applications. Chemical Reviews, Vol. 107, pp 2891-2959.

Chen, D., Feng, H., Li, J. (2012). Graphene oxide: preparation, functionalization, and electrochemical applications. Chemical Reviews, Vol. 112, No. 11, pp 6027-6053.

Chen, Y., Xu, B., Xu, J., Wen, J., Hua, T., Kan, C.W. (2019a). Graphene-based in-planar supercapacitors by a novel laser-scribing, in-situ reduction and

transfer-printed method on flexible substrates. J. Power Sources. Vol. 420, pp 82-87.

Chen, J., Sun, K., Zhang, Y., Wu, D., Jin, Z., Xie, F., Zhao, X., Wang, X. (2019b). Plasmonic MoO_2 nanospheres assembled on graphene oxide for highly sensitive SERS detection of organic pollutants. Analytical and Bioanalytical Chemistry, Vol. 411, pp 2781-2791.

Cheng, H., Zhou, X., Gao, A., Yi, F., Shu, D., Song, X., Zeng, R., He, C., Li, S., Zeng, D. (2018). Supermolecule polymerization derived porous nitrogen-doped reduced graphene oxide as a high-performance electrode material for supercapacitors. Electrochimica Acta, Vol. 292, pp 20-30.

Chien, H. J., Lai, S. M., Wang, W. C., Lin, H. Y., Juang, Y. M., Lai, P. S., Lai, C. C. (2020). Preparation and comparison of Fe_3O_4@graphene oxide nanoclusters for analysis of glimepiride in urine by surface-assisted laser desorption/ionization timeof-flight mass spectrometry. Analytical and Bioanalytical Chemistry, Vol. 412, pp 4057-4065.

Choi, J., Ide, A., Truong, Y. B., Kyratzis, I. L., Caruso, R.A. (2013). High surface area mesoporous titanium–zirconium oxide nanofibrous web: a heavy metal ion adsorbent. Journal of Materials Chemistry A, Vol. 1, No. 19, pp 5847-5853.

Chowdhury, I., Duch, M. C., Mansukhani, N. D., Hersam, M. C., Bouchard, D. (2014). Interactions of graphene oxide nanomaterials with natural organic matter and metal oxide surfaces. Environmental Science and Technology, Vol. 48, pp 9382-9390.

Chu, D. Q., Mao, B. G., Wang, L. M. (2013). Microemulsion-based synthesis of hierarchical 3D flowerlike CuO nanostructures. Materials Letters, Vol. 105, pp 151-154.

Cotolan, N., Rak, M., Bele, M., Cor, A., Muresan, L. M., Milosev, I. (2016). Sol-gel synthesis, characterization and properties of TiO_2 and Ag-TiO_2 coatings on titanium substrate. Surface and Coatings Technology, Vol. 307, pp 790-799.

Dağcı, K. and Alanyalıoğlu, M. (2016). Preparation of free-standing and flexible graphene/Ag nanoparticles/poly(pyronin-y) hybrid paper electrode for amperometric determination of nitrite. ACS Applied Materials and Interfaces, Vol. 8, pp 2713-2722.

Dalvandi, M. and Ghasemi, B. (2013). Synthesis of titanium dioxide nano-powder via sol-gel method at ambient temperature. Journal of Sol-Gel Science and Technology, Vol. 66, pp 68-72.

Danks, A. E., Hall, S. R., Schnepp, Z. (2016). The evolution of sol-gel chemistry as a technique for materials synthesis. Materials Horizons, Vol. 3, pp 91-112.

Danso-Boateng, E., Shama, G., Wheatley, A. D., Martin, S. J., Holdich, R. G. (2015). Hydrothermal carbonisation of sewage sludge: effect of process conditions on product characteristics and methane production. Bioresource Technology, Vol. 177, pp 318-327.

Dave, P. N. and Chaturvedi, S. (2011). A review on nano-TiO_2 sol-gel type synthesis and its applications. Journal of Material Science, Vol. 46, pp 3669-3686.

Debecker, D. P., Hulea, V., Mutin, P. H. (2013). Mesoporous mixed oxide catalysts via nonhydrolytic sol-gel: a review. Applied Catalysis A: General, Vol. 451, pp 192-206.

Delben, J. R. J., Pereira, K., Oliveira, S. L., Alencar, L. D. S, Hernandes, A. C., Delben, A. A. S. T. (2013). Bioactive glass prepared by sol-gel emulsion. Journal of Non-Crystalline Solids, Vol. 361, pp 119-123.

Dintcheva, N. T., Al-Malaika, S., La Mantia, F. P. (2009). Effect of extrusion and photooxidation on polyethylene/clay nanocomposites. Polymer Degradation and Stability, Vol. 94, pp 1571-1588.

Dogan, A. U., Dogan, M., Önal, M., Sarıkaya, Y., Aburub, A., Wurster, D. E. (2006). Baseline studies of the clay minerals society source clays: specific surface area by the Brunauer, Emmett, Teller (BET) method. Clays and Clay Minerals, Vol. 54, pp 62-66.

Dos Anjos, V. E., Rohwedder, J. R., Cadore, S., Abate, G., Grassi, M. T. (2014). Montmorillonite and vermiculite as solid phases for the preconcentration of trace elements in natural waters: adsorption and desorption studies of As,

Ba, Cu, Cd, Co, Cr, Mn, Ni, Pb, Sr, V, and Zn. Applied Clay Science, Vol. 99, pp 289-296.

Dukic, A. B., Kumric, K. R., Vukelic, N. S., Dimitrijevic, M. S., Bascarevic, Z. D., Kurko, S. V., Matovic, L. L. (2015). Simultaneous removal of Pb^{2+}, Cu^{2+}, Zn^{2+} and Cd^{2+} from highly acidic solutions using mechano chemically synthesized montmorillonite-kaolinite/TiO_2 composite. Applied Clay Science, Vol. 103, pp 20-27.

Dumeignil F., Sato K., Imamura M., Matsubayashi N., Payen E., Shimada H. (2003). Modification of structural and acidic properties of sol-gel prepared alumina powders by changing the hydrolysis ratio. Applied Catalysis A: General, Vol. 241, pp 319-329.

Duo, S., Li, Y., Liu, Z., Zhong, R., Liu, T., Xu, H. (2017). Preparation of ZnO from 2D nanosheets to diverse 1D nanorods and their structure, surface area, photocurrent, optical and photocatalytic properties by simple hydrothermal synthesis. Journal of Alloys and Compounds, Vol. 695, pp 2563-2579.

Eastoe, J., Hollamby, M. J., Hudson, L. (2006). Recent advances in nanoparticle synthesis with reversed micelles. Advances in Colloid and Interface Science, Vol. 128, No. 130, pp 5-15.

Elliott, D. C., Biller, P., Ross, A. B., Schmidt, A. J., Jones, S. B. (2015). Hydrothermal liquefaction of biomass: Developments from batch to continuous process. Bioresource Technology, Vol. 178, pp 147-156.

Ensafi, A. A., Alinajafi, H. A., Jafari-Asl, M., Rezaei, B., Ghazaei, F. (2016). Cobalt ferrite nanoparticles decorated on exfoliated graphene oxide, application for amperometric determination of NADH and H_2O_2. Materials Science & Engineering C-Materials for Biological Applications, Vol. 60, pp 276-284.

Erçarıkcı, E., Dağcı, K., Topçu, E., Alanyalıoğlu, M. (2014). Electrochemical preparation of poly(methylene blue)/graphene nanocomposite thin films. Materials Research Bulletin, Vol. 55, pp 95-101.

Escala, M., Zumbuhl, T., Koller, C., Junge, R., Krebs, R. (2013). Hydrothermal carbonization as an energy-efficient alternative to established drying

technologies for sewage sludge: a feasibility study on a laboratory scale. Energy Fuel, Vol. 27, pp 454-60.

Fan, J. P., Kalia P, Di Silvio, L, Huang, J. (2014). In vitro response of human osteoblasts to multistep sol-gel derived bioactive glass nanoparticles for bone tissue engineering. Materials Science and Engineering C, Vol. 36, pp 206-214.

Fterich, M., Nasr, F. B., Lefi, R., Toumi, M., Guermazi S. (2016). Effect of concentration of hexamethylenetetramine in structure, microstructure and optical properties of CuO nanoparticles synthesized by hydrothermal route. Materials Science in Semiconductor Processing, Vol. 43, pp 114-122.

Gao, F. (2004). Clay/polymer composites: The story. Materials Today, Vol. 7, No. 11, pp 50-55.

Gao, Z., Zhang, H., Ao, W., Li, J., Liu, G., Chen, X., Fu, J., Ran, C., Liu, Y., Kang, Q., Mao, X., Dai, J. (2017). Microwave pyrolysis of textile dyeing sludge in a continuously operated auger reactor: Condensates and non-condensable gases. Environmental Pollution, Vol. 228, pp 331-343.

Gedanken, A. (2004). Using sonochemistry for the fabrication of nanomaterials. Ultrasonics Sonochemistry, Vol. 11, pp 47-55.

Gerbec, J. A., Magana, D., Washington, A., Strouse, G.F. (2005). Microwave-enhanced reaction rates for nanoparticle synthesis. Journal of the American Chemical Society, Vol. 127, pp 15791-15800.

Gill, J. K., Orsat, V., Kermasha, S. (2018). Screening trials for the encapsulation of laccase enzymatic extract in silica sol-gel. Journal of Sol-Gel Science and Technology, Vol. 85, No. 3, pp 657-663.

Gordon, T. R., Cargnello, M., Paik, T., Mangolini, F., Weber, R. T., Fornasiero, P., Murray, C. B. (2012). Nonaqueous synthesis of TiO_2 nanocrystals using TiF_4 to engineer morphology, oxygen vacancy concentration, and photocatalytic activity. Journal of the American Chemical Society, Vol. 134, pp 6751-6760.

Guo, K., Qian, K., Zhang, S., Kong, J. L., Yu, C. Z., Liu, B. H. (2011). Bioelectrocatalysis of NADH and ethanol based on graphene sheets modified electrodes. Talanta, Vol. 85, No. 2, pp 1174-1179.

Guruprasad, K., Maiyalagan, T., Shanmugam, S. (2019). Phosphorus-doped MoS_2 nanosheet promoted with nitrogen, sulfur dual-doped reduced graphene oxide as an effective electrocatalyst for hydrogen evolution reaction. ACS Applied Energy Materials, Vol. 2, pp 6184-6194.

Han, W., Ren, L., Qi, X., Liu, Y., Wei, Y., Huang, Z., Zhon J. (2014). Synthesis of CdS/ZnO/graphene composite with high-efficiency photoelectrochemical activities under solar radiation. Applied Surface Science, Vol. 299, pp 12-18.

Hanifah, M. F. R., Jaafar, J., Aziz, M., Ismail, A. F., Rahman, M. A., Othman, M. H. D. (2015). Synthesis of graphene oxide nanosheets via modified hummers method and its physicochemical properties, Jurnal Teknologi, Vol. 74, No. 1, pp 189-192.

Hashemian, S., Saffari, H., Ragabion, S. (2015). Adsorption of cobalt (II) from aqueous solutions by Fe_3O_4/bentonite nanocomposite. Water, Air, Soil Pollution, Vol. 226, No. 1, pp 2212.

He, C., Giannis, A., Wang, J.Y. (2013). Conversion of sewage sludge to clean solid fuel using hydrothermal carbonization: hydrochar fuel characteristics and combustion behavior. Applied Energy, Vol. 111, pp 257-266.

Hibino, H., Kageshima, H., Nagase, M. (2010). Epitaxial few-layer graphene: towards single crystal growth. Journal of Physics D-Applied Physics Vol. 43, No. 37

Hu, X., Li, C., Song, J., Zheng, S., Sun, Z. (2020). Multidimensional assembly of oxygen vacancy-rich amorphous TiO_2-BiOBr-sepiolite composite for rapid elimination of formaldehyde and oxytetracycline under visible light. Journal of Colloid and Interface Science, Vol. 574, pp 61-73.

Huang, M. F., Yu, J. G., Ma, X. F. (2004). Studies on the properties of montmorillonite-reinforced thermoplastic starch composites. Polymer, Vol. 45, No. 20, pp 7017-7023.

Huang, P., Zhang, X., Wei, J., Feng, B. (2010). ZnO hierarchical structures synthesized via hydrothermal method and their photoluminescence properties. Journal of Alloys and Compounds, Vol. 489, pp 614-619.

Hussain, S., Jacob, J., Riaz, N., Mahmood, K., Ali, A., Amin, N., Nabi, G., Isa, M., Mahmood, M. H. R. (2019). Effect Of growth temperature on catalyst free hydrothermal synthesis of crystalline SnO_2 micro-sheets. Ceramics International, Vol. 45, pp 4053-4058.

Hwa, K. Y., Ganguly, A., Tata, S. K. S. (2020). Influence of temperature variation on spinel-structure $MgFe_2O_4$ anchored on reduced graphene oxide for electrochemical detection of 4-cyanophenol. Microchimica Acta, Vol. 187, pp 633.

Istrate, O. M., Rotariu, L., Marinescu, V. E., Bala, C. (2016). NADH sensing platform based on electrochemically generated reduced graphene oxide-gold nanoparticles composite stabilized with poly(allylamine hydrochloride). Sensors and Actuators B-Chemical, Vol. 223, pp 697-704.

Jadhav, U. M., Patel, S. N., Patil, R. S. (2013). Room Temperature Deposition of Nanocrystalline CdS Thin Film by Successive Ionic Layer Adsorption and Reaction (SILAR) Method. Research Journal of Material Sciences, Vol. 1, pp 21-25.

Jamshidi, M., Ghaedi, M., Dashtian, K., Hajati, S., Bazrafshan, A.A. (2016). Sonochemical assisted hydrothermal synthesis of ZnO: Cr nanoparticles loaded activated carbon for simultaneous ultrasound-assisted adsorption of ternary toxic organic dye: derivative spectrophotometric, optimization, kinetic and isotherm study. Ultrasonics. Sonochemistry, Vol. 32, pp 119-131.

Jiang, L.P., Xu, S., Zhu, J.M., Zhang, J.R., Zhu, J.J., Chen, H.Y. (2004). Ultrasonic-assisted synthesis of monodisperse single-crystalline silver nanoplates and gold nanorings. Inorganic Chemistry, Vol. 43, pp 5877-5883.

Kakihana, M. (1996). Invited review sol-gel preparation of high temperature superconducting oxides. Journal of Sol-Gel Science and Technology, Vol. 6, pp 7-55.

Kalantari, K., Ahmad, M. B., Masoumi, H. R. F., Shameli, K., Basri, M., Khandanlou, R. (2015). Rapid and high capacity adsorption of heavy metals by Fe_3O_4/montmorillonite nanocomposite using response surface methodology: preparation, characterization, optimization, equilibrium isotherms, and adsorption kinetics study. Journal of the Taiwan Institute of Chemical Engineers, Vol. 49, pp 192-198.

Kang, D., Kim, T.W., Kubota, S.R., Cardiel, A.C., Cha, H.G., Choi, K.S. (2015). Electrochemical synthesis of photoelectrodes and catalysts for use in solar water splitting. Chemical Reviews, Vol., 115, pp 12839-12887.

Kannaki, K., Ramesh, P. S., Geetha, D. (2012). Hydrothermal synthesis of CuO Nanostructure and Their Characterizations. International Journal of Scientific & Engineering Research, Vol. 3, No. 9, pp 2229-5518.

Karuppuchamy, S., Iwasaki, M., Minoura, H. (2006). Electrochemical properties of electrosynthesized TiO_2 thin films. Applied Surface Science, Vol. 253, pp 2924-2929.

Kathiryelu, S. D., Souza, L., Dhurai, B. (2008). Nanotechnology applications in textiles. Indian Journal of Science and Technology, Vol. 1, No. 5, pp 2-9.

Kesavan, G., Nataraj, N., Chen, S. M., Lina, L.H. (2020). Hydrothermal synthesis of $NiFe_2O_4$ nanoparticles as an efficient electrocatalyst for the electrochemical detection of bisphenol A. New Journal of Chemistry, 2020, 44, 7698-7707.

Khaleed, A. A., Bello, A., Dangbegnon, J. K., Ugbo, F. U., Barzegar, F., Momodu, D. Y., Madito, M. J., Masikhwa, T. M., Olaniyan, O., Manyala, N. (2016). A facile hydrothermal reflux synthesis of $Ni(OH)_2$/GF electrode for supercapacitor application. Journal of Materials Science, Vol. 51, No. 12, pp 6041-6050.

Kim, P., Joo, J. B., Kim, H., Kim, W., Kim, Y., Song, I. K., Yi, J. (2005). Preparation of mesoporous Ni-alumina catalyst by one-step sol-gel method: control of textural properties and catalytic application to the hydrodechlorination of o-dichlorobenzene. Catalysis Letters, Vol. 104, pp 181-189.

Kim, C. H., Kim, B. H., Yang, K. S. (2012). TiO_2 nanoparticles loaded on graphene/carbon composite nanolifs by electrospinning for increased photocatalysis. Carbon, Vol. 50, No. 7, pp 2472-2481.

Kim, Y. K., Seo, H. J., Kim, S., Hwang, S. H., Park, H., Lim, S. K. (2016). Effect of ZnO electro deposited on carbon film and decorated with metal nanoparticles for solar hydrogen production. J Mater Sci Technol. Vol. 32, No. 10, pp 1059-1065.

Konios, D., Stylianakis, M. M., Stratakis, E., Kymakis, E. (2014). Dispersion behaviour of graphene oxide and reduced graphene oxide. Journal of Colloid and Interface Science, Vol. 430, pp 108-112.

Kuang, M., Zhang, J., Wang, W., Chen, J., Cao, Y., Wang, J., Ji, Z. (2019). Ternary Ag deposited TiO_2/palygorskite composites with synergistic effect for enhanced photocatalytic activity. Solid State Sciences, Vol. 97, pp 106015.

Kurajica, S. (2019). A brief review on the use of chelation agents in sol-gel synthesis with emphasis on β-diketones and β-ketoesters. Chemical and Biochemical Engineering Quarterly, Vol. 33, pp 295-301.

Lambert, T. N., Chavez, C. A., Sanchez, B., Lu, H. P., Bell, N. S., Ambrosini, A., Friedman, T., Boyle, T. J., Wheeler, D. R., Huber, D. L. (2009). Synthesis and characterization of Titania-Graphene nanocomposites. The Journal of Physical Chemistry C, Vol. 113, pp 19812-19823.

Lepry, W. C., Nazhat, S. N. (2015). Highly bioactive sol-gel derived borate glasses. Chemistry of Materials, Vol. 27, pp 4821-4831.

Li, X., He, G., Xiao, G., Liu, H., Wang, M. (2009). Synthesis and morphology control of ZnO nanostructures in microemulsions. Journal of Colloid and Interface Science, Vol. 333, pp 465-473.

Libra, J. A., Ro, K. S., Kammann, C., Funke, A., Berge, N. D., Neubauer, Y., Titirici, M. M., Fühner, C., Bens, O., Kern, J. (2011). Hydrothermal carbonization of biomass residuals: A comparative review of the chemistry, processes and applications of wet and dry pyrolysis. Biofuels, Vol. 2, pp 71-106.

Lichtenberger, R. and Schubert, U. (2010). Chemical modification of aluminium alkoxides for sol-gel processing. Journal of Materials Chemistry, Vol. 20, pp 9287-9296.

Lidstrom, P., Tierney, J., Wathey, B., Westman, J. (2001). Microwave assisted organic synthesis-A review. Tetrahedron, Vol. 57, pp 9225-9283.

Lin, J. C. and Yates, M. Z. (2005). Altering the crystal morphology of silicalite-1 through microemulsion-based synthesis. Langmuir, Vol. 21, pp 2117-2120.

Lin, Z., Liu, G., Zheng, Y., Lin, Y., Huang, Z. (2018). Three-dimensional hierarchical mesoporous flower-like TiO_2@graphdiyne with superior electrochemical performances for lithium-ion batteries. Journal of Materials Chemistry A, Vol. 6, No. 45, pp 22655-22661.

Liu, L. L., An, M. Z., Yang, P. X., Zhang, J. Q. (2015). Few-layer graphene prepared via microwave digestion reduction and its electrochemical performances in lithium ion batteries. International Journal of Electrochemical Science, Vol. 10, No. 2, 1582-1594.

Liu, R., Ji, Z., Wang, J., Zhang, J. (2018a). Microporous and mesoporous materials solvothermal synthesized Ag-decorated TiO_2/sepiolite composite with enhanced UV–vis and visible light photocatalytic activity. Microporous and Mesoporous Materials, Vol. 266, pp 268-275.

Liu, J., Yang, C., Shang, Y., Zhang, P., Liu, J., Zheng, J. (2018b). Preparation of a nanocomposite material consisting of cuprous oxide, polyaniline and reduced graphene oxide, and its application to the electrochemical determination of hydrogen peroxide, Microchimica Acta, Vol. 185, pp 172.

Liu, M. X., Zhang, H., Chen, S., Yu, Y. L., Wang, J. H. (2021). MnO_2-graphene oxide hybrid nanomaterial with oxidase-like activity for ultrasensitive colorimetric detection of cancer cells. Analytical and Bioanalytical Chemistry, Vol. 413, pp 4451-4458.

Livage, J. and Sanchez, C. (1992). Sol-gel chemistry. Journal of Non-Crystalline Solids, Vol. 145, pp 11-19.

Lukowiak, A., Lao, J., Lacroix, J., Nedelec, J. M. (2013). Bioactive glass nanoparticles obtained through sol-gel chemistry. Chemical Communications, Vol. 49, pp 6620-6632.

Lyons, J.L., Janotti, A., Van de Walle, C. G. (2013). Theory and modeling of oxide semiconductors. In: Semiconductors and Semimetals. Elsevier, pp 1-37.

Ma, Y., Lv, L., Guo, Y., Fu, Y., Shao, Q., Wu, T., Guo, Z. (2017). Porous lignin based poly (acrylic acid)/organo-montmorillonite nanocomposites: swelling behaviors and rapid removal of Pb (II) ions. Polymer, Vol. 128, pp 12-23.

Maeda, H., Nakano, Y., Kasuga, T. (2013). Preparation of $CaO\text{-}SiO_2$ glass-ceramic spheres by electro spraying combined with sol-gel method. Journal of Nanomaterials, Vol. 2013, pp 10-14.

Maitani, M. M., Tsukushi, Y., Hansen, N. D. J., Sato, Y., Mochizuki, D., Suzuki, E., Wada, Y. (2016). Low-temperature annealing of mesoscopic TiO_2 films by interfacial microwave heating applied to efficiency improvement of dye-sensitized solar cells. Solar Energy Materials & Solar Cells, Vol. 147, pp 198-202.

Malengreaux, C. M., Pirard, S. L., Leonard, G., Mahy, J. G., Herlitschke, M., Klobes, B., Hermann, R., Heinrichs, B., Bartlett, J. R. (2017). Study of the photocatalytic activity of Fe^{3+}, Cr^{3+}, La^{3+} and Eu^{3+} single-doped and co-doped TiO_2 catalysts produced by aqueous sol-gel processing. Journal of Alloys and Compounds, Vol. 691, pp 726-738.

Mandic, V. and Kurajica, S. (2015). The influence of solvents on sol-gel derived calcium aluminate. Materials Science in Semiconductor Processing, Vol. 38, pp 306-313.

Mao, S., Pu, H. H., Chen, J. H. (2012). Graphene oxide and its reduction: modeling and experimental progress. RSC Advances, Vol. 2, pp 2643-2662.

Mao, X., Kang, Q., Liu, Y., Ali, A., Ran, C., Fu, J., Deng, Z., Song, Y., Siyal, J., Dai, W. A. (2018). Microwave-assisted pyrolysis of furfural residue in a continuously operated auger reactor: Biochar characterization and analysis. Energy, Vol. 168, pp 573-584.

Marcano, D. C., Kosynkin, D. V., Berlin, J. M., Sinitskii, A., Sun, Z., Slesarev, A., Tour, J. M. (2010). Improved synthesis of graphene oxide. ACS Nano, Vol. 4, No. 8, pp 4806-4814.

Marchesi, L. F., Freitas, R. G., Spada, E. R., Paula, F. R., Goes, M. S., Garcia, J. R. (2015). Photoelectrochemical characterization of ITO/TiO_2 electrodes obtained by cathodic electrodeposition from aqueous solution. Journal of Solid State Electrochemistry, Vol. 19, pp 2205-2211.

Marcussen, H., Holm, P. E., Strobel, B. W., Hansen, H. C. B. (2009). Nickel sorption to goethite and montmorillonite in presence of citrate. Environmental Science & Technology, Vol. 43, No. 4, pp 1122-1127.

Meng, H., Zheng, S., Mi, B. (2016). Organic fouling of graphene oxide membranes and its implications for membrane fouling control in engineered osmosis. Environmental Science & Technology, Vol. 50, pp 685-693.

Meshram, S., Limaye, R., Ghodkec, S., Nigam, S., Sonawane, S., Chikate, R. (2011). Continuous flow photocatalytic reactor using ZnO-bentonite nanocomposite for degradation of phenol. Chemical Engineering Journal, Vol. 72, pp 1008-1015.

Miao, S., Liu, Z., Han, B., Zhang, J., Yu, X., Du, J., Sun, Z. (2006). Synthesis and characterization of TiO_2-montmorillonite nanocomposites and their application for removal of methylene blue. Journal of Materials Chemistry, Vol. 16, pp 579-584.

Mishra, A., Mehta, A., Kainth, S., Basu, S. (2018). Effect of g-C_3N_4 loading on TiO_2/ Bentonite nanocomposites for efficient heterogeneous photocatalytic degradation of industrial dye under visible light. Journal of Alloys and Compounds, Vol. 764, pp 406-415.

Morales-Torres, S., Pastrana-Martinez, L. M., Figueiredo, J. L., Faria, J. L., Silva, A. M. T. (2012). Design of graphene-based TiO_2 photocatalysts-a review. Environmental Science and Pollution Research, Vol. 19, pp 3676-3687.

Morgan, A. B. and Gilman, J.W. (2003). Characterization of polymer-layered silicate (clay) nanocomposites by Transmission Electron Microscopy and

X-Ray Diffraction: A comparative ctudy. Journal of Applied Polymer Science, Vol. 87, pp 1329-1338.

Mori, K. (2004). Photo-functionalized materials using nanoparticles: photocatalysis. Journal of the Society of Powder Technology, Vol. 41, pp 750-756.

Mosleh, S., Rahimi, M. R., Ghaedi, M., Dashtian, K., Hajati, S. (2018). Sonochemical-assisted synthesis of $CuO/Cu_2O/Cu$ nanoparticles as efficient photocatalyst for simultaneous degradation of pollutant dyes in rotating packed bed reactor: LED illumination and central composite design optimization. Ultrasonics Sonochemistry, Vol. 40, pp 601-610.

Mushtaq, F., Mat, R., Ani, F. N. (2014). A review on microwave assisted pyrolysis of coal and biomass for fuelproduction. Renewable and Sustainable Energy Reviews, Vol. 39, pp 555-574.

Na, P., Jia, X., Yuan, B., Li, Y., Na, J., Chen, Y., Wang, L. (2010). Arsenic adsorption on Ti-pillared montmorillonite. Journal of Chemical Technology & Biotechnology, Vol. 85, pp 708-714.

Nathaniel, E., Kurniawan, A., Soetaredjo, F. E., Ismadji, S. (2011). Organo-bentonite for the adsorption of Pb(II) from aqueous solution: temperature dependent parameters of several adsorption equations. Desalination and Water Treatment, Vol. 36, pp 280-288.

Neaman, A. and Singer, A. (2000). Reology of mixed palygorskite-montmorillonite suspensions. Clays and Clay Minerals, Vol. 48, pp 713-715.

Nguyen, D. L., Gillot, S., Souza, D. O., Blanchard, P., Lamonier, C., Berrier, E., Kotbagi, T. V., Dongare, M. K., Umbarkar, S. B., Cristol, S., Payen, E., Lancelot, C. (2012). One-pot sol-gel preparation for efficient cobalt-molybdenum-titania hydrotreating catalysts. ChemCatChem, Vol. 4, pp 2112-2120.

Ning, N., Yin, Q., Luo, F., Zhang, Q., Du, R., Fu, Q. (2007). Crystallization behavior and mechanical properties of polypropylene/halloysite composites. Polymer, Vol. 48, No. 25, pp 7374-7384.

Nistico, R., Scalarone, D., Magnacca, G. (2017). Sol-gel chemistry, templating and spin coating deposition: a combined approach to control in a simple way

the porosity of inorganic thin films/coatings. Microporous and Mesoporous Materials, Vol. 248, pp 18-29.

Novoselov, K. S., Geim, A. K., Morozov, S. V., Jiang, D., Zhang, Y., Dubonos, S. V., Grigorieva, I. V., Firsov, A. A. (2004). Electric field effect in atomically thin carbon films. Science, Vol. 306, No. 5696, pp 666-669.

Novoselov, K. S., Geim, A. K., Morozov, S. V., Jiang, D., Katsnelson, M. I., Grigorieva, I. V., Dubonos, S. V., Firsov, A. A. (2005). Two-dimensional gas of massless Dirac fermions in graphene. Nature, Vol. 438, No. 7065, pp 197-200.

Obeid, R., Lewis, D., Smith, N., Van Eyk, P. (2019). The elucidation of reaction kinetics for hydrothermal liquefaction of model macro molecules. Chemical Engineering Journal, Vol. 370, pp 637-645.

Ogawa, T., Murata, N., Yamazaki, S. (2003). Devolepment of anti-fogging mirror coated with SiO_2-ZrO_2-colloidal SiO_2 film by sol-gel process. Journal of Sol-Gel Science and Technology, Vol. 27, pp 237-238.

Oliveira, A. G., Nascimento, J. P., Gorgulho, H. F., Martelli, P. B., Furtado, C. A., Figueiredo, J. L. (2016). Electrochemical synthesis of TiO_2/Graphene oxide composite films for photocatalytic applications. Journal of Alloys and Compounds, Vol. 654, pp 514-522.

Pang, X., Zhitomirsky, I., Niewczas, M. (2005). Cathodic electrolytic deposition of zirconia films. Surface Coating Technology, Vol. 195, pp 138-146.

Pappas, G. S., Liatsi, P., Kartsonakis, I. A., Danilidis, I., Kordas, G. (2008). Synthesis and characterization of new SiO_2-CaO hollow nanospheres by sol-gel method: bioactivity of the new system. Journal of Non-Crystalline Solids, Vol. 354, pp 755-760.

Park, S. J. and Ruoff R. S. (2009). Chemical methods for the production of graphenes. Nature Nanotechnology, Vol. 4, pp 217-224.

Passos, F., Carretero, J., Ferrer, I. (2015). Comparing pretreatment methods for improving microalgae anaerobic digestion: Thermal, hydrothermal, microwave and ultrasound. Chemical Engineering Journal, Vol. 279, pp 667-672.

Pei, S., Zhao, J., Du, J., Ren, W., Cheng, H. M. (2010). Direct reduction of graphene oxide films into highly conductive and flexible graphene films by hydrohalic acids. Carbon, Vol. 48, pp 4466-4474.

Peng, S., Zhang, X., Sun, M., Cui, X., Lin, Y. (2012). Graphene oxide modified TiO_2 nanotube arrays: Enhanced visible light photoelectrochemical properties. Nanoscale, Vol. 4, pp 1800-1804.

Peterson, A. A., Vogel, F., Lachance, R. P., Froling, M., Antal, J. M. J., Tester, J. W. (2008). Thermochemical biofuel production in hydrothermal media: A review of sub- and supercritical water technologies. Energy & Environmental Science, Vol. 1, No. 1, pp 32.

Pfitzner, A., Dankesreiter, S., Eisenhofer, A., Cherevatskaya, M. (2013). Heterogeneous semiconductor photocatalysis. In: König B., Editor, Chemical Photocatalysis, De Gruyter.

Platero, E., Fernandez, M. E., Bonelli, P. R., Cukierman, A. L. (2017). Graphene oxide/alginate beads as adsorbents: ınfluence of the load and the drying method on their physicochemical-mechanical properties and adsorptive performance. Journal of Colloid and Interface Science, Vol. 491, pp 1-12.

Potts, J. R., Dreyer, D. R., Bielawski, C. W., Ruoff, R. S. (2011), Graphene-based polymer nanocomposites. Polymer, Vol. 52, pp 5-25.

Powell, C. and Beall, G. (2006). Physical properties of polymer/clay nanocomposites. Current Opinion in Solid State and Materials Science, Vol. 10, No. 2, pp 73-80.

Puetz, J. and Aegerter, M. A. (2004). Dip coating technique. Sol-gel Technologies for Glass Producers and Users, Springer, Boston, MA, pp 37-48.

Pytlakowska, K., Kocot, K., Pilch, M., Zubko, M. (2020). Ultrasound-assisted dispersive micro-solid phase extraction using molybdenum disulfide supported on reduced graphene oxide for energy dispersive X-ray fluorescence spectrometric determination of chromium species in water. Microchimica Acta, Vol. 187, pp 542.

Qi, X., Lian, Y., Yan, L., Smith., R. L. (2014). One-step preparation of carbonaceous solid acid catalysts by hydrothermal carbonization of glucose for cellulose hydrolysis. Catalysis Communications, Vol. 57, pp 50-54.

Raffone, F., Savazzi F., Cicero, G. (2019). 2D Controlled pore generation in single layer graphene oxide for membrane desalination. Chemicals Letters, Vol. 10, pp 7492-7497.

Ramesha, G. K., Kumara, A. V., Muralidhara, H. B., Sampath, S. (2011). Graphene and graphene oxide as effective adsorbents toward anionic and cationic dyes. Journal of Colloid and Interface Science, Vol. 361, pp 270-277.

Randall, J. P., Meador, M. A. B., Jana, S.C. (2011). Tailoring mechanical properties of aerogels for aerospace applications. ACS Applied Materials Interfaces, Vol. 3, pp 613-626.

Ray, S.S. and Okamoto, M. (2003). Polymer/layered silicate nanocomposites: a review from preparation to processing. Progress in Polymer Science, Vol. 28, No. 11, pp 1539-1641.

Reza, M. T., Andert, J., Wirth, B., Busch, D., Pielert, J., Lynam, J. G., Mumme, J. (2014). Hydrothermal carbonization of biomass for energy and crop production. Applied Bioenergy, Vol. 1, pp 11-29.

Sakaushi, K., Oaki, Y., Uchiyama, H., Hosono, E., Zhou, H., Imai, H. (2010). Aqueous solution synthesis of SnO nanostructures with tuned optical absorption behavior and photoelectrochemical properties through morphological evolution. Nanoscale, Vol. 2, pp 2424-2430.

Sanchez-Dominguez, M., Morales-Mendoza, G., Rodriguez-Vargas, M. J., Ibarra-Malo, C. C., Rodriguez-Rodriguez, A. A., Vela-Gonzalez, A. V., Perez-Garcia, S. A., Gomez, R. (2015). Synthesis of Zn-doped TiO_2 nanoparticles by the novel oil-in-water (O/W) microemulsion method and their use for the photocatalytic degradation of phenol. Journal of Environmental Chemical Engineering, Vol. 3, pp 3037-3047.

Sari, A. and Tuzen, M. (2014). Cd(II) adsorption from aqueous solution by raw and modified kaolinite. Applied Clay Science, Vol. 88-89, pp 63-72.

Sengupta, R., Bhattacharya, M., Bandyopadhyay, S., Bhowmick, A. K. (2011). A review on the mechanical and electrical properties of graphite and modified graphite reinforced polymer composites. Progress In Polymer Science, Vol. 36, No. 5, pp 638-670.

Shaban, M., Abukhadra, M. R., Shahien, M. G., Ibrahim, S. S. (2017). Novel bentonite/zeolite NaP composite efficiently removes methylene blue and congo red dyes. Environmental Chemistry Letters, Vol. 16, pp 275-280.

Shah, K. J., Shukla, A. D., Shah, D. O., Imae, T. (2016) Effect of organic modifiers on dispersion of organoclay in polymer nanocomposites to improve mechanical properties. Polymer, Vol. 97, pp 525-532.

Shao, G. N., Imran, S. M., Jeon, S. J., Engole, M., Abbas, N., Haider, M. S., Kim, H. T. (2014). Sol-gel synthesis of photoactive zirconia-titania from metal salts and investigation of their photocatalytic properties in the photodegradation of methylene blue. Powder Technology, Vol. 258, pp 99-109.

Sharma, M., Pathak, M., Kapoor, P. (2018). The Sol-gel method: pathway to ultrapure and homogeneous mixed metal oxide nanoparticles. Asian Journal of Chemistry, DOI:10.14233/AJCHEM.2018.20845.

Silahua-Pavon, A. A., Espinosa-Gonzalez, C. G., Ortiz-Chi, F., Pacheco-Sosa, J. G., Perez-Vidal, H., Arevalo-Perez, J.C., Torres-Torres, J.G. (2019). Production of 5-HMF from glucose using TiO_2-ZrO_2 catalysts: effect of the sol-gel synthesis additive. Catalysis Communications, Vol. 129, pp 105723.

Silva, L. V., Lopes, C. B., Silva, W. C., Paiva Y. G. (2017). Electropolymerization of ferulic acid on multi-walled carbon nanotubes modified glassy carbon electrode as a versatile platform for NADH, dopamine and epinephrine separate detection. Microchemical Journal, Vol. 133, pp 460-467.

Sim, A. Y., Goh, G. K., Tripathy, S., Andeen, D., Lange, F. F. (2007). Photoluminescence of hydrothermally epitaxied ZnO films. Electrochimica Acta, Vol. 52, pp 2933-2937.

Singh, R. K., Kumar, R., Singh, D. P. (2016). Graphene oxide: Strategies for synthesis, reduction and frontier applications. RSC Advances, Vol. 6, pp 64993-65011.

Song, N., Yang, J., Ding, P., Tang, S., Liu, Y., Shi, L. (2014). Effect of covalent-functionalized graphene oxide with polymer and reactive compatibilization on thermal properties of maleic anhydride grafted polypropylene. Industrial & Engineering Chemistry Research, Vol. 53, No. 51, pp 19951-19960.

Song, X., Ma, Y., Wang, J., Liu, B., Yao, S., Cai, Q., Liu, W. (2018). Homogeneous and flexible mullite nanofibers fabricated by electrospinning through diphasic mullite sol-gel route. Journal of Materials Science, Vol. 53, pp 14871-14883.

Sreethawong, T., Ngamsinlapasathian, S., Yoshikawa, S. (2013). Facile surfactant-aided sol-gel synthesis of mesoporous-assembled Ta_2O_5 nanoparticles with enhanced photocatalytic H_2 production. Journal of Molecular Catalysis A: Chemical, Vol. 374-375, pp 94-101.

Stankovich, S., Dikin, D. A., Piner, R. D., Kohlhaas, K. A., Kleinhammes, A., Jia, Y., Ruoff, R. S. (2007). Synthesis of graphene-based nanosheets via chemical reduction of exfoliated graphite oxide. Carbon, Vol. 45, pp 1558-1565.

Stodghill, S. P., Smith, A. E., Haver, J. H. (2004). Thermodynamics of micellization and adsorption of three alkyltrimethylammonium bromides using isothermal titration calorimetry. Langmuir, Vol. 20, No. 26, pp 11387-11392.

Sui, C., Lu, Z., Xu, T. (2013). Effects of annealing temperature on photoluminescence of ZnO nanorods hydrothermally grown on a ZnO: Al seed layer. Optical Materials, Vol. 35, pp 2649-2653.

Sun, Y. Y., Gao, B., Bradford, S. A., Wu, L., Chen, H., Shi, X. Q., Wu, J. C. (2015). Transport, retention, and size perturbation of graphene oxide in saturated porous media: Effects of input concentration and grain size. Water Research, Vol. 68, pp 24-33.

Suslick, S., Bang, H. (2010). Applications of ultrasound to the synthesis of nanostructured materials. Advanced Materials, Vol. 22, pp 1039-1059.

Tadyszak, K., Wychowaniec, J. K., Litowczenko, J. (2018). Biomedical applications of graphene-based structures. Nanomaterials, Vol. 8, pp 944.

Taheriniya, S. and Behboodi Z. (2016). Comparing green chemical methods and chemical methods for the synthesis of titanium dioxide nanoparticles. International Journal of Pharmaceutical Sciences and Research, Vol. 7, No. 12, pp 4927-4932.

Tay, C. B., Chua, S. J., Loh, K. P. (2009). Investigation of morphology and photo luminescence of hydrothermally grown ZnO nanorods on substrates precoated with ZnO nanoparticles. Journal of Crystal Growth, Vol. 311, pp 1278-1284.

Thema, F. T., Moloto, M. J., Dikio, E. D., Nyangiwe, N. N., Kotsedi, L., Maaza, M., Khenfouch, M. (2013). Synthesis and characterisation of graphene thin films by chemical reduction of exfoliated and intercalated graphite oxide. Journal of Chemistry, Vol. 3, pp 1-6.

Therese, G. H. A. and Kamath, P. V. (2000). Electrochemical synthesis of metal oxides and hydroxides. Chemistry of Materials, Vol. 12, pp 1195-1204.

Thompson, L.H. and Doraiswamy, L.K. (1999). Sonochemistry: science and engineering. Industrial & Engineering Chemistry Research, Vol. 38, pp 1215-1249.

Titirici, M. M., Antonietti, M., Thomas, A. (2006). A generalized synthesis of metal oxide hollow spheres using a hydrothermal approach. Chemistry of Materials, Vol. 18, pp 3808-3812.

Tokudome, Y., Fujita, K., Nakanishi, K., Miura, K., Hirao, K. (2007). Synthesis of Monolithic Al_2O_3 with Well-Defined Macropores and Mesostructured Skeletons via the Sol-Gel Process Accompanied by Phase Separation, Chemistry of Materials, Vol. 19, pp 3393-3398.

Tong, L., Liu, Y., Rong, H., Gong, L. (2013). Microwave-assisted synthesis of hierarchical ZnO nanostructures. Materials Letters, Vol. 112, pp 5-7.

Tran, K. Q. (2016). Fast hydrothermal liquefaction for production of chemicals and biofuels from wet biomass - the need to develop a plug-flow reactor. Bioresour Technology, Vol. 213, pp 327-332.

Tyagi, B., Chudasama, C. D., Jasra, R. V. (2006). Determination of structural modification in acid activated montmorillonite clay by FT-IR spectroscopy. Spectrochimica Acta. Part A, Molecular and Biomolecular Spectroscopy, Vol. 64, No. 2, pp 273-278.

Ullah, H., Khan, I., Yamani, Z. H., Qurashi, A. (2017). Sonochemical-driven ultrafast facile synthesis of SnO_2 nanoparticles: growth mechanism structural electrical and hydrogen gas sensing properties. Ultrasonics Sonochemistry, Vol. 34, pp 484-490.

Varadwaj, G. B. B., Rana, S., Parida, K., Nayak, B. B. (2014). A multi-functionalized montmorillonite for co-operative catalysis in one-pot Henry reaction and water pollution remediation. Journal of Materials Chemistry A, Vol. 2, No. 20, pp 7526-7534.

Vilian, A. T. E., Dinesh, B., Rethinasabapathy, M., Hwang, S. K., Jin, C. S., Huh, Y. S., Han, Y. K. (2018). Hexagonal Co_3O_4 anchored reduced graphene oxide sheets for high performance supercapacitors and non-enzymatic glucose sensing. Journal of Materials Chemistry A, Vol. 6, No. 29, pp 14367-14379.

Vinodgopal, K., Neppolian, B., Lightcap, I. V., Grieser, F., Ashokkumar, M., Kamat, P. V. (2010). Sonolytic design of graphene-Au nanocomposites. Simultaneous and sequential reduction of graphene oxide and Au(III). The Journal of Physical Chemistry Letters, Vol. 1, pp 1987-1993.

Wakeland, S., Martinez, R., Grey, J. K., Luhrs, C. C. (2010). Production of graphene from graphite oxide using urea as expansion-reduction agent. Carbon, Vol. 48, pp 3463-3470.

Wang, X., Yang, L., Zhang, J., Wang, C., Li, Q. (2014). Preparation and characterization of chitosan-poly (vinyl alcohol)/bentonite nanocomposites for adsorption of Hg (II) ions. Chemical Engineering Journal. Vol. 251, pp 404-412.

Wang, M., Gao, B., Tang, D., Yu, C.R. (2018). Concurrent aggregation and transport of graphene oxide in saturated porous media: Roles of temperature, cation type, and electrolyte concentration. Environmental Pollution, Vol. 235, pp 350-357.

Wessels, K., Feldhoff, A., Wark, M., Rathousky, J., Oekermann, T. (2006). Low temperature preparation of crystalline nanoporous TiO_2 films by surfactant assisted anodic electrodeposition. Electrochemical and Solid-State Letters, Vol. 9, pp 93-96.

Wu, J., Shen X, Jiang L, Wang K, Chen K. (2010). Solvothermal synthesis and characterization of sandwich-like graphene/ZnO nanocomposites. Applied Surface Science, Vol. 256, No. 9, pp 2826-2830.

Wu, P., Zhang, Q., Dai, Y., Zhu, N., Dang, Z., Li, P., Wang, X. (2011). Adsorption of Cu (II), Cd (II) and Cr (III) ions from aqueous solutions on humic acid modified Ca-montmorillonite. Geoderma, Vol. 164, No. 3, pp 215-219.

Wu, L., Liu, L., Gao, B., Rafael, M. C., Zhang, M., Chen, H., Zhou, Z. H., Wang, H. (2013). Aggregation kinetics of graphene oxides in aqueous solutions: experiments, mechanisms, and modeling. Langmuir, Vol. 29, pp 15174-15181.

Wu, M., Li, T., Li, H., Fan, H., Mi, J. (2017). Desulfurization of hot coal gas over regenerable low-cost Fe_2O_3/mesoporous Al_2O_3 prepared by the sol-gel method. Energy Fuels, Vol. 31, pp 13921-13932.

Xia, J., Li, H., Luo, Z., Shi, H., Wang, K., Shu, H., Yan, Y. (2009). Microwave-assisted synthesis of flower-like and leaf-like CuO nanostructures via room-temperature ionic liquids. Journal of Physics and Chemistry of Solids, Vol. 70, pp 1461-1464.

Xia, T. J., Fortner, J. D., Zhu, D. Q., Qi, Z. C., Chen, W. (2015). Transport of sulfide-reduced graphene oxide in saturated quartz sand: cation-dependent retention mechanisms. Environmental Science & Technology, Vol. 49, pp 11468-11475.

Xia, T. J., Lin, Y. X., Guo, X. T., Li, S. L., Cui, J. S., Ping, H. X., Zhang, J., Zhong, R. W., Du, L. S., Han, C. X., Zhu, L. Y. (2019). Co-transport of graphene

oxide and titanium dioxide nanoparticles in saturated quartz sand: influences of solution pH and metal ions. Environmental Pollution, Vol. 251, pp 723-730.

Xie, H., Zhu, L., Zheng, W., Zhang, J., Gao, F., Wang, Y. (2016). Microwave-assisted template-free synthesis of butterfly-like CuO through $Cu_2Cl(OH)_3$ precursor and the electrochemical sensing property. Solid State Sciences, Vol. 61, pp 146-154.

Yan, X. B., Chen, J. T., Yang, J., Xue, Q. J., Miele, P. (2010). Fabrication of free standing, electrochemically active, and biocompatible graphene oxide-polyaniline and graphene-polyaniline hybrid papers. ACS Applied Materials & Interfaces, Vol. 2, No. 9, pp 2521-2529.

Yang, K., Wan, J. M., Zhang, S., Tian, B., Zhang, Y. J., Liu, Z. (2012). The influence of surface chemistry and size of nanoscale graphene oxide on photothermal therapy of cancer using ultra-low laser power. Biomaterials, Vol. 33, pp 2206-2214.

Yang, H., Kershaw, S. V., Wang, Y., Gong, X., Kalytchuk, S., Rogach, A. L., Teoh, W. Y. (2013). Shuttling photoelectrochemical electron transport in tricomponent CdS/rGO/TiO_2 nanocomposites. The Journal of Physical Chemistry C, Vol. 117, pp 20406-20414.

Yao, Z., Yang, X., Wu, F., Wu, W., Wu, F. (2016). Synthesis of differently sized silver nanoparticles on a screen-printed electrode sensitized with a nanocomposites consisting of reduced graphene oxide and cerium(IV) oxide for non enzymatic sensing of hydrogen peroxide. Microchimica Acta, Vol. 183, pp 2799-2806.

Yasin, G., Khan, M. A., Arif, M., Shakeel, M., Hassan, T. M., Khan, W. Q., Zuo, Y. (2018). Synthesis of spheres-like Ni/graphene nanocomposite as an efficient anti-corrosive coating; effect of graphene content on its morphology and mechanical properties. Journal of Alloys and Compounds, Vol. 755, pp 79-88.

Yayapao, O., Thongtem, S., Phuruangrat, A., Thongtem, T. (2013). Sonochemical synthesis, photocatalysis and photonic properties of 3% Ce-doped ZnO nanoneedles. Ceramics International, Vol. 39, pp 563-568.

Yea, L., Zhang, Y., Song, C., Li, Y., Jiang, B. (2017). Simple sol-gel method to prepare super hydrophilic silica coatings. Materials Letters, Vol. 188, pp 316-318.

Yoon, Y., Zheng, M., Ahn, Y. T., Park, W. K., Yang, W. S., Kang, J. W. (2017). Synthesis of magnetite/non-oxidative graphene composites and their application for arsenic removal. Separation and Purification Technology, Vol. 178, pp 40-48.

You, Z., Qiu, Q., Chen, H., Feng, Y., Wang, X., Wang, Y., Ying, Y. (2020). Laser-induced noble metal nanoparticle-graphene composites enabled flexible biosensor for pathogen detection. Biosensors and Bioelectronics, Vol. 150, pp 111896,

Yu, Y., Qi, S., Zhan, J., Wu, Z., Yang, X., Wu, D. (2011). Polyimide/sepiolite nanocomposite films: Preparation, morphology and properties. Materials Research Bulletin, Vol. 46, No. 10, 1593-1599.

Yu, B., Turdean-Ionescu, C. A., Martin, R. A., Newport, R. J., Hanna, J.V., Smith, M.E. et al. (2012). Effect of calcium source on structure and properties of sol-gel derived bioactive glasses. Langmuir, Vol. 2012, No. 28, pp 17465-17476.

Yu, M., Chen, J. P., Ma, Y. X., Zhang, J. D., Liu, J. H., Li, S. M., An, J. W. (2014). Hydrothermal synthesis of $NiCo_2O_4$ nanowires/nitrogen-doped graphene for high-performance supercapacitor. Applied Surface Science, Vol. 314, pp 1000-1006.

Yun, Y. J., Hong, W. G., Kim, W. J., Jun, Y., Kim, B. H. (2013). A novel method for applying reduced graphene oxide directly to electronic textiles from yarns to fabrics. Advanced Materials, Vol. 25, No. 40, pp 5701-5705.

Zahedi, M., Pirayesh, H., Khanjanzadeh, H., Tabar, M. M. (2013). Organomodified montmorillonite reinforced walnut shell/polypropylene composites. Materials and Design, Vol. 51, pp 803-809.

Zan, X. L., Fang, Z., Wu, J., Xiao, F., Huo, F. W., Duan, H. W. (2013). Free standing graphene paper decorated with 2D-assembly of Au@Pt nanoparticles as flexible biosensors to monitor live cell secretion of nitric oxide. Biosensors & Bioelectronics, Vol. 49, pp 71-78.

Zanetti, M., Lomakin, S., Camino, G. (2000). Polymer layered silicate nanocomposites. Macromolecular Materials Engineering, Vol. 279, pp 1-9.

Zeng, Z. Y., Wang, Y. L., Zhou, Q. B., Yang, K., Lin, D. H. (2019). New insight into the aggregation of graphene oxide in synthetic surface water: Carbonate nanoparticle formation on graphene oxide. Environmental Pollution, Vol. 250, pp 366-374.

Zhang, X., Yao, B., Zhao, L., Liang, C., Zhang, L., Mao, Y. (2001). Electrochemical fabrication of single-crystalline anatase TiO_2 nanowire arrays. Journal of the Electrochemical Society, Vol. 148, pp 398-400.

Zhang, Z., Zhang, J., Liao, L., Xia, Z. (2013a). Synergistic effect of cationic and anionic surfactants for the modification of Ca-montmorillonite. Materials Research Bulletin, Vol. 48, pp 1811-1816.

Zhang, J., Han, Y., Liu, C., Ren, W., Li, Y., Wang, Q., Su, N., Li, Y., Ma, B., Ma, Y., Zhanga, D., Fanga, Y., Miaoa, Z., Maa, M., Dua, X., Takahashib, S., Anzaib, J., Chena, Q. (2013b). Direct electrodeposion of reduced graphene oxide and dendritic copper nanoclusters on glassy carbon electrode for electrochemical detection of nitrite. Electrochimica Acta, Vol. 107, pp 656-663.

Zhang, P., Lu, W., Wang, Y., Jiao, X., Chen, D. (2016). Fabrication of flexible and amphiphobic alumina mats by electrospinning, Journal of Sol-Gel Science and Technology, Vol. 80, pp 690-696.

Zhang, H., Gao, Z., Ao, W., Li, J., Liu, G., Fu, J., Mao, C. R., Kang, Q., Liu, Y., Dai, J. (2017). Microwave pyrolysis of textile dyeing sludge in a continuously operated auger reactor: characterization and analysis. Journal of Hazardous Materials, Vol. 334, pp 112-120.

Zhang, J., Zhou, C. H., Petit, S., Zhang, H. (2019). Hectorite: synthesis, modification, assembly and applications. Applied Clay Science, Vol. 177, pp 114-138.

Zhao, G., Zhang, H., Fan, Q., Ren, X., Li, J., Chen, Y., Wang, X. (2010). Sorption of copper (II) onto super-adsorbent of bentonite-polyacrylamide composites. Journal of Hazardous Materials, Vol. 173, No. 1, pp 661-668.

Zhou, F., Song, H., Wang, H., Komarneni, S., Yan, C. (2018). N-doped TiO_2/sepiolite nanocomposites with enhanced visible-light catalysis: role of N precursors. Applied Clay Science, Vol. 166, pp 9-17.

Zhou, F., Yan, C., Sun, Q., Komarneni, S. (2019). TiO_2/Sepiolite nanocomposites doped with rare-earth ions: preparation, characterization and visible light photocatalytic activity. Microporous and Mesoporous Materials, Vol. 274, pp 25-32.

Zhuang, X. Z., Huang, Y. Q., Song, Y. P., Zhan, H., Yin, X. L., Wu, C. Z. (2017). The transformation pathways of nitrogen in sewage sludge during hydrothermal treatment. Bioresour Technology, Vol. 245, pp 463-70.

Zou, G., Li, H., Zhang, Y., Xiong, K., Qian, Y. (2006). Solvothermal/hydrothermal route to semiconductor nanowires. Nanotechnology, Vol. 17, No. 11, pp 313-320.

Zou, J., Zhong, W., Gao, F., Tu, X., Chen, S., Huang, X., Wang, X., Lu, L., Yu, Y. (2020). Sensitive electrochemical platform for trace determination of Pb2þ based on multilayer Bi-MOFs/reduced graphene oxide films modified electrode. Microchimica Acta, Vol. 187, pp 603.

CHAPTER 7

PHENOLIC COMPOUNDS AS CARBONIC ANHYDRASE INHIBITORS

Asst. Prof. Dr. Ayça AKTAŞ KARAÇELİK[1]

[1] Giresun University, Espiye Vocational School, Department of Food Processing, Giresun, Turkey, 28600. ayca.aktas@giresun.edu.tr, ORCID ID: 0000-0001-5381-2924

INTRODUCTION

Carbonic Anhydrases are extensively distributed in living things, because the substrate of CA is carbon, that forms the basis of the life of all living things. CAs carry out reversibly reaction between bicarbonate ion and carbon dioxide in all organisms and play significant role to regulate numerous pathological/physiological processes. This enzyme is accepted as a target molecule for drugs in many tissues (Supuran ve Scozzafava, 2007). Overactivity of CA enzymes causes different diseases such as especially glaucoma, atherosclerosis, tumor formation, edema, and obesity (Supuran and Scozzafava, 2007). Glaucoma, an eye disease, is characterized by high intraocular pressure. This disease shows its effect by damaging the optic nerve and resulting in progressive vision loss and eventually blindness. The most effective way to reduce high intraocular pressure in glaucoma is to inhibit CA II activity (Renzi et al., 2000). The researches about inhibitors of CA have gained great importance for researchers after discovering that CA activity could be inhibited by many chemicals and drugs (Supuran and Scozzafava, 2002; Gülçin and Beydemir, 2013; Scozzafava et al., 2015; Gocer et al., 2017; Uzunoglu et al., 2020; Karaçelik et al., 2021). Natural, low-toxic, biocompatible, and water-soluble CA inhibitors are mostly preferred as potential drug components because of are without any side effects on health. Recent studies have shown that phenolic compounds in plants exhibited CA inhibition activity.

In the light of this information, it is a promising approach to evaluate natural products in the discovery of new chemotypes with improved drug-like properties to treat CA enzyme-related diseases.

1. PHENOLIC ACIDS AND POLYPHENOLS

The secondary plant metabolites, especially phenolics are produced naturally in all plants. It is a fact that phenolic compounds are important constituents of both human and animal diets. The researches have been still explained the effects of phenolics in foods on health. However, many studies about human health indicated that the diet including foods abundant in polyphenols prevents many different age-related diseases, especially cancers, type II diabetes, and cardiovascular and neurodegenerative diseases (Clifford et al., 2006; Issa et al., 2006; Kelsey et al., 2010; Rashmi and Negi, 2020). Elementary phenols contain one and/or more hydroxyl groups (-OH) bounded on an aromatic ring. Phenolic acids are classified as hydroxycinnamic and hydroxybenzoic acids. Examples of hydroxybenzoic acids with C_6-C_1 phenylmethane structure are protocatechuic, gallic, *p*-hydroxybenzoic, and vanillic acids. On the other hand, hydroxycinnamic acids are in the C_6-C_3 phenylpropane structure and may show different properties thanks to their structure and position of the -OH group attached to the phenyl propane ring. Ferulic, caffeic, *o*-coumaric acids, and *p*-coumaric, are the most abundant hydroxycinnamics in nature (Figure 1).

Polyphenols containing two or more phenolic rings exhibited a wide structural diversity. Polyphenols are composed of the polyketide

(acetate) and shikimate (phenylpropanoid) pathways or metabolisms related to these pathways. The most common polyphenols are flavonoids, which protect plants against UV rays and microorganisms. Up to date, approximately 8000 polyphenolic compounds from different plants have been discovered and more than 4000 of them are flavonoids and this number is increasing (Harborne et al., 1999). Flavonoids, diphenyl propane compounds with a C_6-C_3-C_6 skeleton, contain two benzene rings linked by a 3-carbon chain. -OH groups of flavonoids are rapidly glycosylated due to their reactive properties (Nizamlıoğlu and Nas, 2010). They are structurally divided into five different groups: anthocyanidins, flavones and flavonols, flavanones, flavon-3-ols and proanthocyanidins (Herrmann, 1993). Some of the common flavonoids are myricetin, apigenin, quercetin, morin, chrysin, kaemferol, luteolin, eriodictol, and datiscetin (Figure 1). In addition, glycosides are the most found form of flavonoids in plants (Macheix et al., 1990). Flavonoids are highly effective antioxidants and protect against cardiovascular diseases by reducing oxidation.

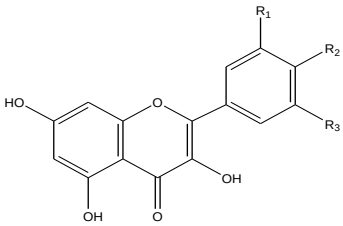

R2= OH; R1=R3= H: Kaempferol

R1=R2=R3= OH: Myricetin

R1=R2= OH; R3= H: Quercetin

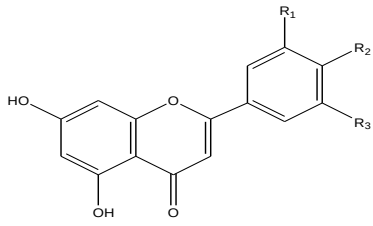

R1=H; R2= OH: Apigenin

R1=R2= OH: Luteolin

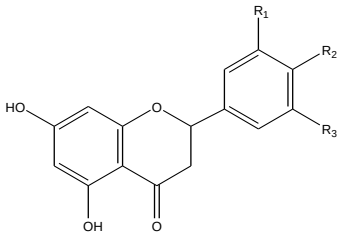

R1= H; R2= 0H: Naringenin

R1=R2= OH: Eriodictol

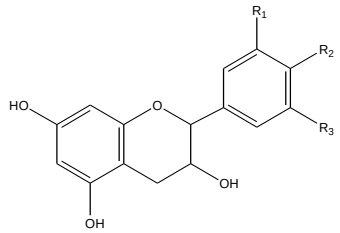

R1=R2= OH; R3= H: Catechin

R1=R2= OH: Epicatechin

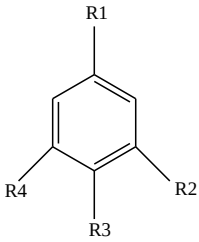

R1= COOH; R2= H; R3= H; R4= H: Benzoic acid

R1= COOH; R2= OH; R3= OH; R4= OH: Gallic acid

R1= COOH; R2= OH; R3= OH; R4= H: Protocatechuic acid

R1= COOH; R2= H; R3= OH; R4= H: *p*-Hydroxybenzoic acid

R1= COOH; R2= OCH_3; R3= OH; R4= H: Vanillic acid

R1= COOH; R2= OCH_3; R3= OH; R4= OCH_3: Syringic acid

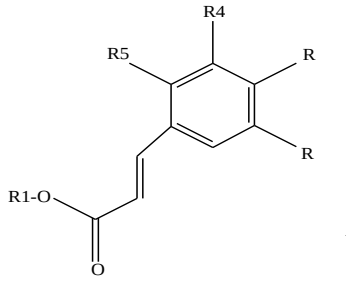

R1= quinic acid; R2= H; R3= OH; R4= OH; R5= H: Chlorogenic acid

R1= H; R2= H; R3= OH; R4= OH; R5= H: Caffeic acid

R1= H; R2= H; R3= H; R4= OH; R5= H: *p*-Coumaric acid

R1= H; R2= H; R3= OCH_3; R4= OH; R5= H: Ferulic acid

R1= H; R2= OH; R3= H; R4= H; R5= H: *o*-Coumaric acid

R1= H; R2= H; R3= OCH_3; R4= OH; R5= OCH_3: Sinapic acid

R1= H; R2= H; R3= H; R4= H; R5=H: Cinnamic acid

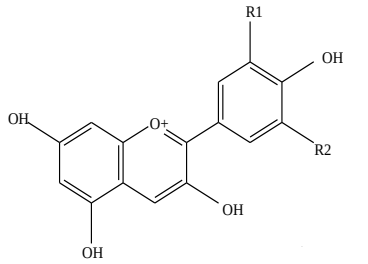

R1= OH; R2= O: Delphinidine

R1=R2= OCH3: Malvidin

R1= OH; R2= H: Cyanidin

R1=R2=H: Pelargonidine

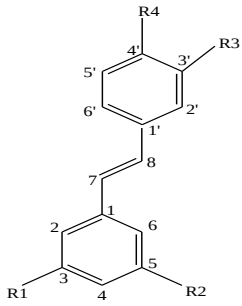

R1= OH; R2= OH; R3= H; R4= OH: *trans*-resveratrol

R1= GlcO; R2= OH; R3= H; R4= OH: *trans*-piseid

R1= GlcO; R2= OH; R3= OH; R4= OH: *trans*-astringin

Figure 1. Some Phenolic Compounds and Chemical Structures

The interactions of plant phenolics with many targets are occurred due to the physicochemical properties of the amphiphilic ring, which is the main structural unit. The planar aromatic ring, which is hydrophobic takes responsibility for hydrophobic interactions (π-stacking), while polar hydroxyl groups involve in hydrogen bonding. The phenolics bind to amino acid residues of various compounds including receptors, proteins, and enzymes due to these reactions. In addition, the formation of *ortho*-hydroxyl groups makes them chelating and antioxidant compounds. The indicated characteristics make phenolics obtained from plants considerable alternative molecules for studying metalloenzyme inhibitions.

2. CARBONIC ANHYDRASE ENZYME AND INHIBITION MECHANISMS

Carbonic anhydrase (EC 4.2.1.1., CA) known as an enzyme, which regulates pH-regulating, is found in many cell types. It performs carbon dioxide (CO_2) regeneration of and CO_2 hydration to bicarbonate (HCO^{3-}) and bicarbonate dehydration in an acidic environment (Gülçin et al., 2004; Zimmerman et al., 2007; Supuran and Scozzafava, 2007; Supuran, 2008). All known CAs today are divided into six different classes as α, β, γ, δ, ζ, η. The enzyme family has been identified in different living things including some bacteria, protozoa, algae, green plants, and vertebrates (Supuran, 2008; Krungkrai and Supuran, 2008). CAs contain one metal ion per protein subunit. All six CA classes can use Zn^{2+} as a metal ion to maintain catalytic activity. While γ-CAs can use Fe^{2+} and maintain their activity with Co^{2+} under anaerobic conditions, Zn^{2+} can be replaced by Cd^{2+} in the structure of ζ-CAs. Similarly, Co^{2+} can be replaced by Zn^{2+} in many α-CAs without remarkable loss of catalytic activity (Iverson et al., 2000; Xu et al., 2008; Zimmerman et al., 2010; Supuran, 2016). α-CAs, the most researched class of CA, possess 16 isoenzymes, which have been identified. Isoenzymes may possess different catalytic activity, intracellular localization, and susceptibility against different classes of inhibitors. CA I, II, III, VII, and XIII are cytosolic CA isoenzymes, and some CA isoenzymes, such as CA IV, IX, XII, and XIV, are also membrane located. The two CA isoenzymes, CA VA and VB are mitochondrial enzymes and CA VI is produced in saliva. It has been shown that the CA XV isoenzyme is not produced in

humans or other primates, but is abundant in other higher vertebrates and rodents. Isoenzymes have active properties in many important biological processes such as CO_2 and ion transportation, acid-base balance, bone resorption, respiration, ureagenesis, lipogenesis, gluconeogenesis, and production of body fluid (Hilvo et al., 2005; Supuran and Scozzafava, 2007; Innocenti et al., 2010a; Supuran, 2016). Among the isoenzymes, CA IX and CA II are the most active enzymes for CO_2 hydration. CA II is located mainly in red blood cells, and many secretory tissues of the eye, kidneys, lungs, central nervous system, and gastrointestinal tract, while CA IX is a tumor-associated isoenzyme (Hilvo et al., 2005; Supuran and Scozzafava, 2007; Supuran, 2008). Many CA isoenzymes are crucial therapeutic targets, which are able to be inhibited or activated for treating diseases (glaucoma, edema, cancer, obesity, epilepsy, and osteoporosis (Supuran and Scozzafava 2002; Supuran and Scozzafava, 2007).

3. INHIBITION MECHANISM OF PHENOLS

In mammals, CAs with 16 known isoenzymes are inhibited by three basic mechanisms. The first is the inhibitor coordination from the active site region of the enzyme to the zinc ion, which is catalytically important and by changing the water/hydroxide ion bound to Zn^{2+} in the active site of the enzyme and leading to the tetrahedral geometry of Zn^{2+}. The second is the mechanism by which the inhibitor binds to a water or hydroxide ion bound to Zn^{2+}. Phenols and polyamines are compounds with this CA inhibition mechanism (Nair et al., 1994). Third, when inhibitors interact to the activator bounding site of CA

active sites, the active enzymes are blocked. Coumarins are bound by this inhibition mechanism. It should be noted that the role of Zn^{2+} in its interaction with the inhibitor decreases continuously when it comes to the last of the CA inhibition mechanisms. This possesses significant implications to design drugs as CA inhibitors. Since 16 CA isoenzymes described so far in mammals have highly conserved active site cavity. The active sites exhibited the highest variation in amino acid sequence and the highest structural variation, which are only those at the active site entrance. This has recently been shown that phenols, coumarins, and other noninteracting inhibitors with Zn^{+2} ion lead to isoenzyme selective CA inhibitors, a target that is difficult to reach with classic sulfonamide/sulfamate inhibitors (Supuran and Scozzafava, 2007). The researches about the potential of phenols as inhibitors of CA indicated that simple phenols are the only competitive inhibitor with CO_2 as the substrate for the major carbonic anhydrase isoenzymes (Nair et al., 1994). It was first reported that phenol is a competitive inhibitor of human CA II (Innocenti et al., 2008b). In the study, the X-ray crystal structure of h CA II and its adduct was examined and it was revealed that two phenol molecules bind to the enzyme. Initially, it is found in a hydrophobic pocket of about 15 Å from the catalytic zinc ion. Therefore, this binding seems not to be connected with catalytic activity of enzyme. However, the second phenol molecule was found in the active site and exhibited a new binding mode. In fact, it is not coordinated with the zinc ion. However, the zinc-bound water/hydroxide ion and the NH amide of Thr 199 are attached to the active site via two hydrogen bonds to the

OH moiety. Moreover, the aromatic ring has been reported to lie in a hydrophobic pocket of the active site bounded by residues Val 121, Val 143, Leu 198, and 197 Trp 209, thereby contributing to complex stabilization as shown in Figure 2 (Supuran, 2016).

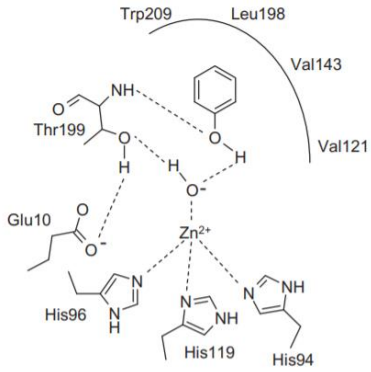

Figure 2. Schematic Illustration of Phenol Binding Mode In The hCA II Active Site (Supuran, 2016)

The findings contributed to the detailed investigation of different polyphenolic and phenolic natural products as carbonic anhydrase enzyme inhibitors. *In vitro* kinetic studies of a number of commercially available phenolic compounds, such as ferulic, caffeic, gallic, *p*-coumaric, salicylic acids, and resorcinol, have shown that they are effective inhibitors of CA in the low micromolar range (Innocenti et al., 2008b; Innocenti et al., 2010b; Davis et al., 2010; Öztürk Sarıkaya et al., 2011; Şentürk et al., 2011; Gülçin and Beydemir, 2013; Adem et al., 2019; Ghiasi et al., 2021).

In another study, inhibitory activities of phenolics such as 4-methyl guaiacol, guaiacol, 4-propyl guaiacol, catechol, 4-methyl catechol,

eugenol, 3-methyl catechol, 3-methoxy catechol, syringaldehyde, isoeugenol, and vanillin against h CAXII, h CAIX, h CAII, and h CAI, isoenzymes were determined (Scozzafava et al., 2015). Except for the catechol, all other compounds showed inhibition potential ranging from 2.2-10.92 μM. In addition, among the phenolic derivatives tested, 3-methoxy catechol and 4-methyl catechol compounds showed potent inhibitory activity on the tumor-associated transmembrane isoenzymes h CAIX and h CAXII. The combination of the phenolic moiety with other functional groups is used to obtain compounds with stronger activity. For example, in the so-called "sugar approach," incorporating the hydrophilic part of sugar allows the molecule to bind to the enzyme cavity in a different way. It also increases its selectivity towards membrane-bound CA isoenzymes over cytosolic ones. Selectivity towards specific h CA isoenzymes reduces side effects. In this context, a series of synthetic *C*-cinnamoyl glycosides have been synthesized and a low micromolar range inhibition potential has been detected against CA I, II, IV, VA, VB, VI, VII, IX, XII, XIII, and XIV (Riafrecha et al., 2013). Structurally containing both phenol and lactone (*α*-pyrone) moieties (K_i: 5.5–10.4 μM), h CA I, III, IV, XIII, and XIV of Dodonein showed inhibitory properties (Carreyre et al., 2013). Rosmarinic acid obtained from medicinal and aromatic plants including rosemary, sage, and thyme, was reported to be a potential CA inhibitor on h CA I (K_i: 86.0 μM) and h CA II (K_i: 57.0 μM) isoenzymes (Topal and Gülçin, 2014). In another study, the inhibitory effects of a series of phenolic acid esters containing ferulic, *p*-coumaric and caffeic acids, benzyl, *p*-hydroxy-

phenetoxy-phenethyl and *m/p*-hydroxyphenethyl- moieties on h CA XIV, XII, and I isoenzymes were investigated (Maresca et al., 2015). A study about inhibition of h CA XII, h CA IX, h CA II, and h CA I isoenzymes with the flavones and aminoflavones showed that these compounds are low micromolar CA inhibitors in the range of 1.88-9.07 μM K_i (Balboni et al., 2012). Studies about the interaction of flavonoids with CAs suggest that they may be another relevant category of CA inhibitors that can be used as a guide to producing more potent CA inhibitors. A number of flavonoids (apigenin, flavones, luteolin, catechin, morin, and quercetin) have been shown to have inhibitory effects against human (CA I, II, IV) and bovine (bCA III) α-CA isoenzymes similar to the standards used (Ekinci et al., 2013). In other studies, the inhibitory effects of a series of flavonoids (apigenin, catechin, epicatechin, rhamnetin, kaempferol, isorhamnetin, fisetin, rutin, silymarin diosmetin, eriocitrin, hesperidin, naringin, taxifolin, and quercetin-3-O-glucoside) on h CA I, h CA II, h CA IV, h CA VI, h CA VA, h CA IX, h CA XII and bCA III isoenzymes were investigated (Sahin et al., 2012; Koz et al., 2013; Gidaro et al., 2015). The results reported above encourage researchers to discover new phenolic compounds against a range of human and bovine CAs.

CONCLUSIONS

Up to now, several discovered phenolic compounds have been deeply researched for their interaction with the main isoenzymes of hCAs. Phenols and polyphenols are the most studied compounds among the natural products and have provided possibility to identify selective

inhibitors of CA. Because of their structural diversity, these compounds are characterized by different selectivity profiles compared to conventional CA inhibitors that have long been used in clinical practice but still have pharmacological side effects. Nevertheless, considering the wide variety of chemotypes of natural phenolics, it illustrates the fact that there is still much to explore. There is a great need new studies, including *in vitro*, *in vivo* testing, and disease models, are required to support these results.

REFERENCES

Adem, S., Akkemik, E., Aksit, H., Guller, P., Tufekci, A. R., Demirtas, I. (2019). Activation and inhibition effects of some natural products on human cytosolic CAI and CAII. Medicinal Chemistry Research, 28, 711-722.

Balboni, G., Congiu, C., Onnis, V., Maresca, A., Scozzafava, A., Winum, J. Y., Maietti, A., Supuran, C. T. (2012). Flavones and structurally related 4-chromenones inhibit carbonic anhydrases by a different mechanism of action compared to coumarins. Bioorganic & Medicinal Chemistry Letters, 22, 3063–3066.

Carreyre, H., Coustard, J. M., Carré, G., Vandebrouck, C., Bescond, J., Ouédraogo, M., Marrot, J. D., Vullo, D., Supuran, C. T., Thibaudeau, S. (2013). Natural product hybrid and its superacid synthesized analogues: Dodoneine and its derivatives show selective inhibition of carbonic anhydrase isoforms I, III, XIII and XIV. Bioorganic & Medicinal Chemistry, 21, 3790–3794.

Clifford, M., Brown, J. E. (2006). Dietary flavonoids and health-broadening the perspective. In flavonoids: chemistry, biochemistry and applications, Andersen, Ø. M., Markham, K. R., (Eds), Taylor & Francis Group: Boca Raton, FL, USA, pp. 319-370.

Davis, R. A., Innocenti, A., Poulsen, S. A., Supuran, C. T. (2010). Carbonic anhydrase inhibitors. Identification of selective inhibitors of the human mitochondrial isozymes VA and VB over the cytosolic isozymes I and II from a natural product-based phenolic library. Bioorganic & Medicinal Chemistry, 18, 14-18.

Ekinci, D., Karagoz, L., Ekinci, D., Senturk, M., Supuran, C. T. (2013). Carbonic anhydrase inhibitors: In vitro inhibition of α isoforms (hCA I, hCA II, bCA III, hCA IV) by flavonoids. Journal of Enzyme Inhibition and Medicinal Chemistry, 28, 283–288.

Ghiasi, M., Goli, N. E., Gholami, S., Supuran, C. T. (2021). QM and QM/MM study on inhibition mechanism of polyphenolic compounds as non-classical inhibitors of alpha-human carbonic anhydrase (II). Theoretical Chemistry

Accounts, 140, 141.

Gidaro, M. C., Alcaro, F., Carradori, S., Costa, G., Vullo, D., Supuran, C. T., Alcaro, S. (2015). Eriocitrin and apigenin as new carbonic anhydrase VA inhibitors from a virtual screening of calabrian natural products. Planta Medica, 81, 533–540.

Gocer, H., Akincioglu, A., Goksu, S., Gulcin, I. (2017). Carbonic anhydrase inhibitory properties of phenolic sulfonamides derived from dopamine related compounds. Arabian Journal of Chemistry, 10, 398-402.

Gülçin, İ., Beydemir, S., Büyükokuroglu, M. E. (2004). In vitro and in vivo effects of dantrolene on carbonic anhydrase enzyme activities. Biological and Pharmaceutical Bulletin, 27, 613-616.

Gülçin, İ., Beydemir, Ş. (2013). Phenolic compounds as antioxidants: Carbonic anhydrase isoenzymes inhibitors. Mini-Reviews in Medicinal Chemistry, 13, 408-430.

Harborne, J. B., Baxter, H., Moss, G. P. (1999). Phytochemical dictionary: Handbook of bioactive compounds from plants (2nd ed.). Taylor and Francis, London.

Herrmann, K. (1993). In pflanzlichen lebensmitteln vorkommende flavonoide als antioxidantien. Gordian, 93, 108-111.

Hilvo, M., Tolvanen, M., Clark, A., Shen, B., Shah, G. N., Waheed, A., Halmi, P., Hänninen, M., Hämäläinen, J. M., Vihinen, M., Sly, W. S., Parkkila, S. (2005). Characterization of CA XV, a new GPI-anchored form of carbonic anhydrase. Biochemical Journal, 392, 83-92.

Innocenti, A., Gülçin, I., Scozzafava, A., Supuran, C. T. (2010a). Carbonic anhydrase inhibitors. Antioxidant polyphenol natural products effectively inhibit mammalian isoforms I-XV. Bioorganic & Medicinal Chemistry Letters, 20, 5050-5053.

Innocenti, A., Öztürk Sarıkaya, S. B., Gülçin, I., Supuran, C. T. (2010b). Carbonic anhydrase inhibitors. Inhibition of mammalian isoforms I-XIV with a series of natural product polyphenols and phenolic acids. Bioorganic & Medicinal Chemistry Letters, 18, 2159-2164.

Innocenti, A., Vullo, D., Scozzafava, A., Supuran, C. T. (2008a). Carbonic anhydrase inhibitors. Interactions of phenols with the 12 catalytically active mammalian isoforms (CA I-XIV). Bioorganic & Medicinal Chemistry Letters, 18, 1583-1587.

Innocenti, A., Vullo, D., Scozzafava, A., Supuran, C. T. (2008b). Carbonic anhydrase inhibitors: Inhibition of mammalian isoforms I–XIV with a series of substituted phenols including paracetamol and salicylic acid. Bioorganic & Medicinal Chemistry, 16, 7424-7428.

Issa, A. Y., Volate, S. R., Wargovich, M. J. (2006). The role of phytochemicals in inhibition of cancer and inflammation: New directions and perspectives. Journal of Food Composition and Analysis, 19, 405–419.

Iverson, T. M., Alber, B.E., Kisker, C., Ferry, J. G., Rees, D. C. (2000). A closer look at the active site of γ-carbonic anhydrases: High resolution crystallographic studies of the carbonic anhydrase from methanosarcina thermophila. Biochemistry, 39, 9222-9231.

Karaçelik, A. A., Küçük, M., Efe, D., Çakır, V., Bıyıklıoğlu, Z. (2021). Carbonic anhydrase inhibition potential and some bioactivities of the peripherally tetrasubstituted cobalt(II), titanium(IV), manganese(III) phthalocyanines. Letters in Drug Design & Discovery, 18, 365-371.

Kelsey, N. A., Wilkins, H. M., Linseman, D. A. (2010). Nutraceutical antioxidants as novel neuroprotective agents. Molecules, 15, 7792–7814.

Koz, Ö., Ekinci, D, Perrone, A., Piacente, S., Çalıskan, O. A., Bedir, E., Supuran, C. T. (2013). Analysis of saponins and phenolic compounds as inhibitors of α-carbonic anhydrase isoenzymes. Journal of Enzyme Inhibition and Medicinal Chemistry, 28, 412–417.

Krungkrai, J., Supuran, C. T. (2008). The alpha-carbonic anhydrase from the malaria parasite and its inhibition. Current Pharmaceutical Design, 14, 631-640.

Macheix, J. J., Fleurit, A., Billot, J. (1990). Fruit Phenolics, Boca Raton, CRC Press.

Maresca, A., Akyuz, G., Osman, S. M., AlOthman, Z., Supuran, C. T. (2015). Inhibition of mammalian carbonic anhydrase isoforms I–XIV with a series of phenolic acid esters. Bioorganic & Medicinal Chemistry, 23, 7181–7188.

Maresca, A., Temperini, C., Vu, H., Pham, N. B., Poulsen, S. A., Scozzafava, A., Quinn, R. J., Supuran, C. T. (2009). Non-zinc mediated inhibition of carbonic anhydrases: Coumarins are a new class of suicide inhibitors. Journal of the American Chemical Society, 131, 3057-3062.

Nair, S. K., Ludwig, P. A., Christianson, D. W. (1994). Phenol as a carbonic anhydrase inhibitor. Journal of the American Chemical Society, 116, 3659-3660.

Nizamlıoğlu, N., Nas, S. (2010). The phenolic compounds in vegetables and fruit; structures and their importance. Electronic Journal of Food Technologies, 5, 20-35.

Öztürk Sarıkaya, S. B., Gülçin, I., Supuran C.T. (2010). Carbonic anhydrase inhibitors. Inhibition of human erythrocyte isozymes I and II with a series of phenolic acids. Chemical Biology & Dug Design, 75, 515-520.

Öztürk Sarıkaya, S. B., Topal, F., Şentürk, M., Gülçin, I, Supuran, C. T. (2011). In vitro inhibition of carbonic anhydrase isozymes by some phenolic compounds. Bioorganic & Medicinal Chemistry Letters, 21, 4259-4262.

Rashmi, H. B., Negi, P. S. (2020). Phenolic acids from vegetables: A review on processing stability and health benefits. Food Research International, 136, 109298.

Renzi, G., Scozzafava, A. Supuran, C. T. (2000). Carbonic anhydrase inhibitors: topical sulfonamide antiglaucoma agents incorporating secondary amine moieties. Bioorganic & Medicinal Chemistry Letters, 10, 673-676.

Riafrecha, L. E., Rodriguez, O. M., Vullo, D., Supuran, C. T., Colinas, P. A. (2013). Synthesis of C-cinnamoyl glycosides and their inhibitory activity against mammalian carbonic anhydrases. Bioorganic & Medicinal Chemistry, 21, 1489–1494.

Sahin, H., Can, Z., Yildiz, O., Kolayli, S., Innocenti, A., Scozzafava, G., Supuran, C. T. (2012). Inhibition of carbonic anhydrase isozymes I and II with natural products extracted from plants, mushrooms and honey. Journal of Enzyme Inhibition and Medicinal Chemistry, 27, 395–402.

Scozzafava, A., Passaponti, M., Supuran, C. T., Gülçin, I. (2015). Carbonic

anhydrase inhibitors: Guaiacol and catechol derivatives effectively inhibit certain human carbonic anhydrase isoenzymes (hCA I, II, IX and XII). Journal of Enzyme Inhibition and Medicinal Chemistry, 30, 586–591.

Supuran C. T. (2016). How many carbonic anhydrase inhibition mechanisms exist?. Journal of Enzyme Inhibition and Medicinal Chemistry, 31, 345-360.

Supuran, C. T. (2008). Carbonic anhydrases: novel therapeutic applications for inhibitors and activators. Nature Reviews Drug Discovery, 7, 168-181.

Supuran, C. T., Scozzafava, A. (2002). Applications of carbonic anhydrase inhibitors and activators in therapy. Expert Opinion on Therapeutic Patents, 12, 217-242.

Supuran, C. T., Scozzafava, A. (2007). Carbonic anhydrases as targets for medicinal chemistry. Bioorganic & Medicinal Chemistry, 15, 4336-4350.

Şentürk, M., Gülçin, I., Beydemir, S; Küfrevioğlu, Ö. I., Supuran, C. T. (2011). In vitro inhibition of human carbonic anhydrase I and II isozymes with natural phenolic compounds. Chemical Biology & Dug Design, 77, 494-499.

Topal, M., Gülçin, I. (2014). Rosmarinic acid: A potent carbonic anhydrase isoenzymes inhibitor. Turkish Journal of Chemistry, 38, 894–902.

Uzunoglu, S. B., Uzunoglu, T., Arslan, O. (2020). Inhibitory effects of anticancer drugs on cytosolic carbonic anhydrase isozymes. Fresenıus Environmental Bulletin, 29, 11461-11465.

Xu, Y., Feng, L., Jeffrey, P. D., Shi, Y., Morel, F. M. M. (2008). Structure and metal exchange in the cadmium carbonic anhydrase of marine diatoms. Nature, 452, 56-61.

Zimmerman, S. A., Ferry, J. G., Supuran, C. T. (2007). Inhibition of the archaeal beta-class (Cab) and gamma-class (Cam) carbonic anhydrases. Current Topics in Medicinal Chemistry, 7, 901-908.

Zimmerman, S. A., Tomb, J. F., Ferry, J. G. (2010). Characterization of camh from methanosarcina thermophila, founding member of a subclass of the γ- class of carbonic anhydrases. Journal of Bacteriology, 192, 1353-1360.

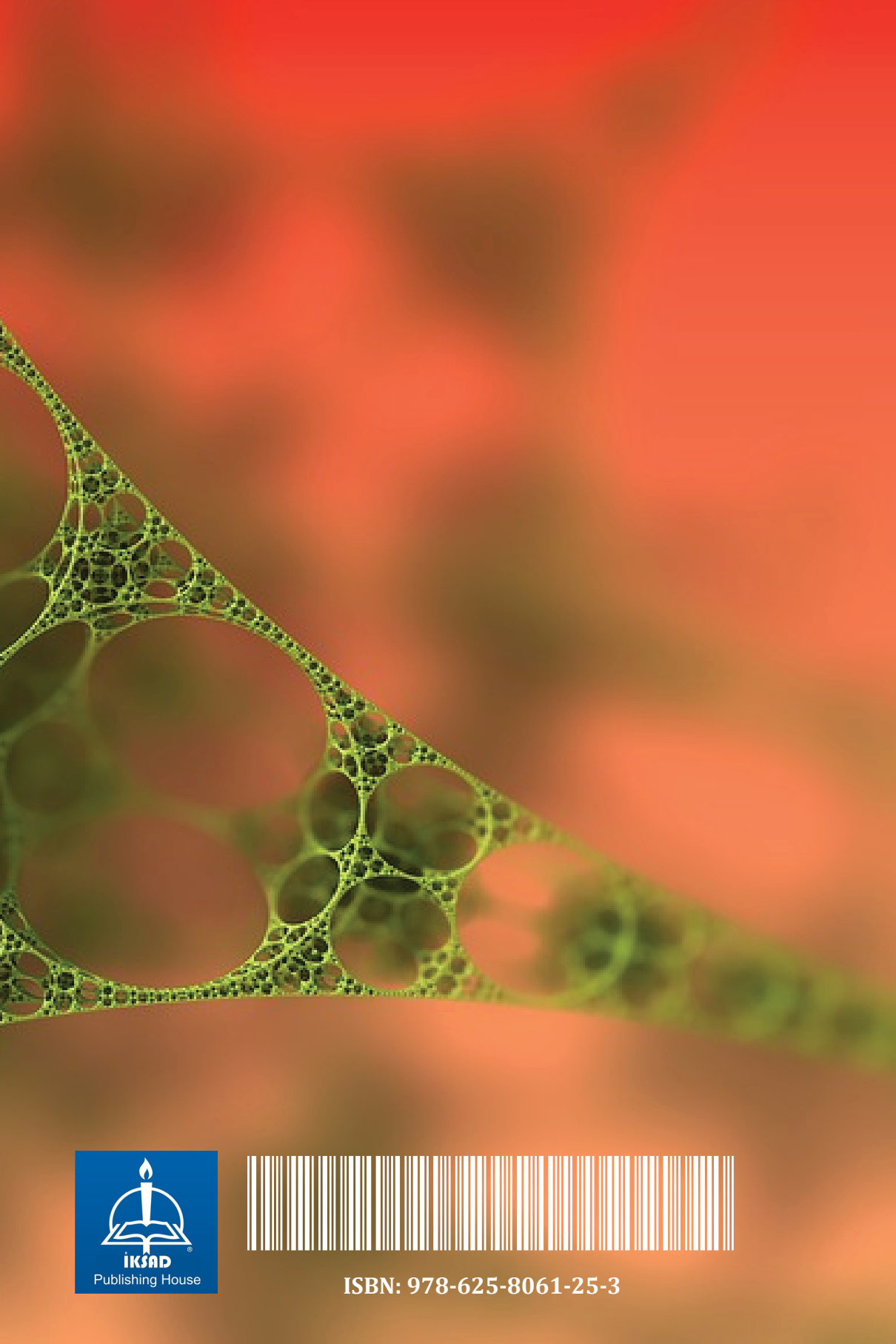

İKSAD Publishing House

ISBN: 978-625-8061-25-3